JOHANN BOCK SEVERIN

SUPERCONDUCTING QUBIT READOUT

IN THEORY, EXPERIMENT AND SIMULATION

SUPERVISED BY: MORTEN KJAERGAARD
JACOB HASTRUP

HANDED IN: OCTOBER 31, 2023

Abstract

For superconducting qubits to be a viable platform for large-scale quantum information processing, a high-fidelity readout is required. This thesis investigates the underlying physics describing the system and time evolution in an initialization and readout sequence in order to study how different physical parameters contribute to the State Preparation and Measurements (SPAM) errors. By calibrating a single superconducting qubit, a simulation model is built using the stochastic master equation to simulate the dispersive approximation of a qubit-resonator system. The model is capable of producing realistic plots of IQ measurements that have similar distributions and SPAM fidelity as measured in the laboratory. The model is used to estimate the contribution to the infidelity from three factors: non-zero temperature, energy decay during measurement, and inefficient measurement. We conclude that non-zero temperature is the biggest contributor to the analyzed system. The model is further used to simulate the system with marginal improvements. This serves as a basis for discussing how to improve superconducting qubit readout.

Acknowledgements

This thesis would not have come to be if it were not for my two truly fantastic supervisors, Jacob Hastrup and Morten Kjaergaard. I deeply appreciate the advice, cooperation, and fruitful discussions of interesting physics we have had along the way.

I want to extend a special thanks to the competent and kindhearted people at SquidLab, who have provided me with technical support, theoretical discussion, and company in a perhaps unhealthy amount of coffee breaks. A particular thanks goes to Malthe Nielsen, who has been my guide in the laboratory and has been building the software to support whatever experiment I thought of.

Outside the laboratory, I want to thank my friends, family, and girlfriend, who have been encouraging, supportive, and lenient while I immersed myself in the field of superconducting qubits.

With the submission of this thesis, I now conclude five amazing years of learning physics at the University of Copenhagen. I am grateful for all the people I met along the way. I could never have hoped for such amazing people to work, study, laugh, live, and be myself among.

Contents

1 Introduction

The demand for power to run computational tasks is accelerating. To overcome the increasing complexity, the transistors, which do the heavy lifting of storing and computing the singular 0's and 1's, have been stacked closer and closer. Now, they span only a few nanometers, a size where they are susceptible to quantum effects, leading to new challenges. [1]. The same quantum effects also provide hope since they can be utilized in a new form of computing on different devices, quantum computers.

By considering quantum bits with the ability to be in a superposition of 0 and 1, some large problems can be formulated compactly and run efficiently [2]. That is, if one has a working quantum computer. Many different implementations of quantum computers are well on their way. They take many very different forms. Some promising candidates are singular atoms trapped in electric fields and controlled by lasers [3], single photons capable of storing quantum information [4], or superconducting circuits that are controlled by microwave pulses at temperatures just above absolute zero [5]. The latter will be the focus of this thesis.

Superconducting qubits are rapidly developing and have seen multiple big accomplishments in the last few decades: the design and fabrication of superconducting circuits capable of processing quantum information [6, 7], microwave pulses that can control and measure it with high precision [8, 9], and schemes to entangle qubits with their neighbors [10]. Recent progress has significantly improved the ability to do operations on single superconducting qubits [11] and multi qubit gates have surpassed the 99.9 % fidelity mark [12]. Improvements have also been made for qubit initialization and readout [9, 13], but this is still a challenge. State Preparation and Measurement errors (SPAM) are inherent parts of the quantum algorithm and hard, if not impossible, to separate in tomography [14]. In this thesis, we will instead examine the physics behind the measurement process. This will allow us to build a model of our system in simulation, where we investigate the effect physical parameters have on SPAM errors.

1.1 Outline of Thesis

The thesis is built up in the following way: The first few chapters will mainly be theoretical. In the rest of Chapter 1, we will cover some fundamentals of quantum mechanics, and in Chapter 2, we will

focus in particular on the theory of circuit Quantum Electrodynamics (cQED). Chapter 3 will go into more depth on how superconducting qubits can be connected with control hardware and resonators to allow control and readout of the qubit. Furthermore, we will investigate how interactions with the environment affect our qubit. This is done by discussing open quantum systems in Chapter 4 and weak continuous measurements in Chapter 5.

The second half of the thesis will focus on readout in experiment and our efforts to recreate it in simulation. We will in Chapter 6 present the experiment to investigate the performance of readout in our system. In Chapter 7, we will calibrate our device to determine the necessary parameters for simulating it. The simulation is created and discussed in Chapter 8. Finally, we will in Chapter 9 use our model to investigate how different parameters contribute to the readout and state preparation infidelity.

1.2 Qubits

Improving classical computer hardware can take many shapes: more processing power, bigger memory size, or faster data transfers. Ultimately, these improvements increase our capability of storing, transferring, or manipulating single entities, bits. Bits are the smallest piece of information in classical computers, corresponding to an on/off switch. Often, they are represented with binary numbers, such that "1" is on and "0" is off. Combining billions or even trillions of bits, we can store data, media, or even programs.

While most everyday computing tasks can easily be done using classical computers, some problems scale exponentially and unforgivably when the size of the problem is increased. Among these problems, we find prime factorization and simulation of quantum mechanical systems, a challenge that will hunt us throughout this thesis. Instead of building classical computers of exponentially increasing size, quantum mechanics provides hope to solve these problems by replacing the bit with the quantum bit (qubit). The qubit is not bound by the discreteness of the classical bit but can be in a superposition of "0" and "1" at the same time [15].

1.2.1 A Quantum Mechanical State

In quantum mechanics, the properties of our system can be continuous, like the position of a particle, or discrete, like the spin of an electron, pointing either up or down. When considering a quantum mechanical object, all possible physical configurations span a Hilbert Space of finite or infinite dimensions. A set of configurations that completely describe all the information one could measure about an object is an element in the Hilbert Space and is called a quantum mechanical state. Mathematically, we represent it with a ket: $|\psi\rangle$, where ψ is a label that could refer to some characteristic information about the configuration [16].

Observable information about the state of the system can be found by applying operators to it. Applying an operator is represented as multiplication from the left: $A|\psi\rangle$, which illustrates the linearity of quantum mechanics. Of special interest are eigenstates to an operator, which are states satisfying $A|a\rangle = a|a\rangle$, where a is the eigenvalue and $|a\rangle$ is the eigenstate. Most importantly, perhaps, is the energy of the system and the corresponding energy eigenstates. These are states associated with the Hamiltonian operator, which, like in classical mechanics, is a generator of the equations of motion in quantum mechanics [16].

1.2.2 The Two Level System

To create a qubit, one needs a quantum mechanical system with two levels. There are multiple ways of achieving this. A straightforward approach is by using an observable in a 2-dimensional Hilbert space like the spin of an electron.

Another approach is to limit ourselves to only a subspace of a larger Hilbert space. If the quantum mechanical states is connected to an environment, they are subject to Boltzmann statistics [1] [17]. At low enough temperatures where the energy difference is much larger than the temperature $\Delta E \gg k_b T$, the system will occupy the ground state unless we change it. By limiting our operation to the subspace of "0" and "1", we will effectively have a qubit. After choosing a two level system, the states of the system can be described with $|0\rangle, |1\rangle$ and can be combined to construct superpositional states:

$$|\psi\rangle = a|0\rangle + b|1\rangle \tag{1.1}$$

where a and b are complex numbers and $|a|^2, |b|^2$ are the respective probabilities that the state will collapse to either $|0\rangle$ or $|1\rangle$ if measured. Since the probabilities must sum to one, we have normalization constraint. We are also allowed to freely choose a global phase since only phase differences have physical meaning[16]. These constraints allow us to write a general state of the two level system:

$$|\psi\rangle = \cos(\theta/2)|0\rangle + e^{i\phi}\sin(\theta/2)|1\rangle \tag{1.2}$$

where our description have two angles θ and ϕ which determine the relative occupation in these two states and a phase between them. With these two angles, the state of a qubit can be visualized geometrically [5].

[1] That is the relative probability of finding a qubit in two different states (say $|1\rangle$ and $|0\rangle$) can be found as the fraction between their Boltzmann factor: $e^{-E_1/k_bT}/e^{-E_0/k_bT}$.

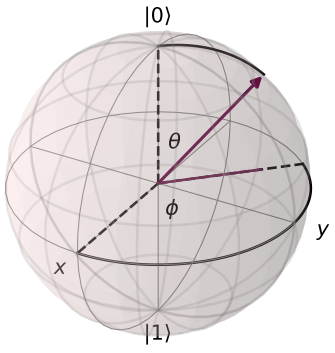

Figure 1.1: Representation of a qubit state on the Bloch sphere. The angles ϕ and θ are displayed along with the projection onto the x-y plane.

1.2.3 The Bloch Sphere

With two angles θ and ϕ and a vector with magnitude 1, the perfect place for visualization is the unit sphere. The depiction of a qubit state on a sphere is called a Bloch Sphere and an example can be seen in 1.1. On the Bloch Sphere, the state $|0\rangle$ will be on the north (positive) pole along the z-axis and $|1\rangle$ at the south pole (negative). With this mapping the projection of the state vector unto the z-axis

gives the probabilities of finding $|0\rangle$ or $|1\rangle$ respectively and the phase difference is mapped unto the x-y plane [15].

1.3 Time Evolution of a Quantum System

Let us now take a look at the dynamics of a quantum system. A process which transforms a state into another must leave the inner product unchanged to keep the normalization. By applying unitary transformation this is guaranteed[2]. Quantum dynamics can then be described by a unitary transformation taking a state at some time $t = t_0$ into a the state at a later time $t = t_0 + \Delta t$. At the later time the inner product should be conserved:

[2] For unitary transformations we have: $\mathcal{U}^{-1} = \mathcal{U}^\dagger$ or equally $\mathcal{U}^\dagger\mathcal{U} = \mathbb{1}$

$$\langle\psi; t_0|\psi; t_0\rangle = \langle\psi; t_0..\Delta t|\psi; t_0..\Delta t\rangle = \langle\psi; t_0|\mathcal{U}^\dagger(t_0, t_0+\Delta t)\mathcal{U}(t_0, t_0+\Delta t)|\psi; t_0\rangle \tag{1.3}$$

which is satisfied since $\mathcal{U}$ is unitary. An additional requirement is that the transformation should reduce to identity if no time has passed: $\mathcal{U}(t_0, t_0 + \Delta t) \to \mathbb{1}$ when $\Delta t \to 0$. Expanding the transformation to first order in the infinitesimal timestep, dt, the unitary transformation is described by:

$$\mathcal{U}(dt) = \mathbb{1} - i\Omega dt \tag{1.4}$$

Where Ω is a hermitian operator with units of frequency[3]. The actual operator is proportional to the Hamiltonian operator and is given by : $\Omega = \frac{H}{\hbar}$. From eq. 1.4 and by defining $d|\psi; t\rangle = |\psi; t..dt\rangle - |\psi; t\rangle$ we find a differential equation for state evolution:

[3] To see why this keeps the normalization, we write $\mathcal{U}^\dagger(dt)\mathcal{U}(dt) = (\mathbb{1} + i\Omega dt)(\mathbb{1} - i\Omega dt) = \mathbb{1} + dt^2\Omega^2$ which goes to identity in the limit of $dt \to 0$ as the dt^2 term vanishes.

$$|\psi; t..dt\rangle = \mathcal{U}(dt)|\psi; t\rangle = \left(\mathbb{1} - i\frac{H}{\hbar}dt\right)|\psi\rangle \tag{1.5}$$

$$|\psi; t..dt\rangle - |\psi; t\rangle = i\frac{H}{\hbar}dt|\psi\rangle \tag{1.6}$$

$$i\hbar\frac{d}{dt}|\psi\rangle = H|\psi\rangle \tag{1.7}$$

This is known as the Schrödinger's equation and governs unitary time evolution of quantum mechanical system given that it is closed from the environment and is not measured [16]. We will return to these two assumptions and relax them later.

Depending on the Hamiltonian, we can express the time-evolution operator. If the Hamiltonian is independent of time, we can solve the equation above to find:

$$\mathcal{U}(t_0, t_0 + \Delta t) = e^{-iH\Delta t/\hbar} \tag{1.8}$$

which entirely removes the time-dependence from the state such that $|\psi; t\rangle = \mathcal{U}(t)|\psi; t = 0\rangle$. If on the contrary, the Hamiltonian is dependent on time and commutes at different times, we can write it as:

$$\mathcal{U}(t_0, t_0 + \Delta t)|\psi; t_0\rangle = \exp\left(-\frac{i}{\hbar}\int_{t_0}^{t_0+\Delta t} dt H(t)\right)|\psi; t_0\rangle \tag{1.9}$$

If the Hamiltonian at different times do not commute with itself, one could introduce the Dyson series[16]. Another approach is to solve the differential equation numerically.

1.3.1 Numerical Implementations

Schrödinger's Equation gives a simple linear relation between the time derivative of a state and the Hamiltonian. If we can represent the states as vectors and the Hamiltonian as a matrix, we can naively solve the differential equation by doing finite size step. With $dt \to \Delta t$ The state at $t + \Delta t$ will approximately be:

$$\vec{\psi}(t + \Delta t) = \vec{\psi}(t) - \frac{i\Delta t}{\hbar} \boldsymbol{H} \vec{\psi}(t) \tag{1.10}$$

Of course this is a crude approximation which improves as Δt is reduced and the equation is repeated iteratively. While this method, known as Euler integration [18], is simple to implement, it quickly loses precision if the time steps become large (see example in figure 1.2). Instead of improving accuracy by increasing the amount of steps, we instead look at a more sophisticated algorithm.

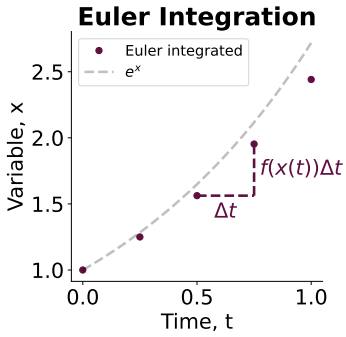

Figure 1.2: A visualized example of Euler integration for the differential equation $x'(t) = x$

In this thesis, integration will primarily be performed using the Qutip Library[19], where the Schrödinger equation is integrated by the Adams method. In this method the last n calculations are used in order to approximate the higher order differentials of the function. If we have a differential equation:

$$y'(t) = f(y(t)) \tag{1.11}$$

We can approximate the point $y(t + \Delta t)$ by a Taylor expanding around t:

$$y(t) + \Delta t y'(t) + \frac{1}{2}\Delta t^2 y''(t) + \frac{1}{3!}\Delta t^3 y'''(t) \dots \tag{1.12}$$

The idea in the Adams algorithm is to approximate the differential up to order n by using finite difference methods. The first and second order derivative can then be approximated by:

$$y'(t) = f(t), \quad y''(t) = \frac{f(y(t)) - f(y(t - \Delta t))}{\Delta t} \tag{1.13}$$

And the third order differential by:

$$y'''(t) = \frac{y''(t) - y''(t - \Delta t)}{\Delta t} = \frac{f(y(t)) - f(2y(t - \Delta t)) + f(y(t - 2\Delta t))}{\Delta t^2} \tag{1.14}$$

and on wards. A visualization of the second order method can be seen in Figure 1.3. The computation of the Adams algorithm is more precise since it considers higher order terms and it runs fast since it reuses the old calculations.

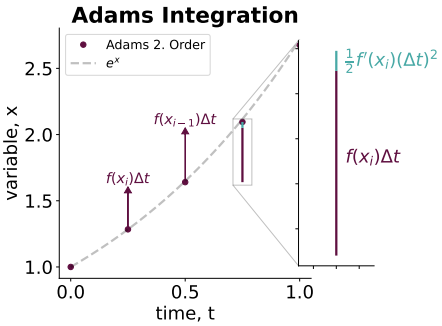

Figure 1.3: A visualization of the second order Adams algorithm. Here the second order derivative is found by the finite difference method to be $f'(x_i) = (f(x_i) - f(x_{i-1}))/\Delta t$

One challenge is that the algorithm requires n points to get started. Until n points are calculated, we can assume no higher order differentials, such that we effectively perform Euler integration for the first step and a second order Adams for the second and so on. Alternatively, we can use another algorithm which moves forward in time to approximate the higher order differentials. An example of such an algorithms is the Runge-Kutta method, which is used in most modern solvers for ordinary differential equations [18].

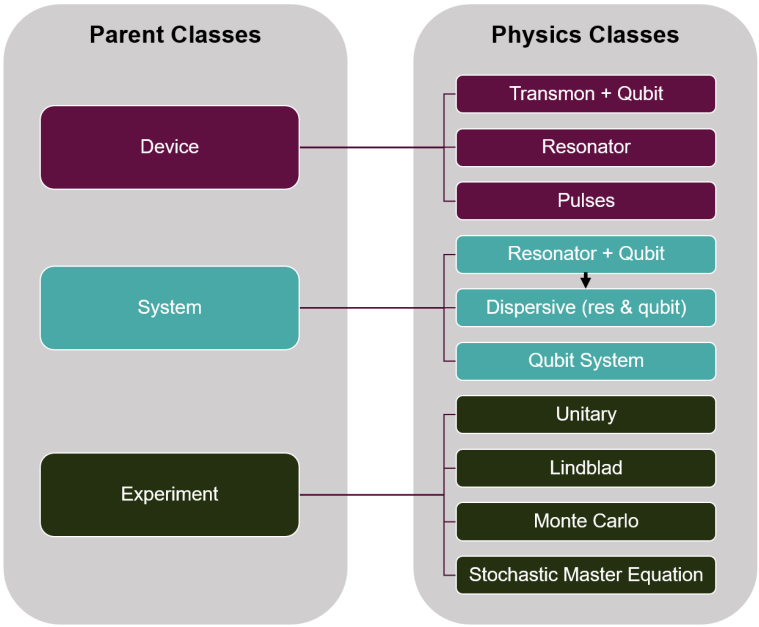

Figure 1.4: Module structure for the code used in the thesis. It is divided into Parent Classes and the Physics classes which inherit attributes from their respective parents.

1.4 Computational Framework of the Thesis

It is by no means a new idea to solve quantum mechanical problems by numerical simulations, so multiple well-optimized and versatile libraries exist. In this thesis, we base most of the calculations on the integration methods present in the Qutip Library [19]. To make faster progress and hopefully contribute to the software in the laboratory, a module to make numerical superconducting qubit experiments was developed during this project. The package is a wrapper around the Qutip Library, but eases the setup of calculating Hamiltonians in superconducting systems, running simulations and managing data. The documentation for the module QuantumDeviceSimulation can be found in Appnedix A.

An overview of the module is shown in Figure 1.4. In general, it is built in three main parts:

- **Devices** are the physical devices placed in the system. This includes different qubits, resonators and pulses.
- **Systems** are combinations of devices along with descriptions of how they interact.
- **Experiments** are organizing the different sweeps of parameters and apply the proper integration technique.

2 Circuit Quantum Electrodynamics

While many platforms can be used as quantum processors, our focus will be on circuits consisting of superconducting materials. In this chapter, we will go through how these qubits are designed to create qubits and how we can model them numerically.

2.1 Circuit QED

Classically, we describe the dynamics of a circuit in terms of its current, $I(t)$, and its voltage drop, $V(t)$. If we consider a simple circuit with one capacitor and one inductor, we have an LC circuit. The energy and subsequent equations of motion are found by summing the energy contributions from each of its elements. The capacitor stores a charge which gives an energy contribution:

$$E_{\text{capacitor}} = \frac{1}{2}CV^2 = \frac{Q^2}{2C} \tag{2.1}$$

where Q is the charge on the capacitor and C is the capacitance related to the distance between two capacitance plates, the area and the permittivity of the material. We can relate the charge in the capacitor to the current by $Q(t) = Q(t_0) + \int_{t_0}^{t} dt' I(t')$. The other component is an inductor which can take many different form, one example is a coil. The inductor stores energy in a magnetic flux through it, giving an associated energy contribution:

$$E_{\text{inductor}} = \frac{\Phi^2}{2L} \tag{2.2}$$

Where Φ is the flux through the inductor and L is the impendance. If the inductor was a coil, the inducatance would be related to the amount of windings, the permability materials, and its length and area. By using Faradays law, one find a relation between the current drop over the inductor and its flux: $\Phi(t) = \Phi(t_0) + \int_{t_0}^{t} V(t')dt'$. The total energy of the LC circuit is now [20]:

$$\mathcal{H} = \frac{1}{2C}Q^2 + \frac{1}{2L}\Phi^2 \tag{2.3}$$

Which is of particular interest since Q is a canonical momentum to the coordinate Φ[1].

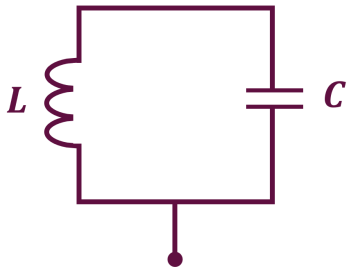

Figure 2.1: Circuit diagram for the LC circuit.

[1] To see this, we can rewrite the capacitor energy in terms of the flux: $\frac{1}{2}C\dot{\Phi}^2$ and define the lagrangian as the difference between kinetic and potential energy: $\mathcal{L} = E_{\text{capacitor}} - E_{\text{inductor}}$. Differentiating the Lagrangian with respect to the time-derivative of flux, we find $\frac{\partial}{\partial\dot{\Phi}}\mathcal{L} = Q$. [5]

2.1.1 Going quantum

Usually, classical circuits exhibit energy loss due to the resistance in the material. However, by utilizing the superconducting phase

at cold temperatures, where electrons pair up as Cooper Pairs to travel through materials with no loss, circuits can achieve no energy dissipation[2]. This allows us to quantize the variables and use the superconducting circuit as a type of artificial atom. [21]

[2] at least not through resistance. Many other outside factors can still interact with the qubit. The limited coherence is still a big obstacle for superconducting qubits.

Since Φ and Q are conjugate variables, they satisfy the classical Poisson bracket equation:

$$\{\Phi, Q\} = \frac{\partial \Phi}{\partial \Phi}\frac{\partial Q}{\partial Q} - \frac{\partial \Phi}{\partial Q}\frac{\partial Q}{\partial \Phi} = 1 \tag{2.4}$$

Quantizing these parameters are done by replacing the variables with the corresponding operators: $Q \to \hat{Q}$ and $\Phi \to \phi$, and applying the correspondence principle. Here we replace the Poisson brackets with the commutator $\{.,.\} \to i\hbar[.,.]$, such that operators satisfy [5]:

$$[\hat{\phi}, \hat{Q}] = i\hbar \tag{2.5}$$

The rest of this thesis will concern quantum mechanics, so we drop the hats from the operators and set $\hbar = 1$. We can reintroduce it later if we need to determine physical quantities. However, we will often refer to energies in terms of the associated frequency $f = \omega/2\pi = E/h$.

2.1.2 Solving the LC Circuit

Since Q and Φ are conjugate variables like position x and momentum p, we can equally choose to represent it in the flux basis or the charge basis. If we picking the flux basis Q takes a differential form:

$$Q = i\frac{\partial}{\partial \Phi} \tag{2.6}$$

The LC circuit Hamiltonian becomes:

$$H|\psi\rangle = -\frac{1}{2C}\frac{\partial^2}{\partial \Phi^2}|\psi\rangle + \frac{1}{2L}\Phi^2|\psi\rangle \tag{2.7}$$

This is exactly the form of a particle in a harmonic potential and we can follow the same procedure and introduce the ladder operators $a, a^\dagger$. Such that the the Hamiltonian can be written as:

$$H = \omega\left(a^\dagger a + \frac{1}{2}\right) \tag{2.8}$$

Where $\omega = \sqrt{8E_C E_L}$ can be found by comparing the Hamiltonian with the one from the harmonic oscillator.

While the harmonic oscillator has many useful properties, a major problem is its equidistant energy levels. When driving transitions with a pulse of frequency ω, we will not only drive transitions in the computational basis $|0\rangle \leftrightarrow |1\rangle$, but also to the higher order states. To find a circuit, we can control without going out of the computational basis, we must search for an anharmonic potential [5].

2.2 Building Qubits

The solution lies in another component, which exists in the realm of superconducting circuits. By separating two superconductors by

a semiconducting material, the Cooper pairs[3] will no longer travel without resistance through the semi conductor but instead tunnel through. The probability of tunneling is dependent on the distance, the semi-conducting material and most importantly the phase difference between the two superconductors. The probability for tunneling through the superconducting phase is given as $\sin(2e\phi(t))$, where $\phi(t)$ is the time-dependent difference in phase between the two superconductors. Using the flux-quantum $\phi_0 = h/2e$ and adding an external flux, the current through the Josephson Junction is:

$$I(t) = I_0 \sin\left(\frac{\phi(t) + \phi_{ext}}{\phi_0}\right) \tag{2.9}$$

The energy of the Josephson Junction can now be found as[15]:

$$E_{\text{Josephson Junction}} = -E_J \cos\left[\frac{\phi(t) + \phi_{ext}}{\phi_0}\right] \tag{2.10}$$

up to a constant, which can be neglected by moving the zero point of the energy. [22]

[3] Superconductivity is often modelled by creating electron pairs which then have spin 1 and behave like bosons. These pairs are called Cooper pairs. [21]

Figure 2.2: An example of a circuit with a capacitor and a Josephson Junction

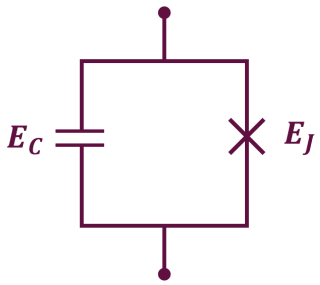

2.2.1 The Cooper Pair Island

Replacing the inductor in the LC circuit with a Josephson Junction, we get a circuit with a non-quadratic potential. The Hamiltonian is given by:

$$H(t) = 4E_C(n - n_g)^2 - E_J \cos\left[\frac{\phi(t) + \phi_{ext}}{\phi_0}\right] \tag{2.11}$$

where $n = Q/2e$ is a amount of cooper pairs on the "island" and $E_C = e^2/2C$[4]. Like flux and charge, the Cooper Pair number n and the superconducting phase difference ϕ form a canonical commutation pair: $[n, \phi] = i$. In the Cooper Pair Box the energy scales of the two contributions are approximately equal $E_C \approx E_J$ [20].

[4] The factor of 4 would disappear if we counted electrons instead of pairs which was historically done

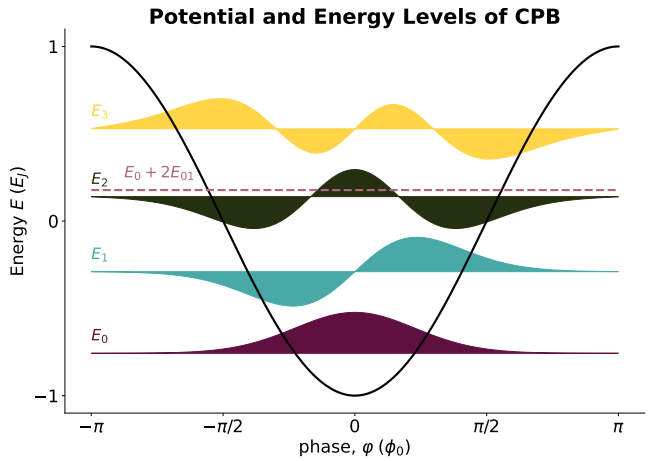

Figure 2.3: The flux-potential of the cooper pair box along with the three lowest energy eigenstates. The eigenstates are shifted according to the their energy and scaled to improve readability. The energy level $E_0 + 2E_{01}$ is shown for comparison. The anharmonicity will be the difference between that line and the E_2

This allows us to think about ϕ as a coordinate where the Josephson Junction energy defines a potential and the charge a kinetic energy. Solving the eigenvaue problem $H\psi(\phi) = E\psi(\phi)$, we can find the

eigenenergies and the eigenvectors of the Cooper Pair Island in ϕ-space. A solution to this problem with $E_C = E_J$ can be seen in Figure 2.3. Most importantly, we note that the that the energy $E_2 - E_1 \neq E_1 - E_0$. This difference is called *anharmonicity* and is defined by $\alpha = (E_2 - E_1) - (E_1 - E_2)$ [15].

2.2.2 The Transmon

With $E_J/E_C \approx 1$ the circuit is susceptible to charge noise, where small variations change the energy significantly. Charge noise is harder to control than flux noise, so the superconducting community has moved toward higher ratios for E_J/E_C. Most commonly the Transmon has a ratio somewhere between 50 and 100. By plotting the energy levels of the cooper pair box and the Transmon as function of n_g, we can see the difference (see Figure 2.4). The insensitivity to charge noise does not come for free but reduces the anharmonicity. With lower anharmonicity, we need longer pulses to make sure, we do not accidental have components of the $E_2 - E_1$ frequency in our pulse, but the wide use of the Transmon indicates that it strikes a good balance [6].

Multiple additions can be made to the Transmon to make its energy tuneable. A possibility is to alter the Josephson Junction with a loop of two. This creates a SQUID, where the flux through the loop can adjust the energy levels of the circuit [20].

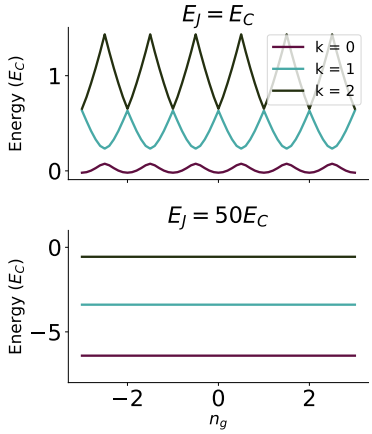

Figure 2.4: The energy levels of the Transmon for different values of n_g. We compare two different settings of E_J/E_C.

2.3 Numerical cQED

To simulate the devices considered in this thesis, we will in this section introduce how the problems at hand can be represented in a suitable way for solving numerically. As mentioned in the previous sections, the Hamiltonian is made out of the two conjugate operators ϕ and n satisfying the commutation relation $[\phi, n] = i$. Like the position and momentum, we now have a choice of which basis to represent the system in. The two basis are related by the Fourier-like transformations[5] [23]:

$$|\phi\rangle = \sum_{n=-\infty}^{\infty} e^{in\phi} |n\rangle \tag{2.12}$$

$$|n\rangle = \frac{1}{2\pi} \int_0^{2\pi} d\phi e^{-in\phi} |\phi\rangle \tag{2.13}$$

Often the problem at hand is easier to formulate in one basis rather than the other. For the transmon, the charge is often localized around 0 since higher $n - n_g$ values give high energies. Since the occupation in the higher levels will be negligible if we control the system properly and keep it at low temperatures, we can set a value for n_{cutoff} to have a finite size of the Hilbert Space. The charge basis is proportional to

[5] This is very similar to the relation between x and p, but with the extra detail that n is discrete and $\phi \in [0, 2\pi]$

n, so we can use that as basis, where n becomes:

$$\hat{n} = \begin{pmatrix} -n_{\text{cutoff}} & 0 & \cdots & \\ 0 & -n_{\text{cutoff}}+1 & & \\ & & \ddots & \\ \vdots & & & n_{\text{cutoff}}-1 \\ & & & & n_{\text{cutoff}} \end{pmatrix} \tag{2.14}$$

To represent the full Hamiltonian we also need $\cos(\phi/\phi_0)$ in the charge basis. Here we will use that:

$$\begin{aligned} e^{\pm i\phi}|n\rangle &= \frac{1}{2\pi}\int_0^{2\pi} d\phi' e^{-in\phi'} e^{\pm i\phi}|\phi'\rangle \\ &= \frac{1}{2\pi}\int_0^{2\pi} d\phi' e^{-i\phi'(n\pm 1)}|\phi'\rangle = |n\mp 1\rangle \end{aligned}$$

Since it is true for all states that the operator $e^{i\phi}$ takes a state $|n\rangle$ to $|n+1\rangle$, we can write it in charge basis as:

$$e^{i\phi} = \sum_n |n\rangle\langle n+1|\,; \quad e^{-i\phi} = \sum_n |n\rangle\langle n-1| \tag{2.15}$$

By writing cosine in terms of the complex exponentials, we now find:

$$\begin{aligned} \cos(\phi/\phi_0+\phi_{ext}) &= \frac{1}{2}\left(e^{-i(\phi/\phi_0+\phi_{ext})} + e^{i(\phi/\phi_0+\phi_{ext}))}\right) \\ &= \frac{1}{2}\left(e^{i\phi_{ext}}e^{i\phi/\phi_0} + e^{-i\phi_{ext}}e^{-i\phi/\phi_0}\right) \\ &= \frac{1}{2}\sum_n\left(e^{i\phi_{ext}}|n\rangle\langle n+1| + e^{-i\phi_{ext}}|n\rangle\langle n+1|\right) \\ &= \frac{1}{2}\begin{pmatrix} 0 & e^{-i\phi_{ext}} & 0 & \cdots \\ e^{i\phi_{ext}} & 0 & e^{-i\phi_{ext}} & \\ 0 & e^{i\phi_{ext}} & 0 & \\ \vdots & & & \ddots \end{pmatrix} \end{aligned} \tag{2.16}$$

With no external flux, $\phi_{ext} = 0$, this reduces to a matrix with $\frac{1}{2}$ on the off-diagonals.

Some systems are more convenient to represent in the flux basis. Again, we would need to find a discrete basis. One could take the $[-\pi, \pi]$ interval and split it in N smaller steps, such that the step size is $\delta = 2\pi/N$. This would give a diagonal representation of ϕ with the elements from $-\pi, -\pi+\delta\ldots$, and we could represent the number basis as a differential between the elements using the finite difference method [24].

With a Hamiltonian represented in a discrete basis, we can calculate the eigenvalues and eigenvectors numerically. We can further reduce the size of the Hilbert space, by representing it in the energy eigenbasis. Here we just include the few lowest energy levels, and can recover the number generator in this basis by $\langle k|\hat{n}|k\rangle$.

3 Computations and Readout

To control and do read out of a superconducting qubit, it is coupled to a control line and a resonator. In this section, we will see how this allows us to control the qubit and measure it by using the resonator as a probe.

3.1 Qubit Control

The state of the qubit is modelled as a two level system and can be visualized as a vector on the Bloch sphere. In this view, any qubit operation can be thought of a rotation of the sphere. While we need two angles to represent a state, we need three to describe an arbitrary rotation.[1]

All possible rotations can be created by three linearly independent generators and the identity. Together they are form a *Universal Gate Set* for a single qubit. Every other rotation can then be made by combining these. A common set of generators spanning a Universal Gate Set is the Pauli matrices $\{\mathbb{1}, \sigma_x, \sigma_y, \sigma_z\}$:

$$\mathbb{1} = \begin{pmatrix} 1 & 0 \\ 0 & 1 \end{pmatrix}, \quad \sigma_x = \begin{pmatrix} 0 & 1 \\ 1 & 0 \end{pmatrix}, \quad \sigma_y = i\begin{pmatrix} 0 & -1 \\ 1 & 0 \end{pmatrix}, \quad \sigma_z = \begin{pmatrix} 1 & 0 \\ 0 & -1 \end{pmatrix}, \tag{3.1}$$

these gates are also considered the generators, since rotations are made by taking the exponential. An example is a $\pi/2$ rotation around the x-axis which is made by:

$$R_X^{\pi/2} = e^{i\frac{\pi}{2}\hat{X}} = \frac{1}{\sqrt{2}}\begin{pmatrix} 1 & -i \\ -i & 1 \end{pmatrix} \tag{3.2}$$

which transforms the $|0\rangle$ to $\frac{1}{\sqrt{2}}(|0\rangle - i\,|1\rangle)$, a state along the y-axis. When Comparing this to the time evolution described in Section 1.3, the gates correspond to the Hamiltonian and by adjusting the gate duration and strength, the angle of the rotation can be adjusted.

If we were to further extend the scope to multi qubit gates, we would also need one fully-entangling two qubit gate to have complete the Universal Gate Set for two qubits. This could be the Control-Not or a Control-phase gate, but in this thesis, we will only deal with one qubit [5].

[1] Since a rotation consist of an axis and the angle of rotation. The vector is represented by two angles θ, ϕ and the rotation amount is determined by a third angle, ψ.

3.1.1 Capacitive Coupling

By running a voltage line to the qubit and coupling it capacitively, we add a term proportional to the charge in the qubit. We have $g_V nV(t)$ to the Hamiltonian, where g_V is the coupling strength and is determined by capacitance of the device and the capacitor coupling them.

In the energy eigenbasis of the LC-circuit, the charge can be written in terms of the ladder operators $n \propto -i(a - a^\dagger)$ which couples the different energy levels. While this is not exactly the case for the Transmon, it is a good approximation[2], and restricting ourselves to the computational basis, we can write $n \propto i(\sigma_+ - \sigma_-)$ for the qubit as well. Here $\sigma_+ = |1\rangle\langle 0|$ and $\sigma_- = |0\rangle\langle 1|$ [5]. The applied voltage gives a contributions to the Hamiltonian of the form:

$$H_{QD} = -\Omega(t) i (\sigma_+ - \sigma_-) = \Omega(t)\sigma_y \tag{3.3}$$

Where the factor of g_V and the constants from the operators are collected in $\Omega(t)$.

[2] And a perfect one, if we just consider two energy levels. For higher level terms, we calculate the n operator in the energy basis and use that operator instead of this approximation.

3.1.2 The Qubit in the Interaction Picture

A truncated qubit capacitively coupled to a control line has a Hamiltonian:

$$H = \frac{1}{2}\omega_q \sigma_z + \Omega(t)\sigma_y \tag{3.4}$$

where the $\omega_q = \omega_{01} = E_1 - E_0$ (where we still omit the factor of $\hbar$). To go into the interaction picture, we consider $H_0 = \frac{1}{2}\omega_q\sigma_z$ and $H_d = \Omega V(t)\sigma_y$, such that the full Hamiltonian is $H = H_0 + H_d$. We now go into a rotating frame using:

$$|\psi\rangle \to |\tilde{\psi}\rangle = \mathcal{U}(t)|\psi\rangle, \quad \text{with} \quad \mathcal{U}(t) = e^{iH_0 t} \tag{3.5}$$

In this basis, the Schrödinger equation becomes:

$$i\partial_t |\tilde{\psi}(t)\rangle = i\partial_t(\mathcal{U}(t)|\psi(t)\rangle) = i\dot{\mathcal{U}}(t)|\psi(t)\rangle + i\mathcal{U}(t)|\dot{\psi}(t)\rangle$$

And using the Schrödinger equation in the original basis: $\partial_t|\psi(t)\rangle = iH|\psi\rangle$ and the transformed state $|\psi(t)\rangle = \mathcal{U}^\dagger(t)|\tilde{\psi}(t)\rangle$, we get:

$$i\partial_t|\tilde{\psi}(t)\rangle = \left[(i\dot{\mathcal{U}}(t)\mathcal{U}^\dagger(t) + \mathcal{U}(t)H\mathcal{U}^\dagger(t)\right]|\tilde{\psi}(t)\rangle \tag{3.6}$$

Such that the effective Hamiltonian in the rotating frame is given as:

$$H_{eff} = i\dot{\mathcal{U}}(t)\mathcal{U}^\dagger(t)) + \mathcal{U}(t)H\mathcal{U}^\dagger(t) \tag{3.7}$$

By splitting the Hamilton in the two terms $H = H_0 + H_d$, we arrive at:

$$H_{eff} = -H_0 + H_0 + \mathcal{U}(t)H_d\mathcal{U}^\dagger(t) \tag{3.8}$$

where we have used that the transformation is unitary $\mathcal{U}^\dagger\mathcal{U} = \mathbb{1}$ and that it commutes with H_0, $[\mathcal{U}, H_0] = 0$. Substituting H_D and $\mathcal{U}(t)$ we get [5]:

$$H_{eff} = \Omega V(t) i \exp\left(it\frac{\omega_q \sigma_z}{2}\right)(|1\rangle\langle 0| - |0\rangle\langle 1|)\exp\left(-it\frac{\omega_q \sigma_z}{2}\right) \tag{3.9}$$

$$= \Omega V(t) i \left(e^{-it\omega_q}|0\rangle\langle 1| - e^{+it\omega_q}|1\rangle\langle 0|\right) \tag{3.10}$$

$$= \Omega V(t) i \left(\left(\cos(\omega_q t) - i\sin(\omega_q t)\right)|0\rangle\langle 1| - \left(\cos(\omega_q t) + i\sin(\omega_q t)\right)|1\rangle\langle 0|\right) \tag{3.11}$$

$$= \Omega V(t)\left(\cos(\omega_q t)\sigma_y - \sin(\omega_q t)\sigma_x\right) \tag{3.12}$$

Here we see that in the rotating frame, the coupling from the control line adds terms proportional to both σ_x and σ_y to the Hamiltonian. [5].

3.1.3 X, Y and virtual Z

To arrive at the gates, we consider the qubit in its rotating frame. Now we apply a pulse through the control line which consists of an oscillating term and an envelope:

$$V(t) = s(t)(\sin(\omega_d t + \phi)) \tag{3.13}$$

where $s(t)$ is the envelope of our pulse with driving frequency ω_d and phase shift ϕ. By defining $I = \cos(\phi), Q = \sin(\phi)$, the pulse can be written as:

$$V(t) = s(t)\left(I\cos(\omega_d t) + Q\sin(\omega_d t)\right) \tag{3.14}$$

Such that the effective driving Hamiltonian becomes:

$$H_{eff} = \Omega s(t)\left(I\cos(\omega_d t) + Q\sin(\omega_d t)\right)\left(\cos(\omega_q t)\sigma_y - \sin(\omega_q t)\sigma_x\right) \tag{3.15}$$

It is now time to perform the infamous rotating wave approximation (RWA). The basic idea is to decompose our Hamiltonian into fast and slow oscillating term $H = H_{slow}(t) + H_{fast}(t)$. The fast part of the Hamiltonian will oscillate quickly and will cancel in the time evolution operator[3] .

[3] This works as the time-evolution operator is given by $U = \exp(i\int dt H)$ so fast oscillating term will cancel if the time interval is sufficiently large.

Rewriting the Hamiltonian with the product to sum trigonometric identities and applying the RWA, we get:

$$H_{eff} = \Omega s(t)\left(\left(I\cos(\omega_d t) + Q\sin(\omega_d t)\right)\cdot\cos(\omega_q t)\sigma_y - \left(I\cos(\omega_d t) + Q\sin(\omega_d t)\right)\cdot\sin(\omega_q t)\sigma_x\right) \tag{3.16}$$

$$H_{eff} \approx \Omega s(t)\left(\left(-I\cos(\delta t) + Q\sin(\delta t)\right)\sigma_y + \left(I\cos(\delta t) - Q\sin(\delta t)\right)\sigma_x\right) \tag{3.17}$$

where $\delta = \omega_q - \omega_d$. The RWA was applied in the the second line to eliminate fast oscillating terms of frequency $\omega_q + \omega_d \gg \omega_q - \omega_d$. In our driving hardware, we can control the driving frequency, the phase ϕ and by extension I and Q. If we want to perform an x-gate, we can set $I = 1, Q = 0$ and drive the qubit at the qubit frequency $\delta = 0$. The y-gate is done in the same way with a $\pi/2$ rotation, such that $I = 0, Q = 1$.

To complete our 1-qubit universal gate set, we now just need the σ_z gate. Since σ_y and σ_x pulses are defined in a rotating frame, we can just virtually rotate the phases to make a "virtual" z-gate. Thus a z-gate is not made by applying a gate, but by simply moving our reference frame, and corresponds to us rotating I and Q into each other. [5]

3.2 Coupling to a Resonator

In order to do readout of the qubit, without altering its state, we couple it to a resonator which will be used as a probe (see Figure 3.1). The resonator is an LC-circuit, so it has a harmonic potential. By coupling the Qubit to an LC-circuit, the physics of the qubit closely resembles that of an atom in a cavity.

In our model, the resonator has an energy given by [4] :

$$H_r = \omega_r \, a^\dagger a \tag{3.18}$$

[4] where we move the energy scale to absorb the zero point energy

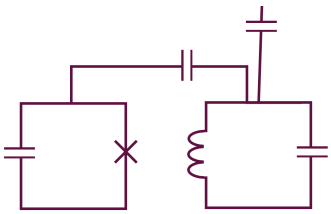

Figure 3.1: A schematic of a Transmon coupled capacitatively to a resonator, which again is coupled to a feed line.

The resonator can now be coupled to the qubit by connecting it capacitively. This gives another interactive contribution: $C_g V_r V_t$. By using $V_{r/t} = 2en_{t/r}/C_{t/r}$ the additional term can be written as $4e^2 C_g n_t n_r / C_r C_t$ or by collected the constants in a coupling strength g:

$$H_{int} = g n_c n_r \tag{3.19}$$

By using that $n_c \propto a + a^\dagger$ and $n_t \propto \sigma_+ + \sigma_-$ we obtain the Jaymes Cunning interaction:

$$H_{int} = g(a + a^\dagger)(\sigma_- + \sigma_+) \tag{3.20}$$

Where the factors of n_c, n_t, C and the other constants are all absorbed into the coupling strength g [5].

3.2.1 Rotating Wave Approximation

To optimize the computation time, it is beneficial to get rid of fast oscillating terms. First we choose to go into the interaction picture, where we cancel the time evolution of the non-interacting Hamiltonian.

$$H_0 = \omega_r \, a^\dagger a + \omega_q \frac{\sigma_z}{2} \tag{3.21}$$

where the associated time evolution operator will be:

$$\mathcal{U}(t) = e^{iH_0 t} \tag{3.22}$$

In the interaction picture, we will now have: $|\psi\rangle \to \mathcal{U} |\psi\rangle$ to counteract the fast oscillations from the H_0 term. The Hamiltonian will transform as: $H \to U(t) H \, U^\dagger(t)$. This yields the effective interaction Hamiltonian given by:

$$H_{int}(t) = H_0 + g \left(e^{it(-\omega_r - \omega_q)} a\sigma_- + e^{it(\omega_r - \omega_q)} a^\dagger \sigma_- \right.$$
$$\left. e^{it(-\omega_r + \omega_q)} a\sigma_+ + e^{it(\omega_r + \omega_q)} a^\dagger \sigma_+ \right)$$

We now perform the rotating wave approximation, where we drop fast oscillating terms:

$$H_{int}(t) \approx H_0 + g \left(e^{it\Delta} a^\dagger \sigma_- + e^{-it\Delta} a\sigma_+ \right) \tag{3.23}$$

Here $\Delta = \omega_r - \omega_q$ is the detuning between the resonator and the qubit. Transforming back to the Schödinger picture, we have [20]:

$$H_S = H_0 + g \left(a^\dagger \sigma_- + a\sigma_+ \right) \tag{3.24}$$

3.2.2 Dispersive Regime

In most resonator-qubit systems, the coupling are designed to have a dispersive interaction, that is:

$$\lambda = \frac{g}{\Delta} \ll 1 \tag{3.25}$$

Here the system can be approximated to simple and interpretable form. We can obtain a form of the Hamiltonian which is diagonal to first order in λ by using the *Schrieffer Wolff transformation*. For a Hamiltonian of type $H = H_0 + \lambda V$, the idea is to apply a transformation $\boldsymbol{D} = e^{\lambda S}$ to get[5]:

$$\begin{aligned} H' = \boldsymbol{D}^\dagger H \boldsymbol{D} &= e^{-\lambda S}(H_0 + \lambda V)e^{\lambda S} \\ &= H_0 + \lambda V + [\lambda S, H_0 + \lambda V] + \frac{1}{2!}[S,[S,H]] + \dots \end{aligned}$$

[5] Here we use, that the exponential of an operator is given by its power series: $e^{\lambda S} = \sum_n (\lambda S)^n/n!$ and $e^{-\lambda S} = \sum_n (-1)^n (\lambda S)^n/n!$

By using $\lambda \ll 1$, we want to approximate the system by neglecting terms of second order or higher in λ. We diagonalize the Hamiltonian to first order if we choose S such that $V + [S, H_0] = 0$. We here use the ansatz:

$$S = (a\sigma_+ - a^\dagger \sigma_-) \tag{3.26}$$

Such that:[6]

$$\begin{aligned} [H_0, S] &= \left[\omega_r a^\dagger a + \omega_q \sigma_z/2, a\sigma_+ - a^\dagger\sigma_-\right] \\ &= -\omega_r \left(a^\dagger\sigma_- + a\sigma_+\right) - \frac{1}{2}\omega_q \left(2a^\dagger\sigma_- + 2a\sigma_+\right) \\ &= -(\omega_r + \omega_q)\left(a^\dagger\sigma_- + a\sigma_+\right) = -\Delta\left(a^\dagger\sigma_- + a\sigma_+\right) \\ &= -\frac{g}{\lambda}\left(a^\dagger\sigma_- + a\sigma_+\right) = -V \end{aligned}$$

[6] Where we can use the commutator relation $[AB, C] = A[B, C] + [A, B]C$ to find $\left[a^\dagger a, a^\dagger\right] = a^\dagger$ and $\left[a^\dagger a, a\right] = -a$. While $[\sigma_z, \sigma_+] = -2\sigma_+$ and $[\sigma_z, \sigma_-] = 2\sigma_-$.

This exactly leads to:

$$V + [S, H_0] = 0$$

While we get a new contribution to the Hamiltonian by:

$$\begin{aligned} [S, V] &= \lambda g\left[a^\dagger\sigma_- - a\sigma_+, a^\dagger\sigma_- + a\sigma_+\right] \\ &= \lambda g\left(a^\dagger a\sigma_-\sigma_+ - aa^\dagger\sigma_+\sigma_-\right) \\ &= 2\lambda g\left(a^\dagger a\sigma_z + \frac{1}{2}\lambda g\sigma_+\sigma_-\right) \\ &= \lambda^2 g^2 \left|1\right\rangle\left\langle 1\right| + 2\chi a^\dagger a\sigma_z \end{aligned}$$

Here we have defined $\chi = g^2/\Delta$ as the dispersive shift, which here is a measure of how much the resonator frequency moves depending on the state of the qubit. The $\lambda^2 g^2 \left|1\right\rangle\left\langle 1\right|$ is a contribution to the first excited state of the qubit and will normally just be absorbed into a new qubit frequency slightly shifted by resonator. The dispersive Hamiltonian now reads:

$$H = \left(\tilde{\omega}_r a^\dagger a + \chi\sigma_z a^\dagger a\right) + \frac{1}{2}\tilde{\omega}_{01}\sigma_z \tag{3.27}$$

Where the qubit and resonator frequency are altered to include the shift they impose on each other [25]. To see the effect, one could

simulate driving the resonator at different frequencies and plot the expected photon number $\langle n \rangle$ at the end of the simulation and repeat for different qubit states. A result of such a simulation can be seen in Figure 3.2. In this case, the width of the curves are dependent on the drive time, often one will however see them Lorentzian shaped, with a width determined by the lifetime of the photons in the resonator.

If we were to consider multiple levels of the qubit, the calculation require a bit more work. This has been done in Appendix B and leads to a general form of the Hamiltonian for a multi level qubit:

$$H' = \left(\omega_r + \sum_k \chi_k |k\rangle \langle k|\right) a^\dagger a + \sum_k (\omega_k + \delta_k) |k\rangle \langle k| \tag{3.28}$$

Where the quantities are derived from a coupling matrix with elements $g_{ij} = g \langle i|n|j\rangle$ and the qubit energies as:

$$\chi_{ij} = |g_{ij}|^2 \left(\frac{1}{\omega_{ij} - \omega_r} + \frac{1}{\omega_{ij} + \omega_r}\right) \tag{3.29}$$

$$\delta_{ij} = \frac{|g_{ij}|^2}{\omega_{ij} - \omega_r} \tag{3.30}$$

$$\chi_i = \sum_j \chi_{ij} \tag{3.31}$$

$$\delta_i = \sum_j \delta_{ij} \tag{3.32}$$

In this form, both the resonator frequency at the ground and first excited state of the qubit is shifted by an amount. This alters the effective dispersive shift between these two [5]:

$$\chi \approx \chi_{01} + \chi_{12}/2 = -g_{01}^2/\Delta \left(\frac{1}{1 + \Delta/\alpha}\right) \tag{3.33}$$

The effect can be seen in Figure 3.3 where the second excited state moves the frequency of the first much closer. This repeats when adding a third, fourth or higher excited state.

When deriving the equations the dispersive model, we neglect terms of order λ^2 or above. If we were to keep this term, it would have been multiplied with a $a^\dagger a$. If the mean photon number would have more than order $1/\lambda^2$, it is no longer valid to throw the terms out. To be sure the dispersive model is a good approximation, one should therefore stay under a critical photon number, where $n_{\text{crit}} = \Delta^2/4g^2$ [5]. When calibrating our qubit in chapter 7, we will find a critical photon number of $n_{\text{crit}} \approx 81$, and since we will be driving the resonator to around $\langle n \rangle \approx 21 \approx n_{\text{crit}}/4$, this is well below the critical number. The dispersive approximation should therefore still provide a good model [25].

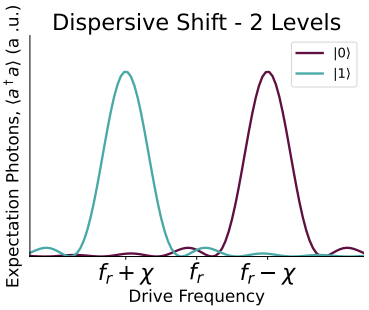

Figure 3.2: Simulated driving of a qubit-resonator system using the dispersive approximation.

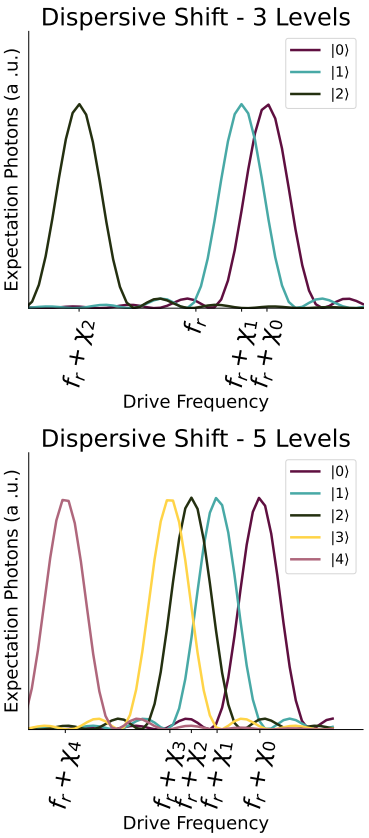

Figure 3.3: Same simulating driving as Figure 3.2, but with a 3 and 5 level qubit respectively.

3.2.3 Readout Drive in the Dispersive Approximation

When we perform a readout, we drive a capactively coupled line on the resonator like what we did with the qubit in Section 3.1. Choosing

a driving pulse with a rectangular envelope and phase 0, we have a contribution to the Hamiltonian of the form:

$$H_{\text{drive}} = \epsilon \cos(\omega_d t)(a + a^\dagger) = \frac{\epsilon}{2}\left(e^{i\omega_d t} + e^{-i\omega_d t}\right)(a + a^\dagger) \tag{3.34}$$

where ϵ is the amplitude of the drive and ω_d is the drive frequency. As with the last few times we encountered fast rotations, we now enter the rotating frame to cancel the rapidly oscillating terms. We choose the time dependent transformation:

$$\mathcal{U}(t) = \exp\left(-it\sum_k(\omega_k + \delta_k)\left|k\right\rangle\left\langle k\right|\right) \otimes \exp\left(-it\omega_d\, a^\dagger a\right) \tag{3.35}$$

To find effective Hamiltoninan:

$$H_{eff} = i\dot{\mathcal{U}}(t)\mathcal{U}^\dagger(t)) + \mathcal{U}(t)H\mathcal{U}^\dagger(t) \tag{3.36}$$

We find the contribution from the "centrifugal" term as:

$$i\dot{\mathcal{U}}(t)\mathcal{U}^\dagger(t)) = -it\sum_k(\omega_k + \delta_k)\left|k\right\rangle\left\langle k\right| - it\omega_d\, a^\dagger a \tag{3.37}$$

The drive hamiltonian transforms as:

$$\begin{aligned} H_{drive} &\to \mathcal{U}(t)H\mathcal{U}^\dagger t \\ &= \frac{1}{2}\epsilon(e^{i\omega_d t} + e^{-i\omega_d t})\left[\,\mathcal{U}(t)(a + a^\dagger)\mathcal{U}^\dagger(t)\right] \\ &= \frac{1}{2}\epsilon(e^{i\omega_d t} + e^{-i\omega_d t})\left[\,ae^{i\omega_d t} + a^\dagger e^{-i\omega_d t}\right] \end{aligned}$$

Neglecting the fast rotating terms ($\propto e^{\pm 2i\omega_d t}$), we get the effective drive Hamiltonian:

$$H_{d,eff} = \epsilon(a + a^\dagger) \tag{3.38}$$

Such that the total effictive Hamiltonian now becomes:

$$H_{eff} = \left(\omega_r - \omega_d + \sum_k \chi_k \left|k\right\rangle\left\langle k\right|\right) a^\dagger a + \epsilon(a + a^\dagger) \tag{3.39}$$

Which gives a nice time-independent Hamiltonian for an m-level qubit resonator system which will prove ideal for simulation purposes. One could have driven with a sine instead of a cosine and the form would have been $i\epsilon(a^\dagger - a)$.

3.3 I-Q Phase Space

In the last section, we showed how the resonator experiences a state dependent shift of its frequency depending on the qubit. A valid way of doing readout is to drive the resonator at the frequency associated with $|1\rangle$. If we experience photon absorption by the resonator, we label the state "1". Often it is however beneficial to drive the resonators in between the two frequencies [26]. In this section, we will built up the tools for visualizing the two dimensional information in an IQ-plane which will allow us to understand why this is the case.

For a quantum harmonic oscillator, we represent the state by introducing the raising and lowering operator from the position and momentum: $a \propto x + ip$ and $a^\dagger \propto x - ip$. We can of course always measure x or p by representing them as $x \propto a + a^\dagger$ and $p \propto i(a^\dagger - a)$. Because of Heisenberg's uncertainty principle, we can however not know both of them at once. This is summed up in the relation between their uncertainties: $\sigma_x \sigma_p \geq 1/2$. The same ideas can also be used to think about the state of the resonator. Here we define the *quadrature operators* which also obey Heisenberg's uncertainty principle. They are defined as[27]:

$$Q = a + a^\dagger \qquad I = i(a^\dagger - a) \tag{3.40}$$

3.3.1 Coherent States

In a Harmonic Oscillator, the number states have expectation values $\langle x \rangle = \langle p \rangle = 0$. To get non-zero values of these expectation values, one is required to have superposition states with adjacent components. An example is $c_n |n\rangle + c_{n+1} |n+1\rangle$, which would satisfy $\langle x \rangle \propto \langle a + a^\dagger \rangle \neq 0$. The more natural states would be the eigenstates to the lowering operator:

$$a |\alpha\rangle = \alpha |\alpha\rangle \tag{3.41}$$

Where we can expand $|\alpha\rangle$ into the Fock basis. This gives us:

$$a \sum_n C_n |n\rangle = \sum_{n=1} C_n \sqrt{n} |n-1\rangle = \alpha \sum_{n=0} C_n |n\rangle \tag{3.42}$$

Here we can extract a relation between their coefficients:

$$\sqrt{n} C_n = \alpha C_{n-1} \tag{3.43}$$

If we know C_0, we can now determine the rest of the series by:

$$C_N = \frac{\alpha^n}{\sqrt{n!}} C_0 \tag{3.44}$$

Ultimately, we can find an expression for the state $|\alpha\rangle$ in terms of the raising operator.

$$|\alpha\rangle = C_0 \sum_n \frac{\alpha^n}{\sqrt{n!}} (a^\dagger)^n |0\rangle \tag{3.45}$$

and C_0 is found from the normalization to be $C_0 = e^{-|\alpha|^2/2}$. To represent the coherent state in the Fock space, we now have:

$$|\alpha\rangle = e^{-|\alpha|^2/2} \sum_n \frac{\alpha^n}{\sqrt{n!}} |n\rangle \tag{3.46}$$

Where each complex α corresponds to a coherent state. If $\alpha = 0$, we have the vacuum state which is the same as the vacuum Fock state $|\alpha = 0\rangle = |n = 0\rangle$ [27].

3.3.2 Phase Space Representations

With the coherent states we have a set of states that span a two-dimensional plane. We can use these to formulate a two dimensional

pseudo-probability density function for values sets of the quadrature components (I, Q). Such a distribution should take the Heisenberg uncertainty principle into account, such that the vacuum state for example should be a two dimensional Gaussian with standard deviation $\frac{1}{2}$. Another desired property of this distribution should be the ability to express expectation values, $\langle O \rangle = \langle \psi | O | \psi \rangle$ in phase space. If we were to represent an operator in a coherent basis, it would take the form:

$$O = \int d\alpha^2 O(\alpha, \alpha^*) \, |\alpha\rangle \, \langle \alpha| \tag{3.47}$$

The expectation value $\langle O \rangle$ will now take the form:

$$\begin{aligned} \langle O \rangle &= \langle \psi | O | \psi \rangle \\ &= \sum_n \langle \psi | \int d\alpha^2 O(\alpha, \alpha^*) \, |\alpha\rangle \, \langle \alpha | \psi \rangle \\ &= \int d\alpha^2 O(\alpha, \alpha^*) | \, \langle \psi | \alpha \rangle \, |^2 \end{aligned}$$

Here $| \langle \psi | \alpha \rangle |$ takes the role of a probability distribution in the coherent phase space. To further ensure that the function is properly normalized, we must have the sum of all probabilities to equal 1. This is enforced by demanding that the expectation value of the identity is equal to 1. But since the set of coherent states are overcomplete (the fact that the integral is two dimensional, should be a hint), the identity has an extra factor of $1/\pi$ [27].

$$1 = \langle \mathbb{1} \rangle = \int d\alpha^2 \frac{1}{\pi} | \, \langle \psi | \alpha \rangle \, |^2$$

This gives us a pseudo-probability function given by:

$$Q(\alpha) = \frac{1}{\pi} | \, \langle \psi | \alpha \rangle \, |^2 \tag{3.48}$$

This even works, when we have non-pure states represented by a density matrix (as we will soon introduce in Section 4.1). Here it is called the Husimi Q-function and is given by:

$$Q(\alpha) = \frac{1}{\pi} \langle \alpha | \rho | \alpha \rangle \tag{3.49}$$

The Q-function is a powerful tool, which allows us to visualize states in the phase space. Some common states like the vacuum state, a Fock state and a coherent state can be seen in Figure 3.4.

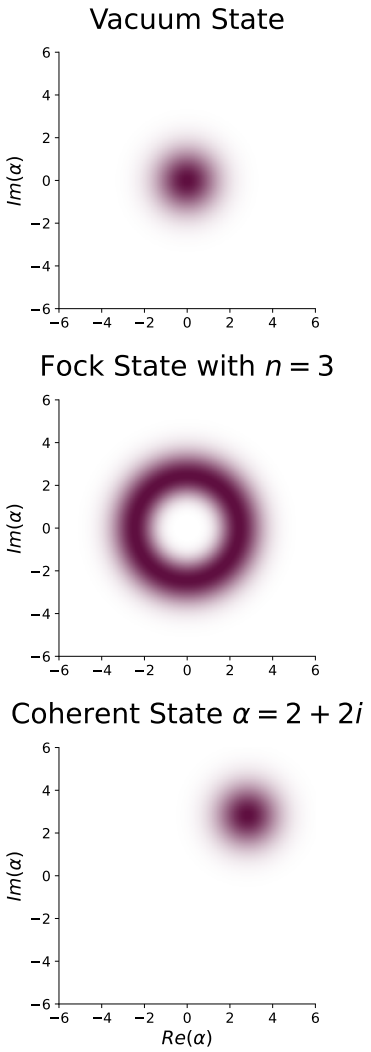

Figure 3.4: Example of Different Q-functions for vacuum state, Fock state ($n = 3$) and a coherent state with $\alpha = 2 + 2i$.

3.3.3 The Driven Resonator in the IQ Plane

With the new formulation of Q-functions, we can visualize the readout drive as a separation in the IQ plane. Let us explore what happens, when we drive the resonator while considering the qubit to be a two level system subject to the Hamiltonian:

$$H_{eff} = (\omega_r - \omega_d + \chi \sigma_z) \, a^\dagger a + \epsilon (a + a^\dagger) \tag{3.50}$$

We can find the equation of motion of the operator a in the Heisenberg picture [16]:

$$\dot{a}(t) = i \Big[H_{eff}, a \Big] = -i \Big[(\omega_r - \omega_d + \chi \sigma_z) \, a^\dagger a + \epsilon (a + a^\dagger), a \Big] \tag{3.51}$$

And using the commutation relations, we find:

$$\dot{a}(t) = -i\left(\left(\omega_r - \omega_d + \chi\sigma_z\right)a(t) - \epsilon\right) \tag{3.52}$$

We now consider the resonator to be in a coherent state $|\alpha\rangle$ (initially we consider $\alpha(t=0)=0$) and the qubit is in $|k\rangle$ with $k=0,1$. By looking at the expectation value of the operator, which will be the same in the Heisenberg and Schrödinger pictures, we get:

$$\begin{aligned}\frac{d}{dt}\langle\alpha,k|\,a\,|\alpha,k\rangle &= \langle\alpha,k| - i\left(\omega_r - \omega_d \pm \chi\right)a(t) + i\epsilon\,|\alpha,k\rangle \\ \frac{d}{dt}\alpha(t) &= -i\left(\omega_r - \omega_d \pm \chi\right)\alpha(t) + i\epsilon\end{aligned} \tag{3.53}$$

Which is a differential equation for the complex number describing the coherent state α. Integrating this equation numerically for the vacuum state coupled to a qubit in either the ground or excited state, we get the results displayed in Figure 3.5. Notice how the phase separation of the two coherent states are better a distinguishing them than their respective distance to Origo.

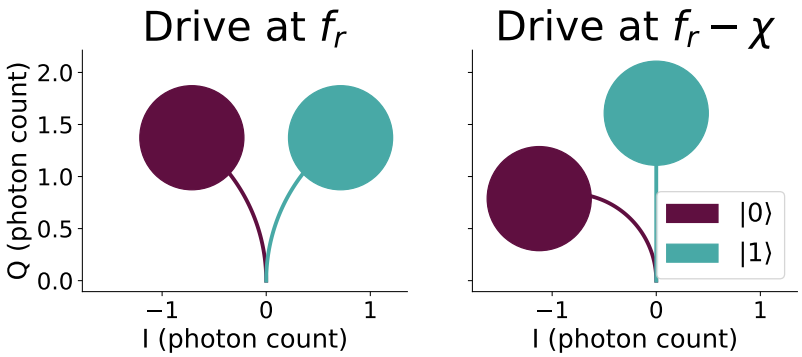

Figure 3.5: Driven resonator in the dispersive model where the qubit state is either 1 or 0. We use the device parameters for the constants in Equation 4.53 which we will calibrate in Chapter 7. The path of I, Q coordinates are displayed along with the standard deviation of a half, which we have for coherent states in the IQ plane.

4 Dynamics of Open Quantum Systems

Up until now, we have considered the qubit and resonator as an isolated system. When not interacting with the environment, the system follows unitary time evolution described by the Schrödinger equation. Ideally, the system would be isolated, but unfortunately, the reality is that our devices interact with the environment. To properly determine its dynamics, we have to consider open quantum systems.

4.1 Density Matrix Formalism

First, we need to reformulate our representation of a quantum state. Up to now, a state has been represented by at state vector $|\psi\rangle$, where the state can be a superposition of states in some basis: $|\psi\rangle = \sum_i c_i |i\rangle$, where c_i is the complex coefficient and the state is normalized such that $\sum |c_i|^2 = 1$. While this is a great formalism when you have knowledge about the entire system, it is not great at handling interactions with an unknown environment. In the density matrix formalism, we represent a single state of a quantum system, not as a vector, but by a matrix. We will here follow the introduction in [28].

To describe an open system, we introduce the formalism of *density matrices*. In this formalism, a classical ket state would be rewritten as:

$$\rho_{\text{pure}} = |\psi\rangle \langle\psi| = \sum_i p_i |i\rangle \langle i| \tag{4.1}$$

where $p_i = |c_i|^2$ is the probability of finding the state $|i\rangle$ on measurement. A ket state is also called a pure state, since there exists some basis, where $p_x = 1$ and $p_i = 0$ for $i \neq x$. Since the trace is independent of basis, a pure state is characterized by the condition:

$$\text{Tr}\left(\rho_{\text{pure}}^2\right) = 1 \tag{4.2}$$

In general, we can however expand the formalism to include more states than pure states. For a density matrix in general, the conditions are that the probabilities must sum to 1 and they should be positive:

$$\text{Tr}(\rho) = 1 \tag{4.3}$$

$$p_i \geq 0 \tag{4.4}$$

Within these conditions we can also formulate non-pure states. An example of such can occur if we have two coupled two level systems and an unknown observer measures one of the systems. Before the measurement, we have an entangled state[1]:

[1] The $\otimes$ references to the product state of two Hilbert spaces: $\mathcal{H}^2 \otimes \mathcal{H}^2$. Sometimes the $\otimes$ will be omitted and the state $|11\rangle$ will represent $|1\rangle \otimes |1\rangle$.

$$|\phi_+\rangle = \frac{1}{\sqrt{2}}(|0\rangle \otimes |0\rangle + |1\rangle \otimes |1\rangle) \tag{4.5}$$

which in density matrix formalism with respect to the basis $|00\rangle$, $|01\rangle$, $|10\rangle$, $|11\rangle$ will be described by:

$$\rho_{\phi+} = \begin{pmatrix} \frac{1}{2} & 0 & 0 & \frac{1}{2} \\ 0 & 0 & 0 & 0 \\ 0 & 0 & 0 & 0 \\ \frac{1}{2} & 0 & 0 & \frac{1}{2} \end{pmatrix} \tag{4.6}$$

Here the entanglement between the states give us off-diagonal elements. These are called coherences since they refer to the entanglement for the two states. If the unknown observer were to measure the state of the second two level system, but not share the outcome, we would have 50 percent chance of getting $|00\rangle$ and 50 for $|11\rangle$, but the systems would no longer be in a superposition. This fact is described by the density matrix:

$$\rho = \begin{pmatrix} \frac{1}{2} & 0 & 0 & 0 \\ 0 & 0 & 0 & 0 \\ 0 & 0 & 0 & 0 \\ 0 & 0 & 0 & \frac{1}{2} \end{pmatrix} \tag{4.7}$$

where the coherences are 0. Without the coherence elements, this is not an entangled superposition, but rather mean that half of an ensemble of this state would in $|00\rangle$ and the other half in $|11\rangle$. This is known as a mixed state, and has $\mathrm{Tr}(\rho^2) < 1$. [2] In general, we write the full density matrix as:

$$\rho = \sum_{ij} \rho_{ij} |i\rangle \langle j| \tag{4.8}$$

[2] This fact can not be represented in the bra-ket notation that we are used to, and here lies the true power of the density matrix formalism: we quantify entanglement versus a fraction of populations.

4.1.1 Expectation Values

The expectation value, $\langle\psi\rangle = \langle\psi|A|\psi\rangle$, is in the density matrix formalism calculated by:

$$\langle A\rangle = \mathrm{Tr}\,(A\rho) \tag{4.9}$$

From this expression, we can recover the expectation value for pure state by:

$$\langle A\rangle = \mathrm{Tr}\,(\rho A) = \mathrm{Tr}\left(\sum_{ij} \rho_{ij} |i\rangle \langle j| A\right) \tag{4.10}$$

$$= \sum_k \langle k| \left(\sum_{ij} \rho_{ij} |i\rangle \langle j| A\right) |k\rangle \tag{4.11}$$

$$= \sum_i |c_i|^2 \langle i|A|i\rangle \tag{4.12}$$

where the sum is over a basis $\{\psi_i\}$.

4.1.2 Interactions with the Environment

The properties of the of the density matrix allows us describe interaction with the environment. Start with considering the combined Hilbert space of two systems:

$$\mathcal{H} = \mathcal{H}_1 \otimes \mathcal{H}_2 \tag{4.13}$$

A measurement in the second system will now have affect the state of both systems. By measuring system 2 it collapses to $|i\rangle\langle i|$ with probability $p_i = \rho_{2,ii}$. If we however, have no knowledge of the second system, we would have to average over all the outcomes. This procedure is done by doing a *partial trace* of the second system. If we define the whole density matrix as $\rho_{\text{total}} = \sum_{ijkl} \rho_{ijkl} |i\rangle\langle j| \otimes |k\rangle\langle l|$ [3], tracing out system 2 would be written:

$$\begin{aligned} \text{Tr}_2(\rho_{\text{total}}) &= \text{Tr}_2\left(\sum_{ijkl} \rho_{ijkl} |i\rangle\langle j| \otimes |k\rangle\langle l|\right) \\ &= \sum_{ij}\sum_{kl} \rho_{ijkl} |i\rangle\langle j| \otimes \sum_{m} \langle m|k\rangle\langle l|m\rangle \\ &= \sum_{ijm} \rho_{ijmm} |i\rangle\langle j| \end{aligned} \tag{4.14}$$

[3] Often we will represent the four-index density matrix as a two dimensional by concatenating the dimensions. In this representation the four indices can be understood as indexes for block matrices. The i,k indexes block matrices and j,l takes the element from the given block matrix.

If we again consider the state $|\rho_+\rangle$ from Equation 4.5 but only have control of the first two level system, then our effective density matrix, would be found as:[4]

$$\rho_{1,eff} = \text{Tr}_2\left(\frac{1}{2}\left(|00\rangle\langle 00| + |00\rangle\langle 11| + |11\rangle\langle 00| + |11\rangle\langle 11|\right)\right) \tag{4.15}$$

$$= \frac{1}{2}\left(|0\rangle\langle 0| + |1\rangle\langle 1|\right) \tag{4.16}$$

[4] effectively we keep all the terms of the first part of the Hilbert space where the second part is the same

Which is exactly the totally mixed density matrix, we had in the previous subsection [28].

4.1.3 Quantum Maps

Allowing for loss of entanglement in a quantum process, we can relax the unitary requirement which came from conserving the inner product of our state vector. Instead we require the mapping of a density matrix to take it into another density matrix:

$$\Lambda(\rho) \to \rho' \tag{4.17}$$

For it to be physical, we need it to fulfill the following two requirements. First, it should be a complete positive (CP) map, such that $\rho_{ii} \geq 0$ for all i. This requirement ensures that a map can not map a density matrix to something with negative probabilities. A CP map can be shown to have a representation of the type [29]:

$$\Lambda(\rho) = \sum_{\alpha} K_\alpha \rho K_\alpha^\dagger \tag{4.18}$$

where K_α is an operator acting on states in the Hilbert space of interest[5]. This representation is called the Kraus representation and

[5] Which does not have to be Hermitian, Unitary or invertible.

K_α are called the Kraus operators. A further requirement is that mappings should preserve the trace of density matrices, $\mathrm{Tr}(\rho) = \mathrm{Tr}(\rho') = 1$. This condition is called to be Trace Preserving (TP). This is fulfilled if[6]:

$$\sum_\alpha K_\alpha^\dagger K_\alpha = \mathbb{1} \tag{4.19}$$

To summarize, a physical quantum map is a complete positive and trace preserving (CPTP) mapping of a density matrix into another [29].

[6] This is seen when writing $1 = \mathrm{Tr}(\rho') = \mathrm{Tr}\left(\sum_\alpha K_\alpha \rho K_\alpha^\dagger\right) = \sum_\alpha \mathrm{Tr}\left(K_\alpha \rho K_\alpha^\dagger\right) = \sum_\alpha \mathrm{Tr}\left(K_\alpha^\dagger K_\alpha \rho\right) = \mathrm{Tr}\left(\sum_\alpha K_\alpha^\dagger K_\alpha \rho\right)$ which is true if $\sum_\alpha K_\alpha^\dagger K_\alpha = \mathbb{1}$.

4.2 Time Evolution of Density Matrices

As mentioned in Section 1.3, the time-evolution of a quantum state follows the Schrödinger equation: $i\partial_t |\psi(t)\rangle = H |\psi(t)\rangle$. This equation can[7] be solved with the time evolution operator $\mathcal{U}(t) = \exp(-iHt)$ to get $|\psi(t)\rangle = \mathcal{U}(t) |\psi(0)\rangle$. Applying this to the density matrices to find the time-dependence gives us:

[7] for a time independent Hamiltonian

$$\begin{aligned}\rho(t) &= \sum_{ij} \rho_{ij} |\psi_i(t)\rangle \langle\psi_j(t)| = \sum_{ij} \rho_{ij} \mathcal{U}(t) |\psi_i(0)\rangle \langle\psi_j(0)| \mathcal{U}^\dagger(t) \\ &= \mathcal{U}(t)\rho(0)\mathcal{U}^\dagger(t)\end{aligned} \tag{4.20}$$

And the derivative:

$$\begin{aligned}\partial_t \rho(t) &= (\partial_t \mathcal{U}(t))\rho(0)\mathcal{U}^\dagger(t) + \mathcal{U}(t)\rho(0)(\partial_t \mathcal{U}^\dagger) \\ &= -iH\rho(t) + i\rho(t)H \\ &= -i[H, \rho(t)]\end{aligned} \tag{4.21}$$

is the differential equation for unitary evolution of a density matrix and is equivalent to Schödinger's equation. We can however extend this to include interactions [28].

4.2.1 Random Unitary Transformation

Before going into the general derivation, we will consider an example where we have an interaction with the environment that alters the dynamics of our system. In this example, the environment can be modelled as randomly adding a white noise term to the Hamilton in form of some hermitian operator θG where θ is a normally distributed variable with variance $\lambda\Delta t$ and mean 0. This leads to a unitary transformation of $e^{-i\theta G}$ over a small time step . When taking the limit to an infinitesimal time step, $\Delta t \to dt$, the probability density function of θ is given by:

$$P(\theta)d\theta = \frac{d\theta}{\sqrt{4\pi\lambda dt}} \exp\left(-\frac{\theta^2}{4\lambda dt}\right) \tag{4.22}$$

Since the contribution is random, we average over all the possibilities. To first order in dt, this leads to the following mapping:

$$\begin{aligned}\rho(t+dt) &= \int_{\infty}^{\infty} d\theta P(\theta) e^{-iG\theta}\rho(t)e^{iG\theta} \\ &= \int_{\infty}^{\infty} d\theta P(\theta)(1 - iG\theta - \frac{1}{2}G^2\theta^2\dots)\rho(t)(1 + iG\theta - \frac{1}{2}G^2\theta^2\dots) \\ &= \int_{\infty}^{\infty} d\theta P(\theta)\left(\rho_t - \frac{1}{2}\theta^2(G^2\rho(t) + \rho(t)G^2 - 2G\rho(t)G\right) + \mathcal{O}(dt^{3/2}) \\ d\rho(t) &= -\frac{\lambda dt}{2}\left(G^2\rho(t) + \rho(t)G^2 - 2G\rho(t)G\right) \end{aligned} \tag{4.23}$$

where we in the third line used, that $\theta P(\theta)$ is odd and its integral 0 while the integral of $\int d\theta P(\theta)\theta^2 = \lambda dt$. Equation 4.23 is our first encounter with a time evolution of a Lindblad form. In Section 4.3 we will look at qubit-environment interactions taking exactly this form, but first we will do a more formal derivation of the Lindblad Master Equation [30].

4.2.2 Lindblad Master Equation

In the above examples, we have shown how unitary or a random unitary transformation looks in density matrix formalism. The Lindblad Master Equation generalizes both of these examples. We will here assume that the Lindblad equation follows a CPTP map, and by doing a Markovian assumption, a proper choice of Kraus operators will lead us to the form. The derivation here follows the methods described by Preskill in [31].

To model this system, we assume that the interact weakly with an environment, such that the information in and out of the system happens at a much slower rate than the environment resets itself. The dynamics of our system is then said Markovian and only depend on the current state of the system and some general parameters of the environment. By using the markovian assumption, the time evolution of a state in an infinitesimal time-interval dt is given by a CPTP map:

$$\rho(t+dt) = \Lambda[\rho(t)] \tag{4.24}$$

For a small time step dt, we can consider the map to be linear in dt.

$$\Lambda(\rho) = \rho + dt\mathcal{L}[\rho] \tag{4.25}$$

Where the Lindbladian $\mathcal{L}[\rho]$ is the *super-operator*[8] of interest since it gives us the differential equation:

$$d\rho(t) = \mathcal{L}[\rho(t)]dt \tag{4.26}$$

[8] A super operator refers to a linear operator acting on a density matrix. It can be some combination of applying operators from both left and right.

To find a representation of $\mathcal{L}$, we can write out the Λ in the Kraus representation:

$$\rho(t+dt) = \Lambda[\rho(t)] = \rho(t) + dt\mathcal{L}[\rho(t)] = \sum_{\alpha} M_\alpha \rho(t) M_\alpha^\dagger \tag{4.27}$$

where the Kraus operators in general can be time-dependent. To find the set of operators that fulfill Equation 4.27 the mapping should be linear in dt and reduce to identity for $dt = 0$. Any mapping linear

in dt can be described by setting $M_0 = \mathbb{1} + O(dt)$ and $M_\alpha = O(\sqrt{dt})$. We now define the mapping as:

$$M_0 = \mathbb{1} + (-iH + K)dt \tag{4.28}$$

$$M_\alpha = \sqrt{dt}L_\alpha \quad \alpha \geq 0 \tag{4.29}$$

Where we will assume H, K to be hermitian[9] and H, K, L_α are all independent of dt. Further introducing the trace preserving condition for the map and keeping terms to first order in dt, we find:

[9] Here we lose generality. We could have kept them general through the whole derivation, but only the hermitian part would stay to the end

$$\mathbb{1} = \sum_\alpha M_\alpha M_\alpha^\dagger = (\mathbb{1} + (-iH + K)dt)(\mathbb{1} + (iH + K)dt) + dt \sum_{\alpha \geq 1} L_\alpha L_\alpha^\dagger \tag{4.30}$$

$$= \mathbb{1} + dt\left(2K + \sum_{\alpha \geq 1} L_\alpha L_\alpha^\dagger\right) + \mathcal{O}(dt^2) \tag{4.31}$$

Which only holds for:

$$K = -\frac{1}{2}\sum_a L_a L_a^\dagger \tag{4.32}$$

where a is reindexing of α by $a = \alpha - 1$. Introducing this back in Equation 4.27:

$$\rho(t) + dt\mathcal{L} = (\mathbb{1} + (-iH + K)dt)\,\rho(t)\,(\mathbb{1} + (iH + K)dt) + dt \sum_{\alpha \geq 1} L_\alpha \rho(t) L_\alpha^\dagger \tag{4.33}$$

$$= \rho(t) + dt\,(-iH\rho(t) + i\rho(t)H) + dt\left(\sum_a L_a \rho(t) L_a^\dagger + K\rho(t) + \rho(t)K\right) + \mathcal{O}(dt^2) \tag{4.34}$$

$$= \rho(t) - idt[H, \rho(t)] + dt\sum_a \left(L_a \rho(t) L_a^\dagger - \frac{1}{2}L_a L_a^\dagger \rho(t) - \frac{1}{2}\rho(t) L_a L_a^\dagger\right) + \mathcal{O}(dt^2) \tag{4.35}$$

We now arrive at the final form of the Lindblad Master Equation:

$$\dot{\rho}(t) = \mathcal{L}[\rho] = -idt[H, \rho(t)] + dt\sum_a \mathcal{D}[L_a]\rho(t) \tag{4.36}$$

where the dissipator, $\mathcal{D}$ is a superoperator defined by:

$$\mathcal{D}[L_a]\rho(t) = L_a \rho(t) L_a^\dagger - \frac{1}{2}L_a L_a^\dagger \rho(t) - \frac{1}{2}\rho(t) L_a L_a^\dagger \tag{4.37}$$

While we assumed that H and K were hermitian this was not necessary. If we were to have them general and decompose them into a hermitian and anti-hermitian part $H = \frac{1}{2}(H + H^\dagger) + \frac{1}{2}(H - H^\dagger)$, the anti hermitian part would cancel out and not be relevant for the dynamics.

With this CPTP map the operators are conveniently named to illustrate the physics. H is of course the Hamiltonian and the equation reduces to the unitary evolution if we set all $L_\alpha = 0$. The L_α are called Lindblad operators and can be interpreted as decoherence of or dissipation from the system. If we were to set $L_0 = \sqrt{\lambda}G$ and L_α for $\alpha \neq 0$, we recover the random unitary transformation which we saw in Section4.2.1 [31].

4.2.3 Numerical Lindblad Master Equation

To solve the Lindblad equation numerically, we need it in a form solveable by the methods covered in Section 1.3.1. To numerical integrate the equation, the Qutip library reformulates the equations to the super operator formalism [19]. The general idea is to represent a density matrix as a vector by concatenating the axis. By representing the density matrices as (very long) vectors, the super operators can be represented as matrices[10]. With this formulation, we again achieve a linear differential equation with a matrix multiplied by vectors which is convenient to implement. Since we also need to keep track of the coherences of the density matrix, the size of the vectors are now n^2 and matrices $n^2 \times n^2$. In conclusion, the Lindblad Master Equation can be solved just like the Schrödinger equation, but we will now have a much larger space to keep track off.

[10] This is much deeper topic one could use to look at the properties of quantum maps. In this thesis, we just use it to make suitable numerical contribution, so the small introduction will have to suffice.

4.2.4 Monte Carlo Approximation

While the Lindblad Equation is a very strong mathematical tool for describing quantum mechanics, numerically simulating it scales heavily with the size of our Hilbert space. To reduce the complexity from $n^2 \times n^2$ back to $n \times n$, we can make use of a Monte Carlo approach to simulating the Lindblad equations. In the Lindblad equations, the Lindbladian terms can be split into an operator and a scalar determining the rate which it is applied $\sqrt{\gamma}L$, where γ is the rate. Instead of simulating the full dynamics, we can instead simulate using the Schrödinger equation and in each time step apply the Lindblad operator with a probability determined by the rate and the size of the time step, $\gamma\Delta t$. Repeating this multiple times, we can estimate the expectation value or the density matrix at a given time by taking averages over the outcomes[11][19].

[11] While this is the general idea, the implementation is more sophisticated, since it draws the time to next application of the operator from the proper distribution. Then the Schrödinger's equation can be integrated up until that point.

4.3 Dissipation and Decoherence in Qubits

We will now take a look, at how coupling to the environment affects the qubit and resonator. While a lot of interesting physics is associated with the interaction with the environment, we will with the Lindblad equation at hand only look at the qubit-resonator system as an open system and consider the environment unchangeable. With this, we will focus in particular on a few parameters describing the interaction: the temperature τ, characteristic time of qubit decay T_1 characteristic time of qubit dephasing T_2 and lastly the rate of photon decay from the resonator κ.

4.3.1 Density Matrix of a Qubit

First, it will be beneficial to expand the representation of a qubit to its density matrix. If we take an arbitrary two level state as described in Section 1.2.2, we find an example of a pure state density matrix by just

taking its product with itself: $|\psi\rangle = \cos(\theta/2)\,|0\rangle + e^{i\phi}\sin(\theta/2)\,|1\rangle$

$$\begin{aligned}\rho_{\text{qubit}} = |\psi\rangle\langle\psi| &= \begin{pmatrix} \cos^2(\theta/2) & e^{-i\phi}\cos(\theta/2)\sin(\theta/2) \\ e^{i\phi}\cos(\theta/2)\sin(\theta/2) & \sin^2(\theta/2) \end{pmatrix} \\ &= \frac{1}{2} + \begin{pmatrix} \cos(\theta) & e^{-i\phi}\sin(\theta) \\ e^{i\phi}\sin(\theta) & -\cos(\theta) \end{pmatrix} \\ &= \frac{1}{2}(\mathbb{1} + \vec{a}\cdot\vec{\sigma}) \end{aligned} \tag{4.38}$$

Where $\vec{\sigma} = [\sigma_x, \sigma_y, \sigma_z]$ and $\vec{a} = [\sin\theta\cos\phi, \sin\theta\sin\phi, \cos\theta]$ is the coefficients[5]. The resemblance to Cartesian coordinates allow us to think about $\vec{a}$ as vector pointing to the state.

The representation in Equation 4.38 provides even more flexibility. When we have a pure state, $|\vec{a}| = 1$, and the vector points to the unit sphere. However $\rho = \frac{1}{2}\,\mathbb{1}$ is also a valid density matrix, namely the fully mixed matrix. Here $|\vec{a}| = 0$. In terms of the Bloch sphere, we can think of pure states as living on the surface while mixed states will have an associated vector pointing somewhere inside $|\vec{a}| < 1 \Leftrightarrow \text{Tr}(\rho^2) < 1$.

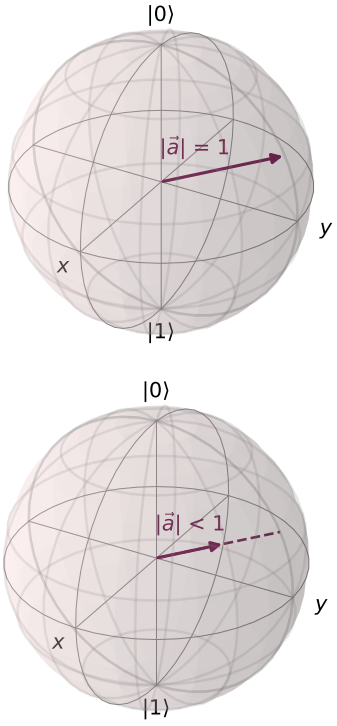

Figure 4.1: Pure state (top) and mixed state (bottom) visualized on the Bloch Sphere.

4.3.2 The Temperature of the System

Even at low temperatures, one should expect to see the temperature have an effect on the qubit. If we consider the qubit connected to the environment as bath, we know from statistical physics that the probability of finding the qubit in different energy states is determined by Boltzmann statistics [17]. Limiting ourselves to a two level system, we would find the qubit in $|0\rangle$ with $\text{prob}(|0\rangle) = 1/(1 + e^{-\beta\omega_{01}})$ and $\text{prob}(|1\rangle) = e^{-\beta\omega_{01}}/(1 + e^{-\beta\omega_{01}})$. While the idea is to initialize the qubit in $|0\rangle$, this fact means that waiting until equilibrium our qubit would be in:

$$\rho_{\text{equilibrium}} = \frac{1}{1 + e^{-\beta\omega_{01}}}\begin{pmatrix} 1 & 0 \\ 0 & e^{-\beta\omega_{01}} \end{pmatrix} \tag{4.39}$$

4.3.3 Longitudinal Relaxation

If the qubit exchanges energy with the environment it could drive transitions between the states $|1\rangle \leftrightarrow |0\rangle$. The relaxation from $|0\rangle \to |1\rangle$ at a rate $\Gamma_\downarrow$ will in the Lindblad equation be described by the Lindblad operator $L_\downarrow = \sqrt{\Gamma_\downarrow}\,|0\rangle\langle 1|$ and correspondingly $L_\uparrow = \sqrt{\Gamma_\uparrow}\,|1\rangle\langle 0|$ will describe the excitement. A qubit which relaxes energy into the environment will have time dynamics which follows[12]:

$$\begin{aligned}\dot{\rho}(t) &= \mathcal{D}[L_\downarrow]\rho(t)) \\ \dot{\rho}(t) &= \Gamma_\downarrow\left(|0\rangle\langle 1|\,\rho(t)\,|1\rangle\langle 0| - \frac{1}{2}\{|1\rangle\langle 0|0\rangle\langle 1|, \rho(t)\}\right) \\ \dot{\rho}(t) &= \Gamma_\downarrow\left(\rho_{11}\,|0\rangle\langle 0| - \rho_{11}\,|1\rangle\langle 1| - \frac{1}{2}\left(\rho_{01}\,|1\rangle\langle 0| + \rho_{10}\,|0\rangle\langle 1|\right)\right)\end{aligned}$$

[12] We use here the anti-commutator $\{A, B\} = AB + BA$ to write the Lindbladian a bit more compactly

By looking at the individual components of the density matrix, we find:

$$\dot{\rho}_{00}(t) = \Gamma_\downarrow \rho_{11}(t) \qquad \dot{\rho}_{10}(t) = -\frac{1}{2}\Gamma_\downarrow \rho_{10}(t)$$
$$\dot{\rho}_{01}(t) = \frac{1}{2}\Gamma_\downarrow \rho_{01}(t) \qquad \dot{\rho}_{11}(t) = -\Gamma_\downarrow \rho_{11}(t)$$

When adding the contribution from $\mathcal{D}[L_\uparrow]\rho(t)$ and introducing $\Gamma_1 = \Gamma_\downarrow + \Gamma_\uparrow$, we find the diagonal elements to:

$$\dot{\rho}_{00}(t) = \Gamma_\downarrow \rho_{11}(t) - \Gamma_\uparrow \rho_{00}(t), \quad \dot{\rho}_{11}(t) = \Gamma_\uparrow \rho_{00}(t) - \Gamma_\downarrow \rho_{11}(t) \tag{4.40}$$

and the off-diagonal to:

$$\dot{\rho}_{01}(t) = -\frac{1}{2}\Gamma_1 \rho_{01}(t), \quad \dot{\rho}_{10}(t) = -\frac{1}{2}\Gamma_1 \rho_{10}(t) \tag{4.41}$$

The diagonal elements make up a set of coupled differential equation, solving for these two[13] and using $\mathrm{Tr}(\rho) = \rho_{00} + \rho_{11} = 1$ gives:

$$\rho_{00}(t) = \frac{\Gamma_\downarrow}{\Gamma_\uparrow + \Gamma_\downarrow} + \left(\rho_{00}(t=0) - \frac{\Gamma_\downarrow}{\Gamma_\uparrow + \Gamma_\downarrow}\right) e^{-t(\Gamma_\uparrow + \Gamma_\downarrow)} \tag{4.42}$$

and

$$\rho_{11}(t) = \frac{\Gamma_\uparrow}{\Gamma_\uparrow + \Gamma_\downarrow} + \left(\rho_{11}(t=0) - \frac{\Gamma_\uparrow}{\Gamma_\uparrow + \Gamma_\downarrow}\right) e^{-t(\Gamma_\uparrow + \Gamma_\downarrow)} \tag{4.43}$$

while the off-diagonals are simply solved by exponential decay:

$$\rho_{01}(t) = e^{-\Gamma_1 t/2}\rho_{01}(t=0), \quad \rho_{10}(t) = e^{-\Gamma_1 t/2}\rho_{10}(t=0) \tag{4.44}$$

From this we see the effects of energy exchange: excitations and relaxations affect the occupation of $|0\rangle$ and $|1\rangle$ until they are in an equilibrium. Further, the energy exchange also leads to decoherence on the diagonal with a rate of $\Gamma_1/2$. The dynamics are visualized in Figure 4.2.

We can also compare the equilibrium position $t \to \infty$ with the equilibrium state described by the Boltzmann statistics in Equation 4.39. Here we find that the rates should satisfy:

$$\frac{\Gamma_\downarrow}{\Gamma_\uparrow + \Gamma_\downarrow} = \frac{1}{1 + e^{-\beta\omega_{01}}} \Rightarrow \frac{\Gamma_\uparrow}{\Gamma_\downarrow} = e^{-\beta\omega_{01}} \tag{4.45}$$

For low temperatures $\beta\omega_{01} \ll 1$, this means that $\Gamma_1 \approx \Gamma_\downarrow$. The characteristic time of the decay from an arbitrary density matrix to the equilibrium is described by the characteristic time $T_1 = \frac{1}{\Gamma_1}$.

[13] This is done by writing the differential equation in matrix representation, by diagonalizing the coefficient we find a basis were the differential equation are decoupled. Solving here and transforming back gives the solution.

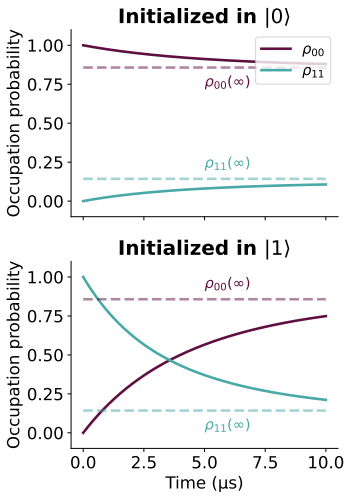

Figure 4.2: Evolution of the diagonal density elements if the qubit is initialized in $|0\rangle$ or $|1\rangle$ respectively.

4.3.4 Dephasing

If the environment couples to σ_z it can alter the eigenenergy. This will lead to dephasing since the rotating frame of the qubit will be different from the one we expect. We can split this interaction in two parts:

A slow part that compared to the experiment we run, such that we can consider it a constant shift of the qubit frequency $\omega \to \omega + \delta_\omega$. We

can look at the consequences of this by simply evolving the equations unitarily.

A faster part which changes multiple times during the experiment. If we consider this a normal distributed contribution to σ_z at each small timestep (as white noise), we can model this like the random unitary example, we considered in Section 4.2.1 in which we would have the operator $L_\phi = \sqrt{\Gamma_\phi}\sigma_z$. If we apply this Lindblad operator, the time evolution would look like:

$$\dot{\rho}(t) = \mathcal{D}[L_\phi]\rho(t)) = \Gamma_\phi \left(\sigma_z \rho(t) \sigma_z - \frac{1}{2}(\sigma_z^2 \rho(t) + \rho(t)\sigma_z^2) \right) \tag{4.46}$$

Since $\sigma_z^2 = \mathbb{1}$ and $\sigma_z \rho(t) \sigma_z$ flips the sign of the off-diagonals, we get:

$$\dot{\rho}(t) = -\Gamma_\phi \left(|0\rangle \langle 1| \rho_{01} - |1\rangle \langle 0| \rho_{10} \right) \tag{4.47}$$

This gives us an extra contribution to the coherence terms, which are simply solved by:

$$\rho_{01}(t) = e^{-\Gamma_\phi t} \rho_{01}(t=0), \quad \rho_{10}(t) = e^{-\Gamma_\phi t} \rho_{10}(t=0) \tag{4.48}$$

So if were to combine the decays from this section and the last, the total dephasing rate would come out to be:

$$\Gamma_2 = \Gamma_\phi + \frac{1}{2}\Gamma_1 \tag{4.49}$$

This is often described by the characteristic time of dephasing:

$$T_2 = \frac{1}{\Gamma_2} = \frac{1}{\Gamma_\phi + \frac{1}{2}\Gamma_1} \tag{4.50}$$

4.3.5 Resonator Decays

The coupled resonator also leaks photon to the environment. This happens with a much higher rate since it is coupled to the feed line. The output of photon also consist of two parts, unwanted dissipation to the environment and leakage to the feed line which we are able to detect. For photon loss the Lindbladian operator is given by $L = \sqrt{\kappa} a$, where kappa is the rate of dissipation.

In Section 3.3.3, we found a differential equation for the pointer state of a coherent state, when we drive the resonator. If we also consider the Lindbladian term, we get a further addition to the time dependence of a in the Heisenberg picture . The time dependent $a(t)$ takes the form of $\frac{d}{dt}a(t) = i[H_{eff}, a(t)] + \mathcal{D}[\sqrt{\kappa}a](a)$[14]. Here $\mathcal{D}[\sqrt{\kappa}a](a)$ is given by:

$$\mathcal{D}[\sqrt{\kappa}a](a) = \kappa \left(a^\dagger a a - \frac{1}{2}\left(a^\dagger a a + a a^\dagger a \right) \right) \tag{4.51}$$

Using the commutator relation $\left[a, a^\dagger\right] = 1$, this can be reduced to

$$\mathcal{D}[\sqrt{\kappa}a](a) = -\frac{1}{2}\kappa a \tag{4.52}$$

[14] While we only discussed the equations of motion the Heisenberg picture above, operators take almost exactly the same form. However, it comes with a changed sign of the commutator. One could check this by writing out the expectation values.

If we reintroduce this into the equations of motion, we find an additional term in the differential equation for the pointer states:

$$\frac{d}{dt}\alpha(t) = -i\left(\omega_r - \omega_d \pm \chi\right)\alpha(t) + i\epsilon - \frac{\kappa}{2}\alpha(t) \tag{4.53}$$

This dissipative term takes the effect of pushing the coherent state towards the origin. If we were to repeat the driving of the resonator with the dissipation, we see that driving off resonance gives a spiral instead of circle towards some steady state. These steady state values can also be found by solving for the steady state equation with $\dot{\alpha}(t) = 0$. We find:

$$\alpha_{ss} = \frac{-\epsilon}{(\omega_r - \omega_d \pm \chi) - i\kappa/2} \tag{4.54}$$

From which we can extract the steady state amplitude from Equation 4.55:

$$|\alpha_{ss}| = \frac{\epsilon}{\sqrt{(\omega_r - \omega_d \pm \chi)^2 + \kappa^2/4}} \tag{4.55}$$

An example of driving the resonator with dissipation can be seen in Figure 4.3.

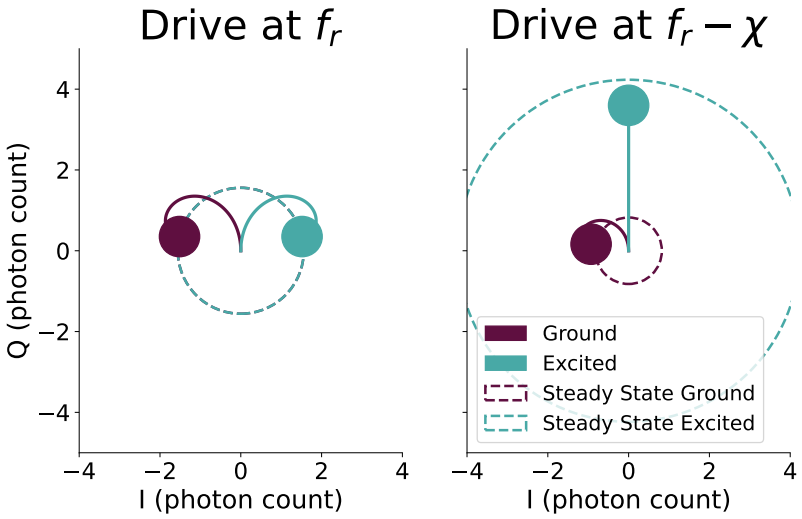

Figure 4.3: Driving of the resonator with the qubit in ground and excited state. The trajectories of the pointer states are shown together with the steady state amplitude.

5 Measurements

In the previous section, we described the effects of a system coupled to its environment. In most cases the interactions of our system is unwanted, but in one case it is necessary: readout. Without interacting with the system, there is no way to gather information about it. Often measurements are portrayed as instantaneous and projective, but the reality is more complicated.

In this chapter, we will introduce the idea of a generalized measurement using a Positive Operator-Value Measure. This will allow us to modify the master equation to include terms representing backaction and measurements. Most of this chapter is based on the excellent introduction to continuous quantum measurements by Jacobs and Steck [32].

5.1 Generalized Measurement

When one first encounter quantum mechanics, a measurement is an instantaneous and complete projection of a state onto the measured quantity. Measuring an observable given by the hermitian operator in its eigenbasis, $\mathcal{O} = \sum_n O_n |n\rangle \langle n|$ (with $|n\rangle$ the eigenstates of O) would result in a projection of a state $|\psi\rangle$ onto the state $|n\rangle$ with probability $|\langle n|\psi\rangle|^2$. In our measurement record, we would find the corresponding value O_n. [1] This is indeed a possible measurement, but this *von Neumann* measurement is just a small set of possibilities which can not explain what happens if we only extract partial information from the system. We will here describe a more general description of measurements.

[1] In the formalism of density matrices the probability is $\langle n|\rho|n\rangle$ and the projected state would be $|n\rangle \langle n|$.

5.1.1 Positive Operator-Valued Measure (POVM)

If we were to start with a state ρ and perform a von Neumann measurement with the projection operator $P_n = |n\rangle \langle n|$, we will get:

$$\rho_f = |n\rangle \langle n| = \frac{P_n \rho P_n}{\mathrm{Tr}(P_n \rho P_n)}, \text{with probability: } \mathrm{Tr}(P_n \rho P_n) = \rho_{nn} \quad (5.1)$$

In describing this projection, we often consider the output n with probability ρ_{nn} but not always recognize that it equally gives us a different value $\neq n$ with probability $1 - \rho_{nn}$. In this case the state will be proportional to $\rho_f \propto \rho - \rho_{nn} |n\rangle \langle n|$. If we were to also represent this with an operator $P_{\text{not n}} = \mathbb{1} - P_n$, we could think of the measure-

ment as applying a set of the operators $\{P_n, P_{\text{not n}}\}$ and applying the operator depending on the outcome.

By expanding this set from two to more operators, we can generalize measurements. The generalization comes as a set of operators $\{\Omega_m\}$ that satisfy:

$$\sum_m \Omega_m^\dagger \Omega_m = \mathbb{1} \tag{5.2}$$

Applying an operator from this set alter the state according to (generalizing Equation 5.1):

$$\rho_f = \frac{\Omega_m \rho \Omega_m^\dagger}{\text{Tr}(\Omega_m \rho \Omega_m^\dagger)}, \text{with probability: } \text{Tr}\left(\Omega_m \rho \Omega_m^\dagger\right) \tag{5.3}$$

Here we are allowed to combine multiple measurements into single questions. An example could be: what is the probability of measuring the operator in an interval $m \in [a, b]$? This will be sum of probabilities:

$$P(m \in [a, b]) = \sum_{m=a}^{b} \text{Tr}\left(\Omega_m \rho \Omega_m^\dagger\right) \tag{5.4}$$

Or rearranging by using linearity and cyclic properties of the trace:

$$P(m \in [a, b]) = \text{Tr}\left(\sum_{m=a}^{b} \Omega_m^\dagger \Omega_m \rho\right) = \text{Tr}(M\rho) \tag{5.5}$$

where the operator $M = \sum_{m=a}^{b} \Omega_m^\dagger \Omega_m$ is the Positive Operator Value Measure (POVM). In this formalism, we can define an M on any subset of $\{\Omega_m\}$ [32].

5.1.2 Continuous set of Gaussian POVMs

We can further extend this from a finite set of operators, to operators measuring a continuous variable. If we imagine a continuous variable, x, that we can measure with a Gaussian precision, then we can formulate the set of POVMS by creating a set of Gaussian measures $\{\Omega_\alpha\}$ with width σ and mean α. The operators take the form:

$$\Omega(\alpha) = \frac{1}{\mathcal{N}} \int_{-\infty}^{\infty} dx \exp\left(-\frac{(x-\alpha)^2}{2\sigma^2}\right) |x\rangle \langle x| \tag{5.6}$$

Where $\mathcal{N}$ is a constant such that the set satisfies Equation 5.2. We can find the normalization by:

$$\begin{aligned}
\mathbb{1} &= \frac{1}{\mathcal{N}^2} \int d\alpha \int dx \exp\left(-\frac{(x-\alpha)^2}{2\sigma^2}\right) |x\rangle \langle x| \int dx' \exp\left(-\frac{(x'-\alpha)^2}{2\sigma^2}\right) |x'\rangle \langle x'| \\
&= \frac{1}{\mathcal{N}^2} \int d\alpha \int dx \exp\left(-\frac{(x-\alpha)^2}{\sigma^2}\right) |x\rangle \langle x| \\
&= \frac{\sqrt{\pi}\sigma}{\mathcal{N}^2} \int dx \, |x\rangle \langle x| = \frac{\sqrt{\pi}\sigma}{\mathcal{N}} \mathbb{1}
\end{aligned}$$

which is true with $\mathcal{N} = (\sigma^2 \pi)^{\frac{1}{4}}$. The set of operators now take the form:

$$\Omega(\alpha) = \frac{1}{(\sigma^2\pi)^{\frac{1}{4}}} \int_{-\infty}^{\infty} dx \exp\left(-\frac{(x-\alpha)^2}{2\sigma^2}\right) |x\rangle \langle x| \tag{5.7}$$

To get some intuition, we can think about the two limiting examples. First a pure state localized in space, $\rho = |x_0\rangle \langle x_0|$. If we measure this state with the of operators $\Omega(\alpha)$ and get α, we find the final state, ρ_f is proportional to:

$$\begin{aligned}\Omega(\alpha) |x_0\rangle \langle x_0| \Omega^\dagger(\alpha) &= \frac{1}{\sqrt{\sigma^2\pi}} \int dx \exp\left(-\frac{(x-m)^2}{2\sigma^2}\right) \int dx' \exp\left(-\frac{(x'-\alpha)^2}{2\sigma^2}\right) |x\rangle \langle x|x_0\rangle \langle x_0|x'\rangle \langle x'| \\ &= \frac{1}{\sqrt{\sigma^2\pi}} \exp\left(-\frac{(x_0-\alpha)^2}{\sigma^2}\right) |x_0\rangle \langle x_0| \end{aligned} \tag{5.8}$$

Which when normalized is simply the same state, as we would expect when measuring in the same basis. The probability of getting the outcome α can also be found as

$$\mathrm{Tr}\Big(\Omega(\alpha) |x_0\rangle \langle x_0| \Omega^\dagger(\alpha)\Big) = \frac{1}{\sqrt{\sigma^2\pi}} \exp\left(-\frac{(x_0-\alpha)^2}{\sigma^2}\right) \tag{5.9}$$

We find that the probability density of a measurement outcome α is normally distributed around x_0. This probability is also the exact normalization, we need in the above. Repeating the measurement, we could come with a more confident estimate of x_0.

If we started with the completely mixed state $\rho = \frac{1}{\mathcal{N}} \int dx |x\rangle \langle x|$ with $\mathcal{N}$ a normalization constant[2]. The outcome after a measurement, α, would be proportional to:

[2] In this there would be some factor of infinity which we would normally remove by considering á finite interval

$$\begin{aligned}\Omega(\alpha)\rho\Omega^\dagger(\alpha) &= \frac{1}{\sqrt{\sigma^2\pi}} \int dx' \exp\left(-\frac{(x'-\alpha)^2}{2\sigma^2}\right) |x'\rangle \langle x'| \int dx \frac{1}{\mathcal{N}} |x\rangle \langle x| \int dx'' \exp\left(-\frac{(x''-\alpha)^2}{2\sigma^2}\right) |x''\rangle \langle x''| \\ &= \frac{1}{\mathcal{N}\sqrt{\sigma^2\pi}} \int dx \exp\left(-\frac{(x-\alpha)^2}{\sigma^2}\right) |x\rangle \langle x| \end{aligned} \tag{5.10}$$

Narrowing the state to be Gaussian around the measured variable and the probability of measuring α will be the same for all values of α

$$\mathrm{Tr}\Big(\Omega(\alpha)\rho\Omega^\dagger(\alpha)\Big) = \frac{1}{\mathcal{N}} \tag{5.11}$$

since it is completely mixed.

5.1.3 Continuous Weak Measurement

We will in this section lay the foundation for making the continuous weak measurement, where information is extracted from the system at some rate. We can construct this process by dividing the time into multiple steps of Δt and applying the Gaussian POVM at each time interval. We wish to formulate this in a way, where no information should be extracted from the system if the duration goes to 0. At small times, we assume the strength of the measurement[3] to be linear in Δt, such that the strength is determined by $k\Delta t$, where k is the rate with which we extract the information. The operator applied in one time step will then be of the form:

[3] We can think off the strength as the concentration of the gaussian proportional to $1/\sigma^2$.

$$\Omega(\alpha) = \left(\frac{4k\Delta t}{\pi}\right)^{\frac{1}{4}} \int dx e^{-2k\Delta t(x-\alpha)^2} |x\rangle \langle x| \tag{5.12}$$

where α is the continuous label. If the state of the system is ρ the probability of measuring the operator Ω_α is then: $P(\alpha) = \mathrm{Tr}\left(\Omega^\dagger(\alpha)\Omega(\alpha)\rho\right)$. We find

$$P(\alpha) = \sqrt{\frac{4k\Delta t}{\pi}} \int_{-\infty}^{\infty} dx |\psi(x)|^2 e^{-4k\Delta t(x-\alpha)^2} \tag{5.13}$$

We will now let the amount of sub-intervals go to ∞ such that $\Delta t \to dt$ while keeping the product constant. In this limit, the Gaussian will be much wider than the wave function[4]. Under the integral, we can the approximate the wave function as being localized $|\psi(x)|^2 \approx \delta(x - \langle x \rangle)$, such that the probability of the instantaneous measurement yielding a specific α gives:

$$P(\alpha) = \sqrt{\frac{4k\Delta t}{\pi}} e^{-4k\Delta t(\langle X \rangle - \alpha)^2} \tag{5.14}$$

[4] If we assume the wave function to be somewhat localized such that the variance of position is much smaller than the variance of an infinitesimal measurement $\langle X^2 \rangle - \langle X \rangle^2 \ll 1/kdt$

Now this means that at each instant, a value for α is drawn from this distribution. The exact value for α also determines which operator in the set $\Omega(\alpha)$ is applied to the state according to Equation 5.3. The measurement introduces stochasticity into the dynamics since there will be drawn a stochastic variable at each time step. Drawing a sequence of these variables and following the dynamics is called *unraveling* the dynamics, and the corresponding list of variables will make up our *measurement record*.

In anticipation for the next section, we will write an α drawn from the distribution in Equation 5.14 as a stochastic variable:

$$\alpha_s = \langle X \rangle + \frac{\Delta W}{\Delta t \sqrt{8k}} \tag{5.15}$$

Where ΔW is a *Wiener process* which produces a normal distributed parameter with variance Δt and mean 0. This formulation often appears in random walks like in Brownian motion[32].

5.2 Stochastic Master Equation

Before arriving at the stochastic master equation, we will introduce some basics of stochastic calculus.

5.2.1 Ito's Rules

In stochastic calculus, we do not only have the limit of $\Delta t \to dt$, but we also need to consider what happens for ΔW. While the properties come from a large field of stochastic calculus which is used in fields from finance to diffusive processes, we will just cover some fundamental rules from Ito calculus. The first rule comes from regular calculus, which states that in the limit of $\Delta t \to dt$ we ignore terms of order dt^2 or higher.

Secondly, if we have a time interval of some duration $t_2 - t_1$, where some dynamical variable W changes. We split the interval in $n = (t_2 - t_1)/\Delta t$ substeps and sum the contributions from ΔW. This

gives us:

$$\sum_{i=1}^{n} \Delta W \tag{5.16}$$

Here we sum an identical variables from a Gaussian distribution with mean 0 and variance Δt. By the central limit theorem, the distribution of the sum will converge to a normal distribution with mean 0 and variance $n\Delta t = t_2 - t_1$. In taking the limit for $n \to \infty$ and correspondingly $\Delta t \to dt$ such that their product is constant, this will not only approximate the Gaussian but will be:

$$\lim_{n\to\infty} \sum_{i=1}^{n} \Delta W = \int_{t=t_1}^{t=t_2} dW = \mathcal{N}(\mu = 0, \text{Var} = t_2 - t_1) \tag{5.17}$$

Which will also mean that integrating the dW^2 or the variance for an infinitesimal random variable would yield:

$$\int_{t=t_1}^{t=t_2} dW^2 = \lim_{n\to\infty} \sum_{i=1}^{n} \Delta W^2 = t_2 - t_1 = \int_{t=t_1}^{t=t_2} dt \tag{5.18}$$

Meaning that the variance of the random process will not itself be random but be dt when integrated over any finite time interval:

$$dW^2 = dt \tag{5.19}$$

The last thing to remark is that we now also neglect terms of $dWdt$. One way to think about this, is that a normal distributed variable will be of the order given by the standard deviation. In a maybe exploitative notation, this can be written as $\sqrt{dt}$ meaning that $dWdt$ is of order $dt^{\frac{3}{2}}$ and in the infinitesimal limit be much smaller than terms of order dW, dt and dW^2 [33].

5.2.2 Stochastic Evolution of a Pure State

With Ito's rules, we are now ready to see how a quantum state evolves while we extract information from it. We will do this in two steps, first we will look how a pure state evolves $\rho = |\psi(t)\rangle \langle\psi(t)| \to \rho(t + dt)$, if its subject to the continuous Gaussian measurement of a hermitian operator X described in Section 5.1.3. To generalize this form, we will try to derive it using the Kraus operators but inevitable fail since measurements are not linear and we will instead force trace preservation.

We will here consider a state $|\psi(x)\rangle \langle\psi(x)|$ which is pure. We split the process of extracting information out in many substeps and let them be infinitesimal $\Delta t \to dt$. This will correspond to applying the POVM based on $\Omega(\alpha)$ with $\Delta t \to dt$. At each application the process will be stochastic, and will correspond to picking a stochastic variable $\alpha_s = \langle X \rangle + dW/dt\sqrt{8k}$ determining which operator and thereby which trajectory to follow. After a step of dt, the state will then be:

$$\rho(t + dt) = \frac{\Omega(\alpha_s)\rho(t)\Omega^\dagger(\alpha_s)}{P(\alpha_s)} = \frac{\Omega(\alpha_s) |\psi\rangle \langle\psi| \Omega^\dagger(\alpha_s)}{P(\alpha_s)} \tag{5.20}$$

The probability of α_s was calculated above in Equation 5.14. Applying the operator $\Omega(\alpha_s)$ gives:

$$\begin{aligned}\Omega(\alpha_s)\left|\psi(t)\right\rangle &= \left(\frac{4k\Delta t}{\pi}\right)^{\frac{1}{4}} \int dx e^{-2kdt(\alpha_s - x)^2} \left|x\right\rangle \left\langle x|\psi(t)\right\rangle \\ &= \left(\frac{4k\Delta t}{\pi}\right)^{\frac{1}{4}} e^{-2k\ dt(\alpha_s - X)^2} \left|\psi(t)\right\rangle\end{aligned}$$

Here capital X is an operator, which in its diagonal form is given by $X \int dx\ x \left|x\right\rangle \left\langle x\right|$. We can now write $\rho(t+dt)$ as:

$$\rho(t+dt) = \frac{\sqrt{\frac{4k\Delta t}{\pi}} e^{-2k\ dt(\alpha_s - X)^2} \left|\psi(t)\right\rangle \left\langle\psi(t)\right| e^{-2kdt(\alpha_s - X)^2}}{\sqrt{\frac{4k\Delta t}{\pi}} e^{-4k\Delta t(\langle X\rangle - \alpha)^2}} \tag{5.21}$$

Canceling the constants and splitting the exponential in the denominator into both exponentials in the numerator, we have:

$$\begin{aligned}\rho(t+dt) &= e^{-2kdt((\alpha_s - X)^2 - (\alpha_s - \langle X\rangle)^2)} \left|\psi(t)\right\rangle \left\langle\psi(t)\right| e^{-2kdt(\alpha_s - X)^2 - (\alpha_s - \langle X\rangle)^2)} \\ &= e^{-2kdt(X^2 - \langle X^2\rangle - 2\alpha_s(X - \langle X\rangle))} \left|\psi(t)\right\rangle \left\langle\psi(t)\right| e^{-2kdt(X^2 - \langle X^2\rangle - 2\alpha_s(X - \langle X\rangle))}\end{aligned}$$

By substituting $\alpha_s = \langle X\rangle + dW/dt\sqrt{8k}$, we can find:

$$\begin{aligned}&-2kdt(X^2 - \langle X\rangle^2 - 2(X - \langle X\rangle)(\langle X\rangle + dW/dt\sqrt{8k})) \\ =& -2kdt(X^2 + \langle X\rangle^2 - 2X\langle X\rangle) - 2\sqrt{k}(X - \langle X\rangle)dW \\ =& -2k(X - \langle X\rangle)^2 dt + 2\sqrt{k}(\langle X\rangle - X)dW\end{aligned}$$

By substituting this back into the exponential, we can expand them while only keeping terms of dt, dW and dW^2:

$$\begin{aligned}\rho(t+dt) = \rho(t) &- 2k\left[(X - \langle X\rangle)^2\rho + \rho(X - \langle X\rangle)^2\right] dt \\ &+ 2\sqrt{k}((X - \langle X\rangle)\rho + \rho(X - \langle X\rangle))dW \\ &+ 4k(X - \langle X\rangle)\rho(X - \langle X\rangle)dW^2 + \mathcal{O}(dt^{3/2})\end{aligned}$$

By using $dW^2 = dt$ and writing $\rho(t+dt) = \rho(t) + d\rho(t)$ we find the differential form of the stochastic differential equation:

$$d\rho(t) = 2k\left(2X\rho X - X^2\rho - \rho X^2\right) dt \tag{5.22}$$

$$+ 2\sqrt{k}(X\rho + \rho X - 2\langle X\rangle\rho)dW \tag{5.23}$$

Comparing this equation with the Lindblad Equation (Equation 4.36) we see, that the first term is exactly $\mathcal{D}[\sqrt{k}X]$. Thus, a continuous measurement gives a contribution which dissipates the system with the applied operator. Further, there is a stochastic contribution, which is dependent on the stochastic variable at each time step. The state is changed by $\mathcal{H}[\sqrt{k}(X)] = 2\sqrt{k}(X\rho + \rho X - 2\langle X\rangle\rho)$ and the measurement record of drawn variables will be:

$$dX = \langle X\rangle dt + \frac{dW}{\sqrt{8k}} \tag{5.24}$$

5.2.3 Stochastic Master Equation

In Section 4.2.2, we derived the Lindblad Master Equation by choosing a set of Kraus operators. In this section, we will follow the same heuristic, however, measurements are not a linear process since we have to renormalize the state after measuring. We will have to enforce normalization of the state by adding an additional term.

If we were to insist on a Linear map in dt we would also have stochastic term according to dW such that we take one Kraus operators of the form:

$$M = \mathbb{1} - (iH - K)dt + cdW \tag{5.25}$$

where we again have H and K hermitian and H, K, c independent of dW and dt. Here we have for convenience only included one Kraus operators, but we could have extended c to be a sum like we did in the derivation for the Lindblad Equation or added other Lindbladian terms with another Kraus operator. The trace preserving condition for Kraus operators, now give

$$1 = \mathrm{Tr}\Big(M\rho(t)M^\dagger\Big) = \mathrm{Tr}\Big(M^\dagger M\rho(t)\Big) \tag{5.26}$$

Expanding:

$$M^\dagger M = \mathbb{1} + 2Kdt + (c^\dagger + c)dW + c^\dagger c dW^2 \tag{5.27}$$

By setting $dW^2 = dt$, we get two constraints, one for dt and one for dW. The first can easily be solved by determining K as:

$$2K = -c^\dagger c \Rightarrow K = -\frac{1}{2}c^\dagger c \tag{5.28}$$

If we were to do the same for the dW expression, we would have:

$$0 = c + c^\dagger \tag{5.29}$$

To preserve the trace, we would need to have $c + c^\dagger = 0$. We could see this as a condition on c, where c is taken to be anti-hermitian [34], or we can do as [32] and accept the non-linearity in the re-normalization step, and actively renormalize at each time step to preserve the trace by subtracting $\langle c + c^\dagger \rangle dW$. If we do this, we write the mapping from $\rho(t)$ into $\rho(t + dt)$:

$$\begin{aligned}
\rho(t + dt) &= M\rho(t)M^\dagger && (5.30)\\
&= \left(-i[H, \rho(t)] + K\rho(t) + \rho(t)K + c\rho(t)c^\dagger\right) dt && (5.31)\\
&+ \left(c\rho(t) + \rho(t)c^\dagger\right) dW - \left\langle c + c^\dagger \right\rangle \rho dW && (5.32)
\end{aligned}$$

Or writing everything in terms of the operator c, we find:

$$d\rho = -i[H, \rho]dt + \mathcal{D}[c]\rho dt + \mathcal{H}[c]\rho dW \tag{5.33}$$

with:

$$\mathcal{D}[c]\rho = c\rho c^\dagger - \frac{1}{2}\left(c^\dagger c\rho + \rho c^\dagger c\right) \tag{5.34}$$

$$\mathcal{H}[c]\rho = c\rho + \rho c^\dagger - \left\langle c + c^\dagger \right\rangle \rho \tag{5.35}$$

The $\mathcal{D}[c]$ is exactly the one we found in the Lindblad equation and describes some dissipation or backaction from measuring the system[5]. The second term is defined by our current trajectory and is how the system changes based on what we learn about it. When comparing with the pure state from above, we see that it can be retrieved by setting $c = \sqrt{2k}X$ in the general form. If we generalize the measurement record from this, we have[32]:

$$dr(t) = \frac{\langle c + c^\dagger \rangle}{2} dt + \frac{dW}{\sqrt{4}} \tag{5.36}$$

[5] In the Lindblad equation, we allowed for multiple dissipation operators, this could also easily introduced here by having multiple c_α and a corresponding L_α for each. The we would just get a set of $\mathcal{D}$ and $\mathcal{H}$ for each c_α

5.2.4 Multiple Observers and Inefficient Measurement

If we consider two observers of a system measuring one operator each c_A and c_B then the full stochastic master equation gets contributions from each:

$$\begin{aligned} d\rho(t) = -i[H,\rho] + \mathcal{D}[c_A]\rho(t)dt + \mathcal{H}[c_A]\rho(t)dW \\ + \mathcal{D}[c_B]\rho(t)dt + \mathcal{H}[c_B]\rho(t)dW \end{aligned}$$

But observer A has no knowledge about the measurements from observer B. Therefore she must average over them. Averaging over all dW gives 0, and observer A will just see the backaction term: $\mathcal{D}[c_B]\rho(t)dt$.

Inefficient measurements leads to similar results. If an observer were to apply some measurement c, but only receive a fraction of the information $\eta \in [0,1]$. The system would still exhibit the full backaction but less information will go into the stochastic update of the density matrix. With inefficient measurement, the stochastic master equation takes the form:

$$d\rho = -i[H,\rho]dt + \mathcal{D}[c]\rho dt + \eta\mathcal{H}[c]\rho dW \tag{5.37}$$

And the record will have its signal scaled by a factor $\sqrt{\eta}$. If we instead normalize the record such that it averages to the expectation value, then we get the scaling on the noise term:

$$dr(t) = \frac{\langle c + c^\dagger \rangle}{2} dt + \frac{dW}{\sqrt{4\eta}} \tag{5.38}$$

5.2.5 Numerical Integration of Stochastic Differential Equations

We are now set with a stochastic differential equation describing the evolution of a quantum system subject to continuous measurement. However, solving this and finding a closed-form expression for $\rho(t)$ analytically is as good as hopeless. Instead, we will perform a numerical integration, where the stochasticity will be a Monte Carlo element. Repeating (or unraveling) the simulation multiple times, will each give multiple trajectories and density matrices associated with our knowledge of the system.

With a stochastic differential equation of the type

$$dX(t) = f(X(t))dt + g(X(t))dW(t) \tag{5.39}$$

In the simplest scheme, one can do a type of Euler integration, by picking a small number Δt and drawing a number ΔW from a normal distribution with standard deviation $\sqrt{\Delta t}$, we can then calculate the evolution of X in increments:

$$X(t + \Delta t) = f(X(t))\Delta t + g(X(t))\Delta W \tag{5.40}$$

In the limit of $\Delta t \to dt$, we had $dW^2 = dt$, but with a finite step, this will not be entirely true, and we need a small correction. This is called the Milstein method [35] and we update according to:

$$X(t + \Delta t) = f(X(t))\Delta t + g(X(t))\Delta W + \frac{1}{2}g(X(t))g'(X(t))\left(\Delta W^2 - \Delta t\right) \tag{5.41}$$

To improve this method further, it is also possible multiple terms in the Ito-Taylor expansion of the stochastic variable like we did with the Adams method in Section 1.3.1. In the Qutip library which is used to simulate the Stochastic Master Equation a Taylor 1.5 method is used with the Milstein correction. This also includes a term proportional to $\Delta W \Delta t$ from the Taylor-Ito expansion. Compared to the 12th order implementation of the regular integration, this is however very imprecise, and we will have to significantly reduce the timesteps to make sure it is reliable. This also makes the trajectories expensive to simulate [19].

5.3 Measurement of a Qubit

With the stochastic master equation, we can look at how the qubit is actually measured. This is not an instantaneous process, but one where the resonator is driven for hundreds of nanosecond while its leakage back into the feed line is monitored. In the formulation of this chapter, this means that we measure with the operator $\sqrt{\kappa}a$. However, the measurement is not perfect, and we both have a decay of photon which do not reenter the feed line but instead leak out in the environment. In addition, the signal from the feed line has to be amplified multiple times for us to detect it at room temperature. These amplification also blur our signal. Together, this leads to an inefficient measurement, where we measure $\sqrt{\kappa\eta}a$ while the back action term is given by $\sqrt{\kappa}a$.

In the experiment, we can choose to measure one or both of the quadratues. These methods are called homodyne where only one is measured, or if we measure both, we have a hetereodyne measurement. This is done by sending the signal into an IQ mixer, and we can split the signal in an I and a Q component, measuring both a half strength.

The corresponding operators to this process, can be thought of by splitting the Heterodyne measurement in two Homodyne processes with half the signal each. Such that we have

$$c_0 = \sqrt{\frac{\kappa}{2}}\,a, \quad c_{\frac{\pi}{2}} = i\sqrt{\frac{\kappa}{2}}\,a \tag{5.42}$$

We can model this as two inefficient observers, where we keep the information of both of them. Combining the two records into a complex number leads to

$$dr_{\text{heterodyne}}(t) = (\langle I \rangle + i \langle Q \rangle)\, dt + \frac{1}{\sqrt{2\eta\kappa}}(dW_I + i dW_Q) \tag{5.43}$$

Where we have associated the two quadratures with I and Q. Both of which come with a noise process. However, we should still notice that $\mathcal{D}[a] = \mathcal{D}[ia]$ such that applying the hetereodyne measurement leads to the same dissipation as in the homodyne case. Physically, this should also make sense since it is the same signal we look at, we just split it in two [36].

5.4 Measurement Induced Backaction on the Qubit

The section above, does not directly measure the qubit, but is indirectly measuring it by determining the state of the resonator. It is however possible[6] to see how the measurements interact with the qubit, if we trace the out the resonator. In Section 3.3.3, we considered how the resonator coherent states: α_g, α_e associated with $|0\rangle$ and $|1\rangle$ behaves under dispersive readout.

[6] but difficult

The idea is to use the transformation $P = |g\rangle \langle g| D(\alpha_g) + |e\rangle \langle e| D(\alpha_e)$ where $D(\alpha)$ is the displacement operator moving the coherent state with an amount α in phase space. By applying this transformation, the dynamics are moved from the resonator and unto the qubit such that we can trace out the resonator and see how the qubit is affected [37]. By transforming the Hamiltonian, and tracing out the resonator, before doing the inverse transformation of the qubit. Gambetta et al. finds that the qubit experiences an effective frequency shift by:

$$\omega_Q \to \omega_Q + 2\chi \,\text{Re}[\alpha_g(t)\alpha_e^*(t)] \tag{5.44}$$

In addition, the resonator decay also affects the qubit with a dephasing term. $\mathcal{D}[a]\rho$ will in this transformation lead to a qubit interaction according to:

$$\kappa\mathcal{D}(a) \to 2\chi \,\text{Im}[\alpha_g(t)\alpha_e^*(t)]\mathcal{D}[\sigma_z] \tag{5.45}$$

Where the corresponding backaction from the measurement will take the form of [36]:

$$\eta\mathcal{H}(\sqrt{\kappa}a) \to \eta\sqrt{2\chi \,\text{Im}[\alpha_g(t)\alpha_e^*(t)]}\mathcal{H}[\sigma_z] \tag{5.46}$$

The equation allow us to see how the qubit is dephased by our measurements. Further, we get an additional approximation, where we can average out the resonator in the dispersive limit, under the further assumption that both the state of the resonator will be coherent when starting from a both $|0\rangle$ and $|1\rangle$. While this significantly reduces the complexity of the simulation since the resonator accounts for the largest part of the Hilbert Space, some of the assumption are very restrictive. An example is that T_1-decay is not modelled well by these equations [7].

[7] In [37] the transformation is done with the assumption that $T_1 \gg 1/\kappa$

6 Readout Experiment

We will now determine how well readout can be done on our experimental setup. In this chapter, we will first present the setup, then describe the metric we use for determining the quality of a readout before doing an experiment to determine it.

6.1 Experimental Setup

We will first provide an overview of the experimental setup consisting of three main parts: the quantum device, the control hardware at room temperature, and the cooling stages in the fridge.

6.1.1 Soprano Chip

The experiments are run on the Soprano Chip with 6 qubits. We run all experiment on qubit 2 (see Figure 6.1) and will effectively think of the whole system as a one qubit system. Qubit 2 is a flux tuneable transmon which is connected to a resonator, a control line and flux line used to tune the frequency. The resonator is connected to a feed line which is further connected to the five other resonators. The qubit is flux tuneable and will throughout all experiments be set at the sweet spot, where it the least sensitive to flux noise.

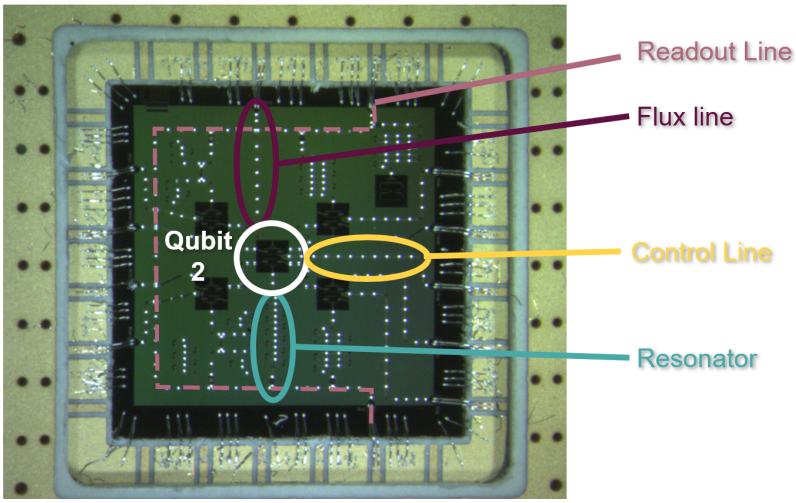

Figure 6.1: The Soprano Chip layout with indicated feed lines and couplings to qubit 2 which is used.

6.1.2 Control Hardware

In order to control the qubit and drive the resonator, we need to be able to create pulses with the right frequency and envelope. For this, we use an arbitrary waveform generator and data processing device. In this experiment, this is done with an OPX [38]. The OPX has two output signals to drive the qubit, two to drive the readout line and two input channels for readout signal. These channels correspond for each to the I and Q signal. The envelope of the pulses can be made with a resolution of 1 GS/s and can process waves with a frequency of 400 MHz. In addition, it has an on-board Field-Programmable Gate Array (FPGA) which is used to compile pulses and demodulate the signal.

Since the signal needed for qubit and resonator control is of order 5-10 GHz, another device for up- and down-conversion is needed. In our experiment, we make use of the Octave [39]. The Octave has three local oscillators for down converting signal, one of which support up conversion. The up conversion is used for the readout line while another local oscillator is used to generate pulses for qubit control. A schematic of the control hardware setup can be seen to the left in Figure 6.2.

The two control devices are controlled by using QUA, a Python API used to write code to be compiled and executed on the hardware [40]. For this thesis, the in-house module OPX_Control[41] was used which significantly simplifies writing and running experiment using the OPX and Octave

In addition to the driving lines, a line from the OPX is also coupled directly to the fridge which is used to adjust the flux in the qubit and thereby its frequency. This will be constant for all experiments at the qubit sweet spot, so we will for the most part ignore it.

6.1.3 Cooling and Amplification

To keep the soprano chip as close to the absolute zero as possible, it is placed in a cryostat capable of cooling to $\approx$ 30mK. In the right side of Figure 6.2, we have illustrated the qubit and resonator drive lines from room temperature to the chip and the returning signal from the resonator and back to room temperature. For simplicity, we have only illustrated one microwave control line, one readout input line and one readout output line[1].

The input lines are cooled at multiple stages from room temperature to approximately 30 mK. This happens in multiple stages and the amplitude of the signal is reduced in each stage by attenuators. At the coldest stage, the signal is filtered with a low-pass filter and goes through a directional filter before entering the lines on the Soprano chip.

Since the output signal is of order 10-100 photons, it is a high risk to be lost to thermal noise in the up-conversion line. Therefore, multiple highly sophisticated amplifications are needed. The first of which is Traveling Wave Parametric Amplifier (TWPA) [42]. The

[1] There are many others which share similar ideas. These consists of other qubit control lines, flux lines and a line for a local oscillator to drive the TWPA

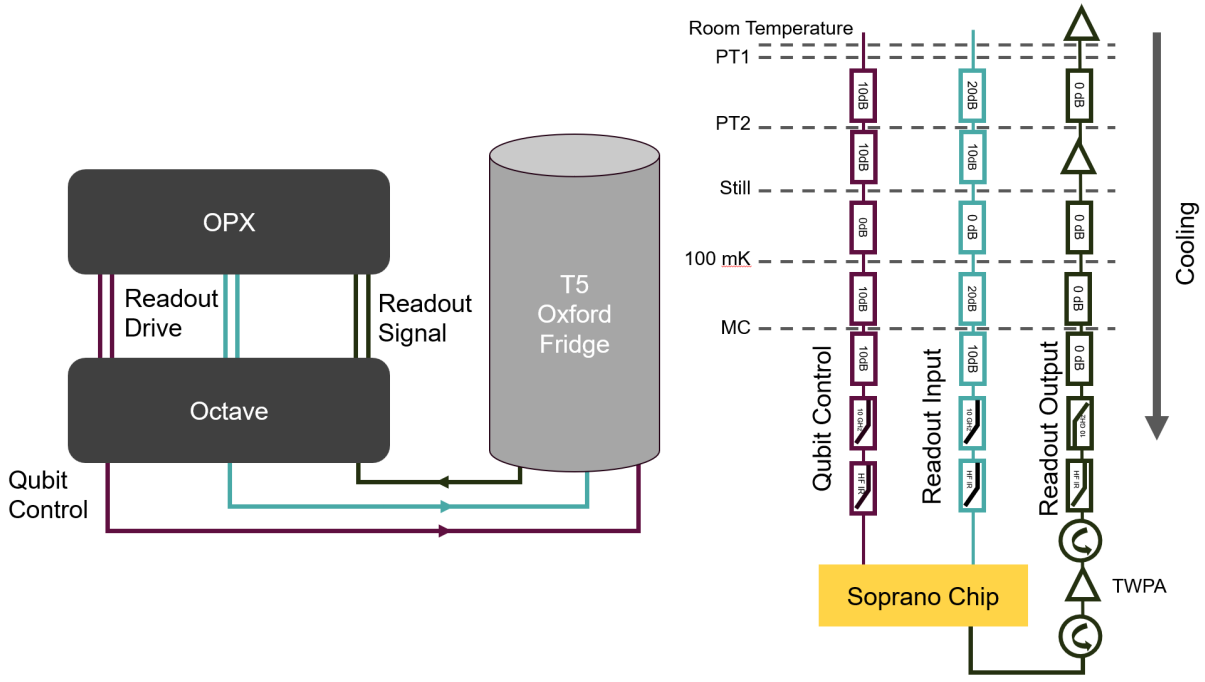

Figure 6.2: A crude schematic of the setup. Qubit control and resonator lines are sent through the octave where they are up converted before going to T5. In the other direction, the signal is down converted and mixed in the IQ mixer before reentering the OPX where it gets demodulated.

TWPA amplifies at low temperature and adds noise close to that of theoretical minimum. After the TWPA two other amplification are performed before the signal exits the fridge and reenters the octave for IQ mixing.

6.1.4 Demodulation of Readout Signal

To do a readout of the resonator, a pulse is send at an intermediate frequency, ω_{IF} from the waveform generator to the octave where it is mixed with a local oscillator signal, ω_{LO}. This results in a high frequency pulse send to the fridge at the readout frequency.

After interacting with the resonator it is amplified and it enters the Octave with the form:

$$s(t) = A\cos(\omega_{RO}t + \theta_{RO}) \tag{6.1}$$

In the heterodyne measurement scheme, the signal is again mixed in an IQ-mixer with a local oscillator. By delaying one part of local oscillator pulse with a phase of $\pi/2$, it is possible to measure two quadratures simultaneously. The signals become:

$$V_0 = A_{RO}A_{LO}\cos(\omega_{IF}t + \theta_{RO}) \tag{6.2}$$

$$V_{\frac{\pi}{2}} = A_{RO}A_{LO}\sin(\omega_{IF}t + \theta_{RO}) \tag{6.3}$$

Which is at frequency slow enough that we can digitize the values. To perform the readout[2], we now combine the two signals into a complex number and demodulate it by multiplying with $e^{-i\omega_{IF}t}$:

$$V(t) = e^{-i\omega_{IF}t}(V_0 + iV_{\frac{\pi}{2}}) = A_{RO}e^{i\theta_{RO}} \tag{6.4}$$

[2] The following can either be done live on the FPGA or in post processing by storing the data

At each timestep, we will now have a value pair for $(I(t), Q(t)) = (\mathrm{Re}\{V(t)\}, \mathrm{Im}\{V(t)\})$ which can be integrated to get a more precise point in the IQ plane [5]:.

6.2 Readout Fidelity

Before determining the performance of our readout, we should define what a good metric for readout is. To help we try to refine the goal of it.

- Given a quantum state ρ a readout process is a scheme that predicts a state σ, such that σ is on average as close to ρ as possible.

While this is a bit easier to work with, we still need to find a quantity for "closeness" between a density matrix and our prediction. Mathematically, we can achieve this by defining a formal distance, such as the trace-norm on the vector space of 2×2 matrices: $\mathcal{M}^2$ [43]:

$$||\rho - \sigma|| = \mathrm{Tr}\left[\sqrt{(\rho-\sigma)^\dagger (\rho-\sigma)}\right] \tag{6.5}$$

which has the desired properties like $||\rho_{\text{pred}} - \rho_{\text{true}}|| = 0$, if our prediction is correct. While the trace-norm is an excellent tool, often a related quantity will be used in quantum physics. We instead use the fidelity, which has a general form defined by[43]:

$$F(\sigma, \rho) = \left(\mathrm{Tr}\sqrt{\sqrt{\rho}\sigma\sqrt{\rho}}\right)^2 \tag{6.6}$$

Here $\sqrt{\rho}$ is the matrix, which satisfies $(\sqrt{\rho})^2 = \rho$. The relation to the trace norm is by bounds of the Fidelity [3]. It also has other beneficial properties like being symmetric in $\sigma \leftrightarrow \rho$ and it reduces significantly if one of the states are pure. In our schemes the readout will be always be pure since we predict either $|1\rangle\langle 1|$ or $|0\rangle\langle 0|$. In this case $\sigma = |k\rangle\langle k|$ and the full equation can be written as:

[3] both upper and lower bound by $1 - \sqrt{F(\rho,\sigma)} \leq \frac{1}{2}||\rho - \sigma|| \leq \sqrt{1 - F(\rho,\sigma)}$ [43]

$$\begin{aligned} F(\sigma,\rho) = F(\rho,\sigma) &= \left(\mathrm{Tr}\sqrt{\sqrt{\sigma}\rho\sqrt{\sigma}}\right)^2 \\ &= \left(\mathrm{Tr}\left(|k\rangle\ \langle k|\rho|k\rangle\ \langle k|\right)\right)^2 \\ &= \langle k|\rho|k\rangle \end{aligned}$$

Because of the stochastic nature of quantum mechanics, estimating this quantity takes multiple measurements. We repeat it N times and take the average over the process.

$$\mathbf{E}\left[F(\sigma,\rho)\right] = \frac{1}{N}\sum_i^N F(\sigma_i, \rho_i) \tag{6.7}$$

In the full readout scheme, we should be able to properly measure both $\rho = |1\rangle\langle 1|$ and $|0\rangle\langle 0|$. For this reason, we also average over the initialization of the qubit.

$$\frac{1}{2}\left(\mathbf{E}\left[F(\sigma(\rho_0),\rho_0)\right] + \mathbf{E}\left[F(\sigma(\rho_1),\rho_1)\right]\right) \tag{6.8}$$

Here ρ_k refers to the best initialization of $|k\rangle\langle k|$, we can make and $\sigma(\rho_i)$ the prediction our readout scheme produces given that state. It is important to note, that if we are not capable of initializing the qubit in a desired pure state[4], the initialization and the readout are both factors in the fidelity measure. Together these two factors are referred to as the State Preparation and Measurement errors or SPAM for short.

[4] which we are not

One drawback of this fidelity scheme is that it is $\frac{1}{2}$ for a completely random classification[5]. For this reason, most definitions of the SPAM fidelity [20, 44] is re-scaled such that the fidelity score lies between 0 and 1:

[5] And a classification scheme with $F < \frac{1}{2}$ can be better by just swapping the output labels

$$F_{\text{SPAM}} = \mathbf{E}[F(\sigma(\rho_1), \rho_1)] + \mathbf{E}[F(\sigma(\rho_0), \rho_0)] - 1 \tag{6.9}$$

Which is the definition we will be using to define the "goodness" of a readout (and initialization). Over many repetitions and with pure state predictions, the expectation value of the fidelity, can be found by probability of classifying correctly:

$$\mathbf{E}[F(\sigma(\rho_k), \rho_k)] = P(\text{ro} = "k" | \text{ init} = k) \tag{6.10}$$

where "ro" is short for readout and "init" for initialization. Or writing it in terms of the infidelities $P(\text{ro} = "0" | \text{ init} = 0) = 1 - P(\text{ro} = "1" | \text{ init} = 0)$, we get the estimate as:

$$F_{\text{SPAM}} = 1 - P(\text{ro} = "0" | \text{ init} = 1) - P(\text{ro} = "1" | \text{ init} = 0) \tag{6.11}$$

6.3 Determining the Readout Fidelity

To determine the readout fidelity of our superconducting qubit, we will now do the following experiment. The scheme is visualized in Figure 6.3 and goes as:

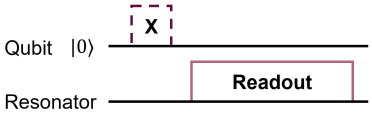

Figure 6.3: Circuit displaying the process of making a readout test. In half the initialization, an X gate is applied to excite the qubit to $|1\rangle$. This is followed by a readout pulse on the resonator.

1. The Qubit is initialized by waiting a duration of 10 times the T_1 such that it is effectively in its equilibrium state. This will be the initialization ρ_0.

2. In half the experiments, we apply an X_π pulse to excite the qubit into the first excited state. This gives us our ρ_1.

3. We now apply a rectangular[6] resonator pulse at frequency $f_d = f_r$ (in between the two states shift) lasting 600ns. This starts movement in the IQ plane analogous to what was described in Section 4.3.5. The feed line output signal is monitored using a heterodyne measurement-scheme. This leads to I and Q signal which is tracked and digitized every ns and stored for post processing.

4. Steps 1-3 are repeated 1000 times for initialization ρ_0 and for initialization ρ_1.

[6] We have a 10 ns ramp-up and ramp-down period to avoid "kicking" the system. This is neglected in our analysis and later in simulations

In the post processing (which is visualized in the top row of Figure 6.4), we have the initialization label and the I and Q trajectories of the readout pulse. By demodulating them at the intermediate

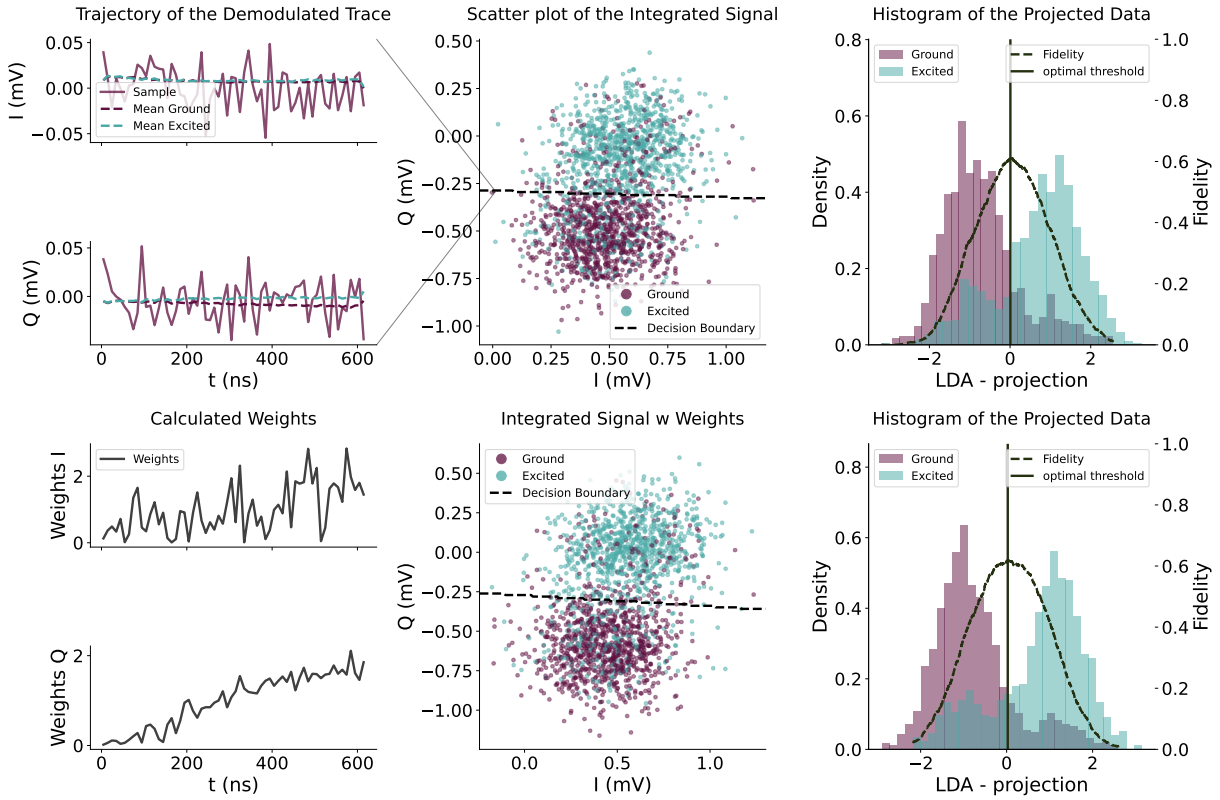

Figure 6.4: Visualization of the Fidelity calculation for no weights (top) and optimal weights (bottom). The top left panel shows an example trajectory along with the mean trajectories. While the bottom left panel are the optimal weights calculated to separate the two distributions. The middle panels are the IQ distributions shown in scatter plots. In the right panels the IQ distributions are projected unto the axis with the biggest separation. Here the Fidelity as a function of threshold is plotted and the optimal is marked.

frequency and integrating the signal we arrive at one value set for (I, Q). Plotting the distribution, we can find the projection line with the largest separation using Linear Discriminant Analysis. This is done by using the implementation in SKLearn [45]. All points are projected onto this axis and summarized in a 1D histogram. By picking the threshold which maximizes the fidelity, we have a measure for the fidelity of this readout protocol. In our experiment this leads to the fidelity.

$$F_{\text{SPAM}} = 0.613 \pm 0.018 \tag{6.12}$$

It is worth noting that this is not the best optimized readout signal, we can achieve. The amplitude of the resonator pulse is here lower than optimal. The goal is however not to do optimal readout but instead study the contribution to the SPAM infidelity, and a stronger pulse would require a bigger Hilbert space in our simulations. We will return to this challenge later.

6.4 Filtering and Weights

Summing the points to get a better classification works well if the points are from a steady distribution. In reality, we might have different other attributes in the readout signal, that we want to weigh differently. A typical example, is that the qubit ramp-up interval will have less separation than in the steady state. Further, the qubit will

also experience energy decay from $|1\rangle \rightarrow |0\rangle$[7] or we might even want to include signal during resonator depletion. A solution to this is by applying different integration weighs at different times.

[7] Or absorb energy to go the other way

6.4.1 Weighting of the Input

Under the assumption that the measured signal from the resonator will be Gaussian in the IQ plane and that points at different times are uncorrelated [46], it is possible to derive optimal linear weights. To do this, we first allow for a weighting parameters at each time step in each quadrature. The integration now takes the form of $\sum_{x=I,Q}\sum_t k_{x,t}\cdot x_t$. If we define the signal as the difference between the integrated signal from the trajectories of $|0\rangle$ and $|1\rangle$, we have:

$$\Delta S = \sum_X \sum_t k_{x,t}(\langle X_0 - X_1\rangle + \xi_t) \tag{6.13}$$

Where we have collected the noise terms from both trajectories into one parameter ξ_t. The Signal to Noise Ratio (SNR) is defined by:

$$\mathrm{SNR}^2 = \frac{|\langle \Delta S\rangle|^2}{\mathrm{Var}(\Delta S)} \tag{6.14}$$

where we can find the mean and variance of the signal as:

$$\langle \Delta S\rangle = \sum_X \sum_t k_{x,t}(\langle X_0 - X_1\rangle \tag{6.15}$$

$$\mathrm{Var}(\Delta S) = \sum_X \sum_t k_{x,t}^2 \left(\mathrm{Var}(\langle X_0 - X_1\rangle) + \mathrm{Var}(\xi)\right) \tag{6.16}$$

The SNR can be maximized by differentiating with respect to the weights and setting the derivative equal to $\partial k_{x,t}\,\mathrm{SNR} = 0$. The weights that maximize the signal is found by setting:

$$k_{x,t} = \frac{\langle X_0 - X_1\rangle}{\mathrm{Var}(\Delta S)} \tag{6.17}$$

Where we will determine the variance and average expected difference experimentally by performing a set of measurement and calculating the mean difference and variance to determine the weights [47].

In the lower row in Figure 6.4 the same experiment as last section was classified using optimal weights. With these weights, we improve the readout fidelity to:

$$F_{\text{readout}} = 0.620 \pm 0.017 \tag{6.18}$$

This is very close to readout fidelity of the simple weights. While it appears that these weights are only a marginal improvement, we should still notice that the two IQ distributions become narrower. In quantifying this, we can calculate the Signal to Noise ratio for the two example. We see that SNR $= 2.54$ goes to SNR $= 2.19$ when we apply the weights. This corresponds to reduce the overlap from the distributions from 1.43% to 0.55%. With 2000 samples (1000 $|0\rangle$ and 1000 $|1\rangle$), we would win around 10-20 additional correct classifications[8], but if the distributions were to be closer, the increase in SNR by 0.25 would have had an even bigger impact on the fidelity.

[8] In the actual experiment, we find 7, but this is subject to some randomness and still a lot smaller than the uncertainties.

6.4.2 Non-Linear Classification Schemes

Classifying with optimal weights is common since it can be combined with the demodulation in one operation (they are both linear operations) and it can be run live on the FPGA. This allows for fast executions and easy calibrations. However, the assumptions are not entirely realistic and the signal is both non-Gaussian and are not uncorrelated at different times.

One example is relaxation during the readout. If the qubit state halfway through the process changes from $|1\rangle \rightarrow |0\rangle$ our measurement record will then start to follow the trajectory of the ground state. In this case, we should weigh the points differently depending on the information provided by the rest of the trajectories. We can do such a generalization either by allowing for a covariant weights [44] or by applying machine learning methods like neural networks [48].

6.5 Postselection

In some instances, we do not mind running with a large overhead in order to increase our readout fidelity. In these cases, we can instead associate a probability of a given trajectory belonging to the 0 or 1 group and then pick the fraction f with the most certain classifications. Since T_1 decay tends to happen somewhere during the measurement, the points will often be placed in some tail going from $1 \rightarrow 0$. Furthermore, the overlap between the two distributions will be in between them. By sacrificing points in the middle, we suspect the leftover errors are mainly due to inseparable distributions.

Wrong initialization gives a mixed state, which will lead to a certain part of "ground state" measurement following the distribution of the excited state. For this reason, the state initialization fidelity can be crudely approximated by taking the fidelity from SPAM in the limit where $f \rightarrow 0$. In Figure 6.5, we have done the post-selection with the trajectories from the readout experiment. By fitting a polynomial, here 3rd order, we can approximate the limit for the fraction of data going to 0 as:

$$F_{\text{init}} \approx \lim_{f \rightarrow 0} F_{\text{SPAM}} = 0.82 \pm 0.02 \tag{6.19}$$

Since the errors on the lower included fractions are large and the points are not uncorrelated, this should just be seen an estimate of the initialization fidelity, but not much weight should be put on it.

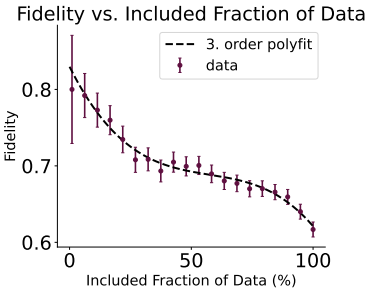

Figure 6.5: The Fidelity of an initialize and measure experiment depending on the fraction of most certain points, we include. The curve is fitted with a second order polynomial to estimate the limit for the fraction going to 0.

7 Calibration Methods

To simulate qubit-resonator trajectories of a readout, we will have to create a model of our system. Throughout chapter 2-5, we introduced theory to describe the system, however, this also came with many parameters, we are still left to determine. Estimating these parameters from the qubit in the laboratory will be the focus in this chapter. Throughout the process, we will perform multiple fits and only present the important outcomes in the main text. A list of fit parameters and goodness of fit metrics can be found in Appendix C.

7.1 Qubit Calibration

We will start with a calibration of the Transmon. While we could solve the system by finding the values of E_C and E_J, we will instead model the Transmon as a three level system and simulate the charge matrix as $\langle k|n|k\rangle = a + a^\dagger$[1]. This leaves us to determine the frequency f_{01} and the anharmonicity α. Furthermore, in order to perform gates, we will calibrate a Rabi pulse from Equation 3.17. In addition to these parameters, we will determine the characteristic time for energy decay and dephasing T_1 and T_2.

[1] This gives us the right correlation between $|0\rangle \leftrightarrow |1\rangle$ and a close to correct connection from $|1\rangle \leftrightarrow |2\rangle$

7.1.1 Spectroscopy

To control the qubit and to simulate its Hamiltonian, perhaps the most important quantity is the frequency. The frequency is found by doing spectroscopy, where a pulse is sent to the qubit at different frequencies. The qubit is then measured to see if it has changed states. The qubit frequency f_{01} will now be the center of a Lorentzian distribution [49]. Thus, we can determine f_{01} by fitting such a curve. This is done in the left panel in Figure 7.1.

Since the design of the transmon gives a negative anharmonicty, we can extend the qubit spectroscopy, to also look for a transition from $|0\rangle \rightarrow |2\rangle$. This can be done either with f_{02} or to stay in the frequency regime, we can instead look for a transition from absorption of two photons, where the photon will will have frequency $f_{02}/2$. We can write it in terms of the anharmonicity at $f_{01} - \alpha/2$. A fit with two Lorenzians can be found in the right panel in Figure 7.1.

From the two experiments, we can extract the qubit frequency and from the difference of the two, we get the anharmonicity. We extract

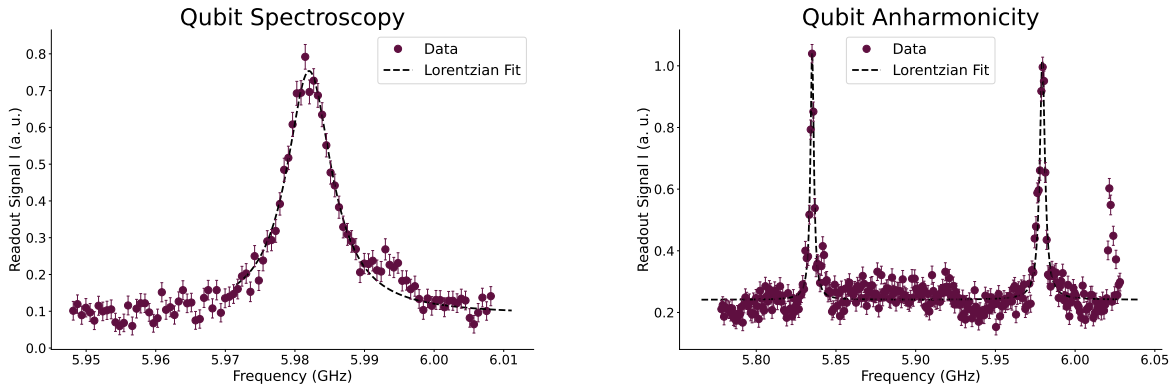

Figure 7.1: Qubit spectroscopy for the f_{01} transition frequency to the left. On the right is an extended scan where another peak is seen, this is the $f_{02}/2$ where two photons are absorbed to go from $0 \rightarrow 2$. The fits are Lorentzian for one peak and the sum of two Lorenzian for the two peak spectroscopy.

the qubit frequency

$$f_{01} = (5.98203 \pm 0.00008)\ \text{GHz} \tag{7.1}$$

And the anharmonicity is calculated as:

$$\alpha = f_{02} - 2f_{01} = (-288.81 \pm 0.15)\ \text{MHz} \tag{7.2}$$

A comment worth making here is that the two-peak Lorentzian curve is not a good fit $\chi^2/\text{ndof} \approx 2.5$. This is largely due to an assumption that the background is constant. In general one should not trust the uncertainties of a poor fit, but to a large degree we do not need it here. If the main purpose was to determine the quantities to the best of our ability, we could have done more work here like fitting the two curves separately or continuing with other experiments were we could get even better estimates of the frequencies. In this thesis, we will suffice with a value "close to" the real value to make a realistic model.

7.1.2 Rabi

In Section 3.1.3, we saw how one can make an x- and y-gates. With a known transition frequency and a set duration and envelope, we just lack the amplitude of the pulse to make sure the unitary evolution exactly corresponds to an X or Y gate.

The amplitude is determined by an experiment, where we initialize the qubit in state $|0\rangle$ and do a pulse with a frequency $\omega_d = \omega_q$ and amplitude Ω before reading it out. We will see oscillations depending on the area of the curve. Each top will correspond to a $\pi + n2\pi$ rotation around the x-axis, where the qubit will be in $|1\rangle$ and the bottoms will be at $2\pi n$ rotations, where the qubit is back in $|0\rangle$. With a cosine fit, we can pick the amplitude yielding us the π rotation. To go from this pulse to a $\pi/2$ rotation, we can simply pick half of the X_π amplitude [50]. A schematic of the experiment is shown in Figure 7.2 and the results from the experiment can be seen along with the cosine in Figure 7.3.

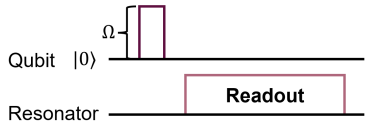

Figure 7.2: The pulse sequence to determine the rabi amplitude. By varying the amplitude depicted with Ω and reading out the signal, the optimal Ω can be determined.

One could further improve the transition from $|0\rangle \rightarrow |2\rangle$ by applying envelopes derived from the DRAG scheme [8]. While these experiments are necessary to create an X-pulse and initilize our qubit

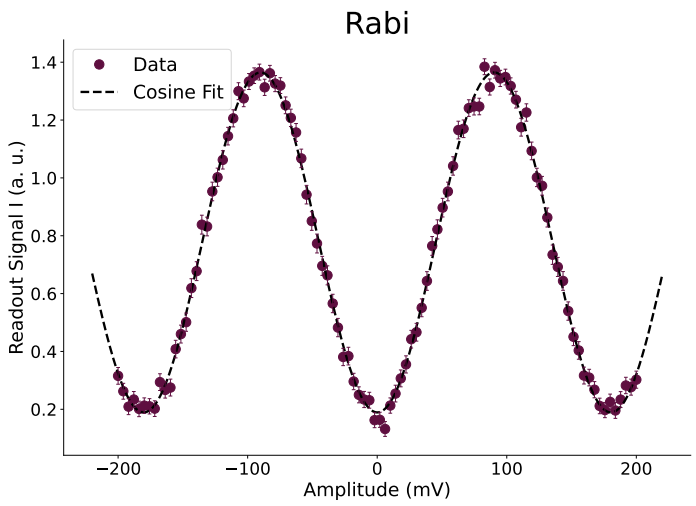

Figure 7.3: The outcome of a Rabi experiment. By varying the amplitude we get a cosine like behaviour which can be fitted to determine the top of the first wave. The curve is fitted with a function of the type: $y = A\cos(2\pi x f + \phi) + b$ where x is the amplitude, y the outcome and A, f, ϕ and B are the fitted parameters.

in the $|1\rangle$ state, this calibration is not necessary for making the initialization in simulation, since we can just apply the x-gate directly.

It is possible to determine the average fidelity of gates by a randomized benchmarking scheme [51]. Without going into much depth, this was done to find an average gate fidelity of $F_{\text{gate}} = 0.9913 \pm 0.0003$. The infidelity contribution here will however be much lower than the other contributions like temperature, so we will assume that we do a perfect X-gate in experiment.

7.1.3 Decay Calibration

In Section 4.3.3, we saw that the characteristic longitudinal decay time, T_1 determines the relationship between $\rho_{00}(t)$ and $\rho_{11}(t)$. For this experiment, we will initialize the qubit in state $|1\rangle$ since this state is the furthest from the steady state. We then wait some time t_{wait} before measuring the qubit. By repeating this experiment multiple times for different waiting times (see Figure 7.4), we can approximate $\rho_{00}(t)$ and $\rho_{11}(t)$ by taking the average at each time step. Now plotting the occupation as a function of time, we will obtain a decaying function going toward the steady state. The exponential coefficient of this decay is given by $1/T_1$ [5].

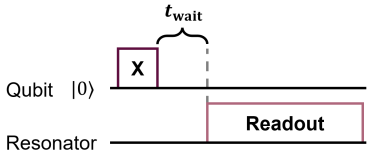

Figure 7.4: The pulse sequence used to do the T_1 calibration experiment.

Doing the experiment on our qubit, we obtain the results displayed in Figure 7.5. The exponential fit gives the value for T_1:

$$T_1 = (4.30 \pm 0.12)\ \mu\text{s} \tag{7.3}$$

The T_1 comes from interaction between qubit and environment which unfortunately changes over time. This leads to a fluctuating T_1 time, so even though one can determine the current T_1 with a high precision, it might change just few hours later. This experiment was run just seconds before the readout sequence described in Chapter 6. But in Section 7.3.1, we will see that an experiment done on the same device just a few months before will have significantly higher T_1. To

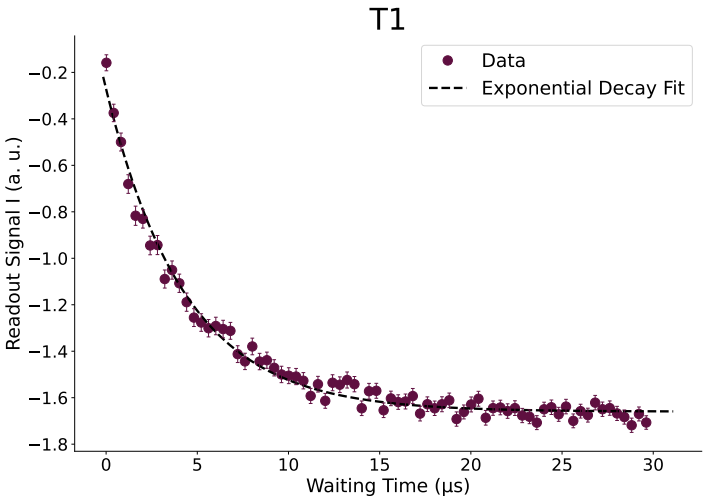

Figure 7.5: Data from an experiment determining the characteristic T_1 decay time. The fit is an exponential decay given by: $y = Ae^{-t/T_1} + b$ where t is the waiting time, y is the outcome of the experiment and A, b and T_1 are fit parameters.

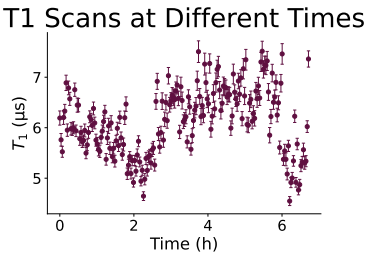

Figure 7.6: The results from repeated T_1-calibrations over a few hours.

see an example of T_1 fluctuations of our device over just a few hours, see Figure 7.6.

7.1.4 Dephasing Calibration

The dephasing of the qubit is not as important a parameter when we look at readout. For completeness and because we also make use of dephasing in the efficiency calibration in Section 7.3.2, we will still do a calibration. To measure T_2, one does a Ramsey style experiment, where a pulse with a frequency slightly offset from the qubit frequency (in our case 5 MHz) is applied to perform an $X_{\pi/2}$ pulse. This state will now start to precess around the z-axis. After some time the pulse is performed again. This leads to time-dependent oscillations which are dependent on the state of the qubit when performing the second pulse. In addition, the qubit will experience dephasing while at the equator of the Bloch sphere, ultimately resulting in a mixed state. This gives an almost exponential envelope of the oscillations where the exponential coefficient is determined by the T_2 time [5].

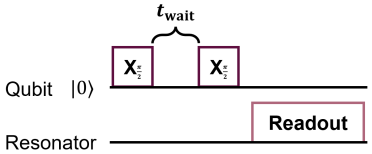

Figure 7.7: Ramsey experiment schematic. Two $X_{\pi/2}$ pulses intentionally detuned from the qubit frequency are applied with a wait time in between them. Afterwards the qubit is measured by performing a readout pulse on the resonator.

In Figure 7.8 two Ramsey experiments are shown. The left one was done before the measurement and the right is a few weeks older. It was run with the same parameters on the same device but this just displays the sensitivity to changes in environment. In the left one, we allowed for two cosine oscillation terms, since we suspect that the system couples to another two level system leading to additional oscillation. The envelope give us:

$$T_2 = (1.65 \pm 0.12)\ \mu s \tag{7.4}$$

Which can further give us the dephasing time, by using Equation 4.50:

$$T_\phi = \left(\frac{1}{T_2} - \frac{1}{2T_1}\right)^{-1} = (1.38 \pm 0.08)\ \mu s \tag{7.5}$$

Where we again should be careful about using this as more than an estimate because of the data does not fit our initial model.

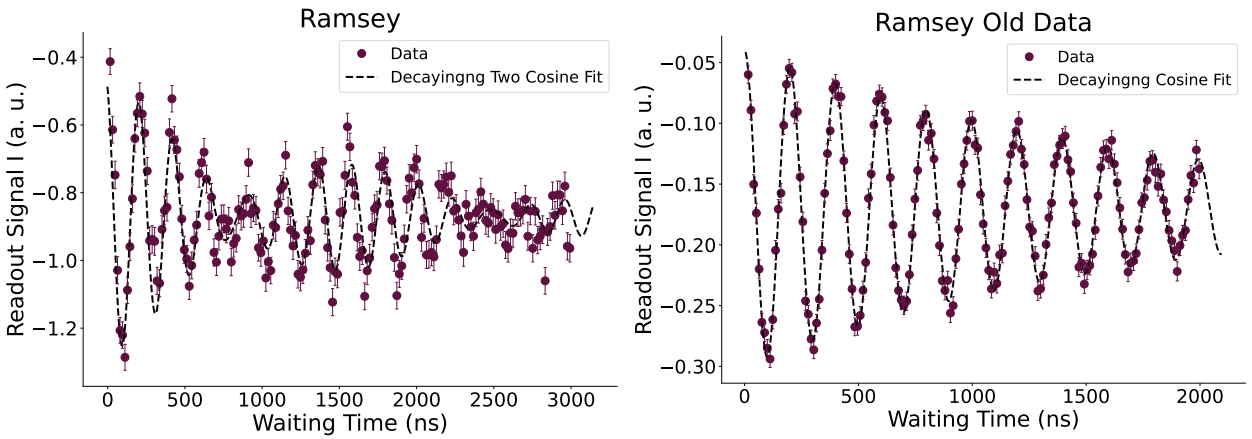

Figure 7.8: Figures showing the T2 experiment. The left shows the Ramsey T_2 while the right shows an older T_2 experiment on the same device. Both are fitted with a function of the type $y = A\cos(2\pi t f + \phi)e^{-t/T_2} + b$ where t is the waiting time, y is the outcome and f, ϕ, A, b and T_2 are fitting parameters. An additional cosine pulse is added to the left one adding the parameters f_1, ϕ_1, A_1.

7.2 Resonator Calibration

With the qubit calibrated, we will move on to the resonator. The resonator is modelled as a quantum harmonic oscillator, so the non-interacting Hamilton is completely determined by its frequency, f_r. However, the interaction with the qubit required us to calibrate the dispersive shift and the coupling strength g. To model the coupling to its environment we determine the photon dissipation rate κ, and lastly we will estimate steady state photon number, $\bar{n}_{ss}$ which is closely related to the amplitude of the drive pulse, ϵ.

7.2.1 Spectroscopy

Like the qubit, we can perform resonator spectroscopy to find the frequency. Because of the dispersive interaction, we will get a different frequency when the qubit is in $|0\rangle$ or in $|1\rangle$ and we will have to do the experiment with both initialization. Since the photons in the resonator have an exponential lifetime, the frequency spectrum will have Lorentzian curve around the resonance frequency. The experiment and the associated fits can be seen in Figure 7.9. Since $|1\rangle$ decays to $|0\rangle$ in many cases, we have added a second Lorentzian to the fit of resonator when the qubit is excited state. In addition, we have limited the fitting points to be around the peak, since the background is not constant but also have some oscillations which we contribute to a finite-size demodulation window [5]. The two frequencies come out to be:

$$f_{r0} = 7.55590 \text{ GHz} \pm 3 \text{ KHz}; \quad f_{r1} = 7.55439 \text{ GHz} \pm 7 \text{ KHz} \quad (7.6)$$

For these parameters, we can extract the resonator frequency f_r and the dispersive shift χ. This can further be used together with the resonator-qubit detuning and anharmonicity to calculate the coupling between qubit and resonator in the dispersive approximation using

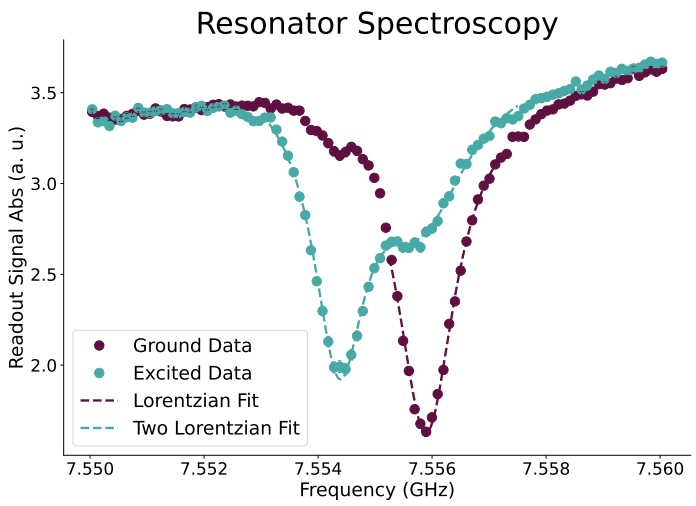

Figure 7.9: Spectroscopy of the resonator signal where the qubit is either in $|0\rangle$ (purple) or in $|1\rangle$ (light blue). Since 1 is somewhat decayed into 0, the curve for 1 is fitted with two Lorentzians.

Equation 3.33:

$$f_r = (f_{r0} + f_{r1})/2 = 7.555130 \text{ GHz} \pm 4 \text{ KHz} \tag{7.7}$$

$$\chi = (f_{r0} - f_{r1})/2 = (763.5 \pm 4) \text{ Khz} \tag{7.8}$$

$$g = \sqrt{\chi(f_r - f_q)\left(1 + \frac{f_r - f_q}{\alpha}\right)} = (87.0 \pm 0.4) \text{ MHz} \tag{7.9}$$

Such that we now can calculate both the resonator Hamiltonian and the full interacting one.

7.2.2 Resonator Decay Rate

To model the resonator dissipation, we will now calibrate κ. We found in Section 4.3.5 that the resonator will decay exponentially when not driven. With this information, we can find κ by simply filling the resonator and watching it deplete. By applying a pulse untill steady state is reached and monitoring the I, Q signal during depletion, we can get the trajectory of mean photon count[2]. An average of 10,000 trajectories are performed of this and the average trace is demodulated and also course grained in 10 ns intervals to reduce the noise. The results along with an exponential fit of the depletion can be seen in Figure 7.10. The exponent factor is found to be:

$$\kappa = 3.8 \pm 0.6 \text{ MHz} \tag{7.10}$$

We can also compare this to the width of the resonator dips. With the Lorentzian distribution the width is given as $2\pi\kappa$ [5]. From the fits above calibrating the resonator frequency, we find $\kappa = (3.87 \pm 0.08)$ MHz when the qubit is in $|0\rangle$ and $\kappa = (3.50 \pm 0.07)$ MHz from $|1\rangle$. For $|1\rangle$ some of the dynamics will however mix with T_1 decay of the qubit and is not as reliable.

[2] Up to a factor which we is not needed to determine the exponential factor

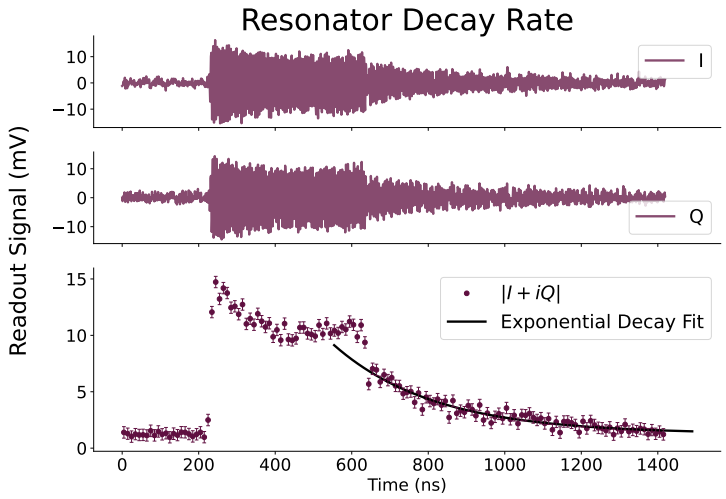

Figure 7.10: Traces from a short drive and a following monitoring of the feed line. In the top panel, the meaned IQ traces are taken. In the lower, the $|I(t) + iQ(t)|$ values are plotted and averaged over 10 ns intervals. The last part (from $t = 600$ ns is fitted with an exponential function: $y = Ae^{-\kappa t} + b$ where t is the time y is proportional to the mean photon number and A, b and κ are fitting parameters.

7.2.3 Photon Counting

To recreate the simulation, we will now need to calibrate the pulse as well. In the experiment, it is determined by some voltage, which we will have to convert to coupling operator going into the Hamiltonian with units of energy. To do this, we will calibrate the amount of photons present in the steady state. This will be done using the two properties:

1. In Section 4.3.5, we described how the resonator goes into a steady state when driven. In the IQ plot, the mean photon number was proportional to the driving amplitude.

2. Like the qubit state shifts the resonator frequency, the qubit frequency is also shifted if we were to fill the resonator with photons. We can use this to rewrite Equation 3.27 to the convenient form: $H = \tilde{\omega}_r a^\dagger a + \left(\frac{1}{2}\tilde{\omega}_{01} + \chi a^\dagger a\right)\sigma_z$

We can now calibrate the photon count in its steady state by driving the resonator until the steady state is reached. Then we do a qubit spectroscopy experiment like the one in Section 7.1.1 to determine the effective qubit frequency. We then repeat the experiment at multiple amplitudes of resonator pulse and multiple frequencies for the qubit pulse. By fitting a second order polynomial we can interpolate the shift at the driving strength ϵ and divide it with the dispersive shift to estimate the mean photon number in the resonator steady state. The experiment is visualized in Figure 7.11. The results for the scan can be seen in the left panel of Figure 7.12, whereas the right panel shows the calculation of mean photon number at different amplitudes.

From this analysis, we extract the mean photon number as:

$$\bar{n}_{ss} = 21 \pm 1 \tag{7.11}$$

Which we can use to extract the driving strength seen by the resonator

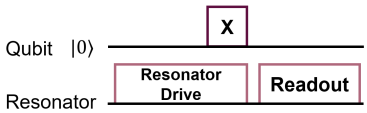

Figure 7.11: An illustration of the photon counting experiment. A pulse is applied with the amplitude of the typical readout pulse. When the steady state is reached an X-gate with a a given frequency is applied. A typical readout is performed thereafter to see if the qubit changed state.

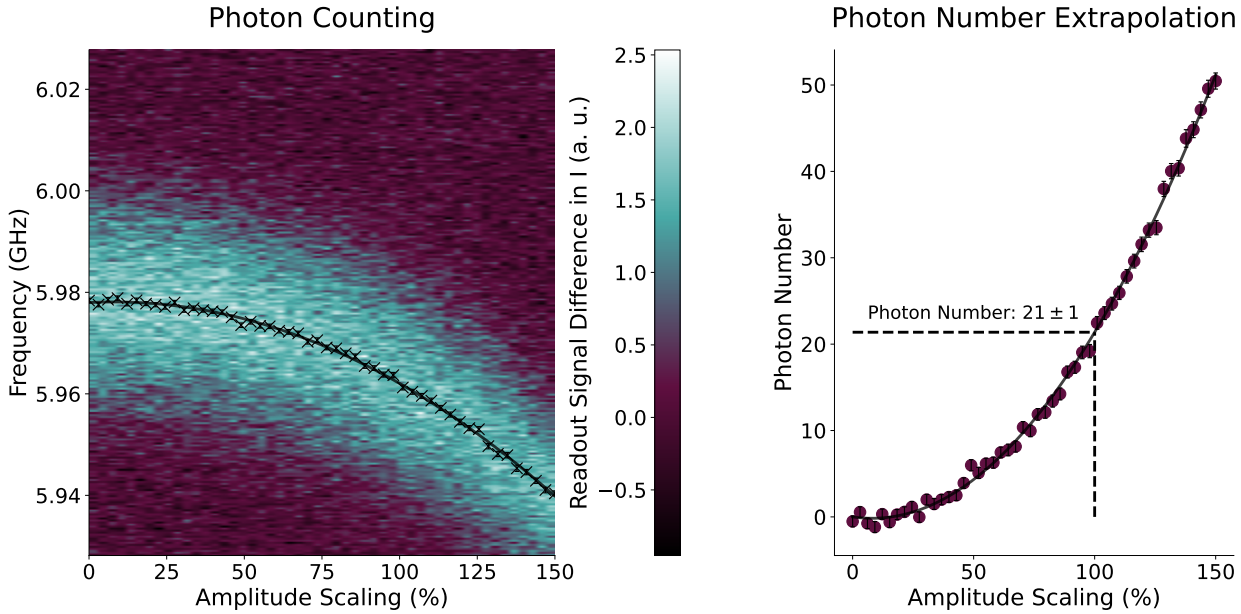

Figure 7.12: Scan of readout-pulse-amplitude and the frequency of qubit-pulse in the left plot. The right shows the calculated mean photon number.

from Equation 4.55

$$\epsilon = \bar{n}\sqrt{\left(\frac{\kappa}{2}\right)^2 + (\chi)^2} = 6.4 \text{ MHz} \tag{7.12}$$

When driving the resonator at its frequency f_r.

7.3 System Parameters

Lastly, the dynamics of the combined system are subject to two additional outside forces: the temperature, τ, and the efficiency of measurements, η.

7.3.1 Temperature and T_1 Calibration in Continuous Time

In Section 4.3.3, we covered how T_1 and τ affect the dynamics and equilibrium positions of the density matrix. In this section, we do a similar method to the T_1 calibration, but instead use continuous time-traces. It should be noted that the experiment run here is made a few months before the other calibration schemes at a time where T_1 was significantly higher. The temperature is however still representative of the state of the qubit when the readout experiment in Chapter 6 was made.

In this experiment, we will do a long continuous readout pulse of the resonator. By splitting it up into small chunks, we will see the state of the qubit at that given time. If we repeat this experiment n times, then we can estimate $\rho_{00}(t)$ and $\rho_{11}(t)$ at a given time during the readout. Since the readout primarily adds dephasing of the qubit, this should not influence the diagonal components of the density matrix. The time dependent elements of the density matrix can now be fitted with the equations derived in Section 4.3.3. The data from a

thousand trajectories of 50 µs classified by demodulating sections of 1 µs is shown in Figure 7.13 and the distributions and classifications from demodulating the first microsecond is displayed in Figure 7.14. By doing 1 µs intervals, we significantly reduce the overlap between the two distributions, such that it can be neglected in the steady state count.

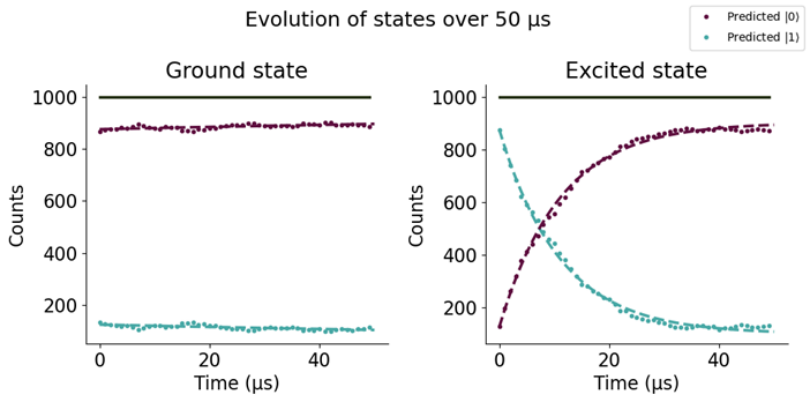

Figure 7.13: The dynamics of our qubit system from 50 µs readout split into 1 µs pieces which are all classified.

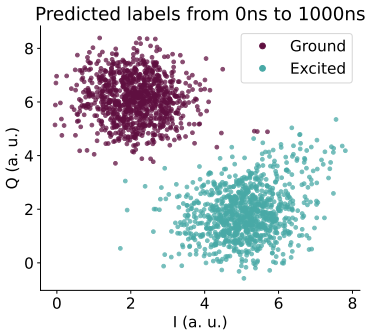

Figure 7.14: The IQ distribution of points from a 1 microsecond demodulation window. The two distributions are well separated, so we expect no overlap.

From the results of the fit, we can extract the decay time, the initial fraction and the steady state fraction of occupancy in the excited state $|1\rangle$. We initialized both in $|1\rangle$ and $|0\rangle$, but since the ground state initialization is already in steady state, we will not trust the fit from the exponential model. While the idea of the method originally was to determine T_1 with a fast scheme, the important aspect for this thesis is to extract the temperature from the steady state fraction. We find the temperature from the Boltzmann factor in the steady state:

$$\frac{\rho_{00}(t=\infty)}{\rho_{11}(t=\infty)} = e^{(E_1-E_0)/k_b\tau} \Rightarrow \tau = -\frac{\hbar\omega_{01}}{k_b} / \log\left(\frac{\rho_{00}(t=\infty)}{\rho_{11}(t=\infty)}\right) = (0.13 \pm 0.04)\ \mathrm{K} \tag{7.13}$$

One might compare the temperature of the superconducting qubit with the temperature of the cryostat of around 30 mK. The difference is suspected to come from electronic heating and other sources of microwaves leaking out into the material. The first run of this analysis gave $\tau = 147.5$ mK which is the value used in simulation. This is however well within the confidence interval.

7.3.2 Readout Efficiency

The amplification chain from the resonator signal and up to room-temperature and digitization is by no means lossless. Each amplification and thermalization step adds noise to the coherent state of the resonator state which we are trying to measure. This ultimately gives us a state which is severely blurred if we compare it to the crisp coherent states with widths of only 1/2. In this subsection, we will estimate the efficiency parameter η. We will follow the method developed by Bultink et al. [52] where they perform this calibration in general for the whole amplification chain.

The general idea can be found in the inefficient stochastic master equation (see Section 5.2.4). Here the backaction term is applied no matter the efficiency we measure with, such that the qubit is dephased. By comparing the amount of extracted information with the amount of dephasing, we can estimate the efficiency.

To use this method, one must first create a readout pulse with a signal that is zero at start and end: $S(t=0) = S(t=T) = 0$. To limit decoherence during the readout, one would choose a short pulse and readout during a cooldown of the resonator for $\approx 5/\kappa$.[3] The shape and resonator signal in pulse is shown in Figure 7.15. With this pulse, the method now consists of two parts:

1. Determine how the SNR changes when we increase the readout amplitude. With a signal starting and ending at 0, this should follow a linear relation: $\mathrm{SNR}(\epsilon) = a\epsilon$.
2. Investigate the backaction of the readout on the qubit. After a pulse, the coherence is related to the readout amplitude by the gaussian relation $|\rho_{01}(T,\epsilon)| = |\rho_{01}(T,0)|e^{-\epsilon^2/2\sigma^2}$

From these parameters, the readout efficiency can then be calculated as [52]:

$$\eta = a^2\sigma^2 \tag{7.14}$$

where our equation deviates from the one in [52] by a factor 2, since they define SNR with respect to the variance of a single trajectory[4]. We combine the two $\mathrm{Var} = \mathrm{Var}_{|0\rangle} + \mathrm{Var}_{|0\rangle}$ reducing the SNR with $1/\sqrt{2}$ compared to their definition.

Amplitude Dependence of SNR To determine the Signal to Noise ratio from the readout pulse, we do a readout experiment like the one in Chapter 6: by initializing the qubit in $|0\rangle$ and then performing an X-gate to every other initialization before reading it out, one can see determine the separation between $|0\rangle$ and $|1\rangle$. We make sure to use optimal weights, to make sure all the available information is used.

By repeating the experiment for drives with different fractions of the readout amplitude ϵ and calculating the SNR from the measurement distributions, we obtain the results in the left panel of Figure 7.16. To the right, the histogram is shown for the I quadrature with amplitude for $\epsilon/4$. The SNR is calculated by taking $\sqrt{\mathrm{SNR}_I^2 + \mathrm{SNR}_Q^2}$. Fitting a linear equation to the results, we obtain $a = (2.43 \pm 0.15)/\epsilon$.

Dephasing from Readout Pulse For finding the relation between the amplitude and dephasing, the qubit is initialized in $|0\rangle$ and a $R^x_{\pi/2}$ pulse is performed to send the qubit into $\frac{1}{\sqrt{2}}(|0\rangle + i|1\rangle)$. With the pulse in this state, the density matrix will be:

$$\rho(t=0) = \frac{1}{2}\begin{pmatrix} 1 & -i \\ i & 1 \end{pmatrix} \tag{7.15}$$

the readout drive will now be applied[5]. During the readout signal

[3] One can optimzie this further by applying a stimulated depopulation pulse.

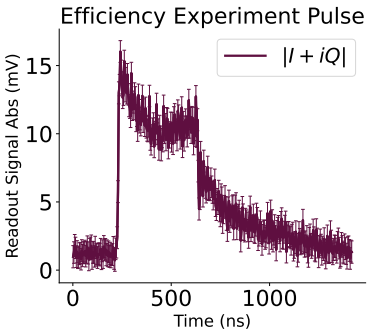

Figure 7.15: The signal in the resonator during the readout pulse used for the efficiency calibration.

[4] assuming that the trajetory for the ground and excited state has the same variance.

[5] while ignoring the output

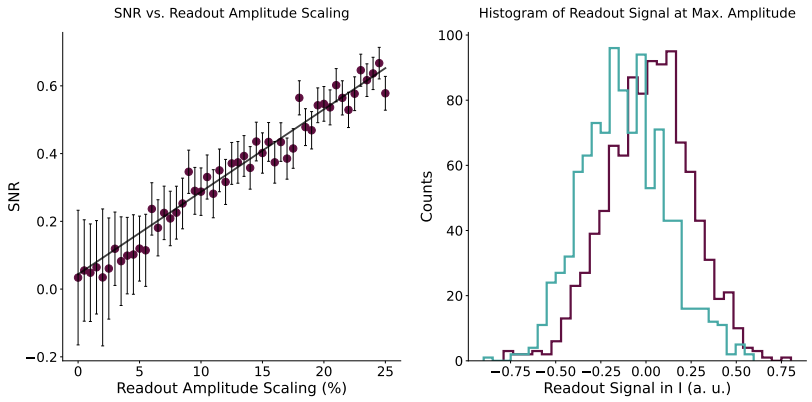

Figure 7.16: Figure showing the experiment for extracting SNR as a function of readout amplitude. An example at the highest amplitude is shown to the right, where the two distributions are separated. The left figure displays the result of this analysis for all values of ϵ as well as a linear fit applied to it.

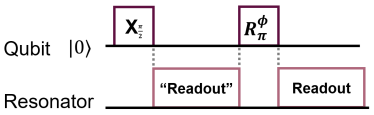

Figure 7.17: The dephasing experiment circuit. First the qubit is rotated $\pi/2$ around the X-axis, where after it is subject to the readout pulse without demodulating and saving the signal. Now the qubit is rotated π around a vector ϕ in the $x-y-$plane and finally readout.

the off-diagonal elements will be reduced by two factors: inherent dephasing by T_2-processes and qubit back action by the signal. To determine the amount of dephasing, we will perform a $\pi/2$ rotation around an axis along the ϕ angle in the x-y-plane before reading out the signal. The entire sequence is illustrated in Figure 7.17.

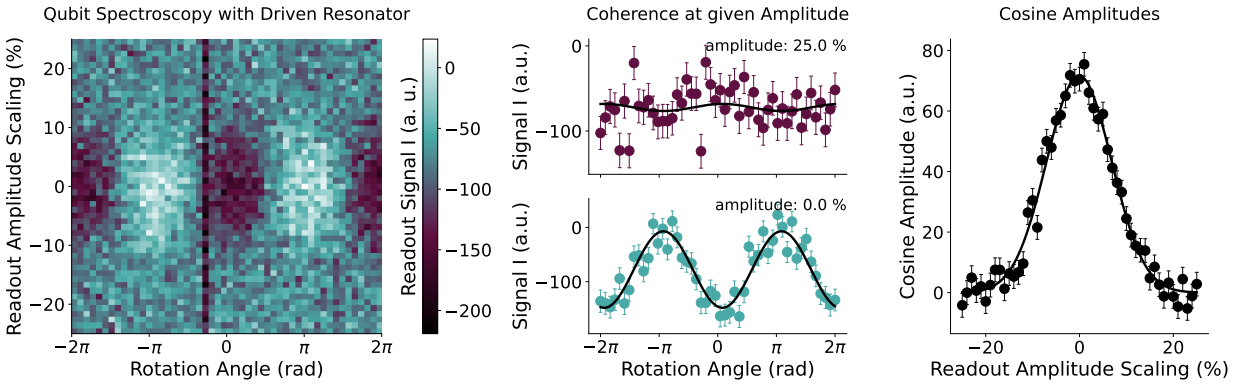

Figure 7.18: Results from the dephasing experiment. The 2D scan is shown along with the cosine-way for amplitude $\epsilon = 0$ and $\epsilon = \epsilon_{max}$. Fitting the cosine function and plotting the amplitude as function of the readout amplitude gives the last figure, where they are are fitted by a Gaussian distribution.

By comparing the readout signal for different angles of ϕ, we expect a cosine shape: $\langle \sigma_z \rangle = 2|\rho_{01}(t = T)| \cos(\phi + \phi_0)$. The phase and frequency of the cosine shape is fitted in the case where most signal is present (at 0 amplitude) and kept constant for all other amplitudes.

By fitting the amplitude for different fractions of the readout amplitude, we can fit a Gaussian distribution to determine σ. Here the T_2 dephasing will just contribute to an overall dephasing, which will be constant throughout all the experiment and will scale the amplitude of the Gaussian. However, this does not affect the width, which we are interested in. The outcome of the distributions can be seen in Figure 7.18 where we find a value for $\sigma = (7.42 \pm 0.17)\ 10^{-2}\ \epsilon$.

We note that there is some problem along a specific rotation axis. When using the OPX, there is sometimes an accumulation of phases, which can give specific errors, so we will here ignore data along that axis.

Calculating the Efficiency In the last two experiment we have extracted a and σ. By combining them, we can find the efficiency of the readout chain:

$$\eta = a^2\sigma^2 = (3.3 \pm 1.2)\% \tag{7.16}$$

Giving us a only around 1/30 of the information available. This leaves huge opportunities for improvements in the amplification chain.

7.4 Overview of Device Parameters

In this chapter, we have calibrated the necessary values of the qubit, resonator and system to be able to simulate the quantum system. The parameters are summarized in Table 7.1. In determining some parameters and uncertainities, the model was not a good fit for our data. These parameters are marked with a star * to illustrate that not much weight should be contributed to the listed value.

Qubit		value	error	unit
Frequency	f_{01}	5.98203	0.00008*	Ghz
Anharmonicity	α	-288.81	0.15*	MHz
Decay Time	T_1	4.30	0.12	µs
Dephasing Time	T_ϕ	1.38*	0.08*	µs
Resonator		value	error	unit
Frequency	f_r	7.555130	0.000004*	Ghz
Dispersive Shift	χ	763.5	4*	KHz
Decay rate	κ	3.8	0.6	Mhz
Mean Photon Number	$\bar{n}$	21	1	-
System		value	error	unit
Coupling	g	87.0	0.4	Mhz
Efficiency	η	3.3	1.2	%
Temperature	τ	0.13	0.04	K
Pulse		value	error	unit
Duration	T_{dura}	1000	-	ns
Drive Frequency	f_{drive}	7.555130	-	GHz
Drive Amplitude	ϵ	6.4	-	MHz

Table 7.1: The outcome of calibrating the qubit with the methods presented in this chapter. A star * illustrates that a value comes from a modified fit or that the uncertainty is taken from a fit with a very high or very low reduced χ^2.

8 Building a Model of the System

With a set of parameters that describe our system, we will in this chapter build the simulation. We will will present this simulation work in three steps. First, we will take a look at four different methods of simulating the system. Next, we will argue for the use of the dispersive model compared to the full time-dependent Hamilton. Finally, we will adjust some parameters of the simulation such as the dimensions of our Hilbert Space and the size of the time steps.

8.1 Different Simulation Approaches

Throughout the first few chapter, we covered different ways of representing and numerically integrating a quantum system. In this section, we will summarize the few methods (see for example a quick overview in Table 8.1. The four methods are:

- **Unitary** - This is a time evolution of the Schrödinger Equation (presented in Section 1.3). In Qutip this is done by the Adams algorithm which we covered in Section 1.3.1. This is the fastest and simplest to run, but does not support interaction with the environment.
- **Lindblad Equation** - The Lindblad equation simulates the density matrix and allows us to include dissipation terms. Like the Schrödinger equation, the Lindblad Master Equation is also deterministic, so it is only necessary to run it once for each configuration. All dynamics can then be extracted from ρ.
- **Monte Carlo** - The Monte Carlo method is described in Section 4.2.4 and the main idea is that dissipation are applied stochastically while the Schrödinger Equation describes the unitary evolution in between application of the Lindblad operators. This allows for faster simulation than the Lindblad Master Equation. However, multiple trajectories will have to be taken to make sure the dynamics represent the full dynamics.
- **Stochastic Master Equation** - The Stochastic Master Equation is described in Chapter 5 and the most complicated of the simulation tools. This includes the dynamics of the Lindblad Equation, but in addition also supports the weak measurement which is obtained during a readout.

Table 8.1: Overview of what the different simulation schemes support. The abbreviations correspond to SE: Schödingers Equation, ME: Master Equation, MC: Monte Carlo, SME: Stochastic Master Equation

	SE	ME	MC	SME
deterministic	x	x		
dissipation		x	x	x
mixed states		x		x
measurements				x
state	ψ	ρ	ψ	ρ
state size	n	n^2	n	n^2

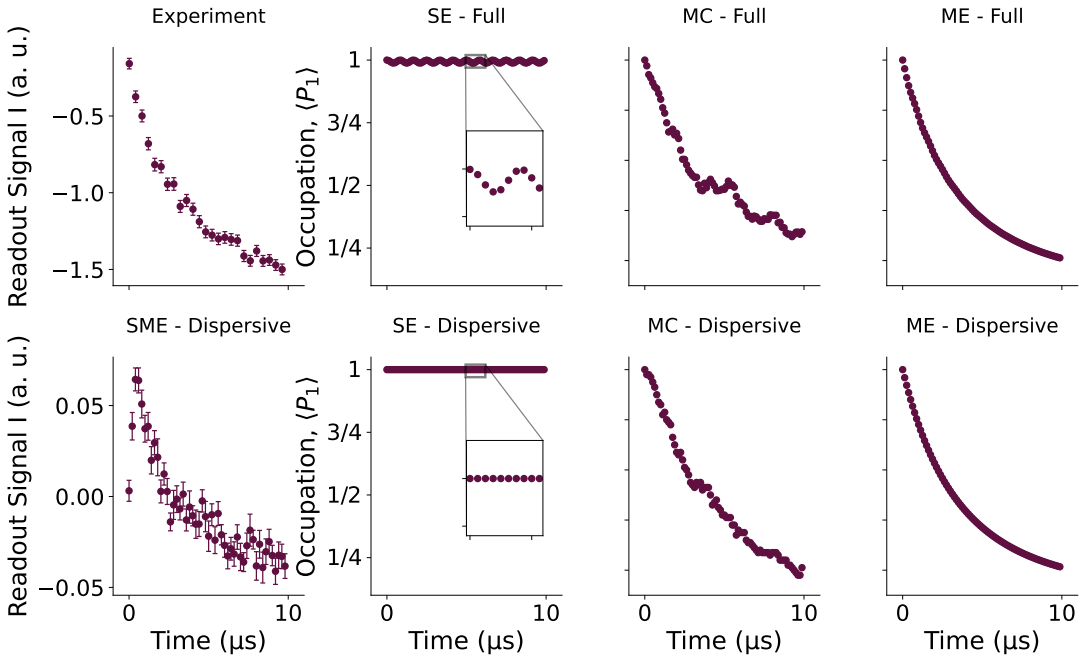

Figure 8.1: Illustration of the T_1 experiment run with different simulation techniques. In the Schrödinger experiment, a zoom-in is made to show the oscillations from qubit-resonator interaction which are not present in the dispersive model.

8.1.1 Comparing Simulations for T_1 Calibration

To illustrate the differences of the different simulations and compare the simulation time, we have simulated the T_1 calibration experiment. We do this with the full interacting Hamiltonian in the lab frame (Equation 3.20) without any drive. We run the simulation with the Schrödinger, Monte Carlo and Lindblad approach. These simulations can be seen along with the experimental results in the top panel of Figure 8.1. In the lower panel, we see simulations run on the dispersive Hamiltonian in a rotating frame of the resonator. In addition, we have also simulated the dispersive Hamiltonian with the Stochastic Master Equation to simulate the readout process. Here it is necessary to apply a resonator pulse[1]. All simulations were run in a finite Hilbert space with a 3-level qubit and 10-level resonator.

In Table 8.2, the running time[2] of the simulations are noted. For the stochastic simulations, 100 trajectories were calculated to get representative dynamics. The T_1 experiment is however long (10 μs and we run with a resolution of 0.5 ns, so this will also be a larger experiment compared to the readout process.

The main takeaway from the simulations is the difference in running time for a full Hamiltonian simulation compared to the dispersive approximation[3]. Comparing the dispersive/full Hamiltonian, we see small oscillations in the qubit state of the Schrödinger equation. These oscillations are however small to the dynamics, we introduce with dissipation.

Table 8.2: Running time of the different simulation approaches to running the T_1 calibration scheme. All numbers are in seconds. The Monte Carlo and Stochastic Master Equation was simulated with 100 trajectories parallelized such that 10-12 trajectories were calculated at a time.

	SE	ME	MC	SME
Full	384	1022	7069	-
Dispersive	0.6	1.2	282	614

[1] We did this at a fifth of the calibrated value and upped the efficiency to 50% to get a measurement for illustrating purposes which can be run in the same size Hilbert space.

[2] On a laptop with processor Intel i7-1260P

[3] This is primarily because we omit the fast oscillating terms, we could do similar transformations for the Jaynes Cummings model if we were to study high power readouts

8.1.2 Validity of the Dispersive Approximation

The full Hamiltonian, we simulated to get the results shown in Figure 8.1 are expensive to run. Even without calculating the time-dependent pulses necessary for simulating the readout process. In Section 3.2.2, we mentioned a critical photon number, which in our system is ≈ 80, approximately four times the steady state photon number in our readout. We are far below this number and the dispersive approximation should be fine.

To confirm, we have also done a simulation of a "weak" readout pulse both in the dispersive limit and the full-time-dependent Hamiltonian. This was done with a Lindbladian simulation. The expectation value of I and Q are displayed along with the Q-function at three different times in Figure 8.2. Qualitatively, we see great correspondence between the two figures. However, the full simulation has some numerical artifacts in the Q-function from the simulation. This is probably due to built up of small numerical errors in a fast rotating basis. We conclude that we should not only use the dispersive model because of its significant speed-up, but also to avoid these kind of numerical errors.

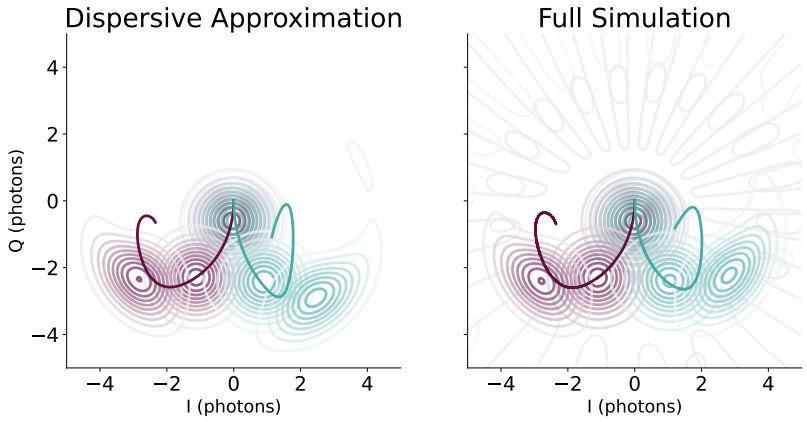

Figure 8.2: Simulated readout drive using the dispersive approximation and full time-dependent Hamiltonian. The expectation value for the I and Q quadratures are shown along with the Q function at three different times.

8.1.3 Q Function and Trajectories

In Section 3.3, we introduced the Q-Function to determine the phase space probability of finding the resonator with a specific I, Q value set. With the speed-up and accuracy[4] for the Lindblad simulation has over the Stochastic Master Equation, one might ask, why we went through the trouble of introducing and coding it. To come with an answer, we will compare the Q function to the measurement trajectories of the Stochastic Master Equation.

As a start, we might have to revisit the interpretation of the density matrix. In the example, we had in Section 4.1.2 the mixed state came from someone (or something) measuring our state without our knowledge. This left us with a state that if we repeat the experiment would yield $|0\rangle$ half of the time and $|1\rangle$ in the other half. In the Lindbladian formulation the density matrix can be formulated as an

[4] Going from order 1.5 $\rightarrow$ 12 reduces errors significantly

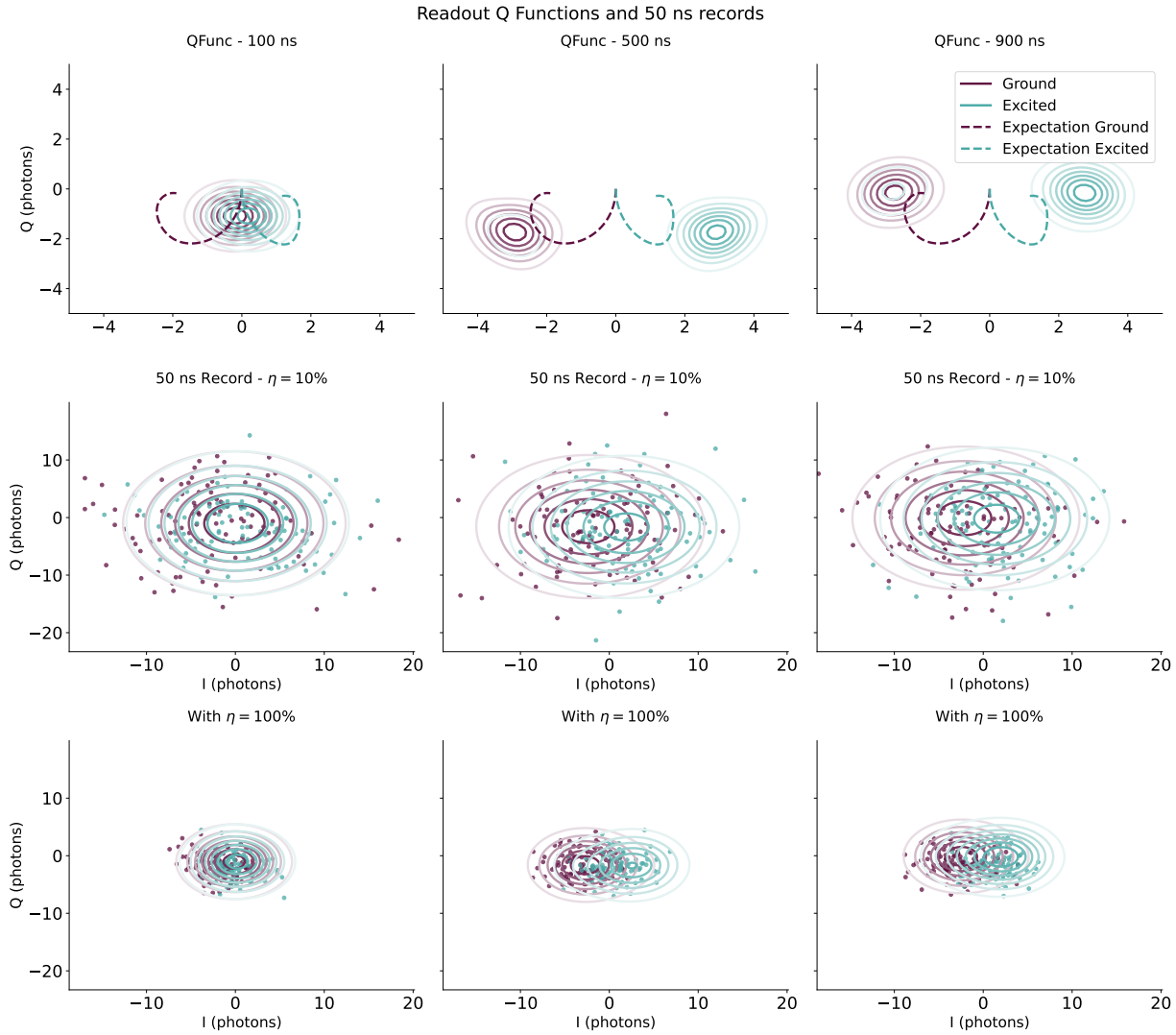

Figure 8.3: Comparison of the Q Function and the scatter plot for a 10 ns readout record. In the top plot the Q Function distribution is shown at $t = 0, 200$ and 400 ns. In the two lower rows the the measurement record for 250 $|0\rangle$ and $|1\rangle$ trajectories are shown. Furthermore, the Q-Function is convolved by a 2d Gaussian with covariance matrix $2\Delta t/\eta \mathbb{1}$ to match the error of the records.

ensemble average, that if we do it multiple times, we would arrive at this outcome. For the SME, we measure it in the meantime. The information here, would no longer be an ensemble average in the same way, but slowly collapse to one of the states in the ensemble. This is what we are calling unraveling.

Averaging over all possible trajectories reduces the Stochastic Master Equation to the Lindblad Equation. And since we model the distribution for trajectories with a Gaussian, we can somewhat find the distribution of measurement records. If we were to assume that the expectation value of I and Q does not change during a small interval. We could use the Q function distribution and convolve it with the expected Gaussian width of our measurement record. This leads to the distribution of measurements records in that time interval. This is illustrated in Figure 8.3.

8.2 Timesteps and the Size of the Hilbert Space

To complete our simulation model, we still have to decide on the proper size of the Hilbert Space and the size of the time steps.

To determine the size of the timestep, we utilize some functionality in the Qutip library. One trick here is that the Adams algorithm actually calculates a 13th order integration step. If the Taylor series converges, then the difference between the 13. and 12. order term will be larger than the leftover error and we can set a threshold on the accuracy we accept [53]. Qutip allows for up to 2500 substeps per timestep and if the error is still to large it terminates and raises an error [19]. This means, we should just set the resolution low without raising an error. A good choice of the 600 ns readout pulse was to split it in 10 ns intervals (which then still could be subdivided in up to 2500 substeps).

The Taylor Milstein 1.5 scheme also checks error bounds. With the stochastic term it is however not as reliable and with a low time resolution the measurement records can include NaN values. A resolution which seems to work is running 2 ns when the efficiency is low, and increasing the resolution to 1 ns when testing the efficiencies $\eta > \frac{1}{3}$ since the stochastic term is larger in this case.

The size of the Hilbert Space affects the complexity of the simulation significantly, since the entries of the density matrix scales as n^2 with n the dimension of the Hilbert Space. However, picking the size is like most of these considerations a trade off between accuracy and simulation time.

For the Qubit we need to have a two dimensional system but we have include a third to be able to calculate the dispersive shift when we are doing the full model. This would further allow for transitions leakage to and from the excited state. This is however not fully implemented in the models since the occupancy would be $< 2\%$ with temperatures around 130 mK. Therefore, other parts of the simulation had a higher priority.

For the resonator, we have to make sure, we do not miss any of the dynamics. The size of the Hilbert space should therefore be significantly larger than the maximum number of photon, we will have at any point during the simulation. The coherent states are decomposed into Fock space states near the mean photon number. With the values of κ and χ in our system, the resonator does not directly enter the steady state, but overshoots it by a bit[5]. When we further add the stochastic nature in the SME, we had to increase it even more to make sure, we do not get near the border. With 50 dimensions in our resonator Hilbert space the model included the desired dynamics without too many errors. A few trajectories with high η had some numerical problems which results in incorrect movements in the IQ plane, one can for example see a couple of points lying near Origo even without T_1 and with well separated distributions.

[5] We saw this when calculating the trajectories in Section 4.3.5

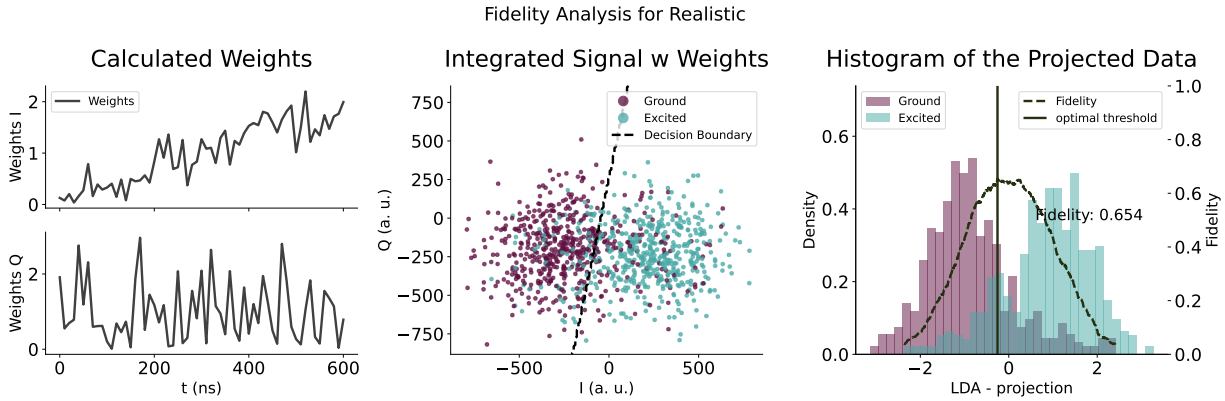

Figure 8.4: The weights, IQ plots and a histrogram of the simulated dataset. The histogram is combined with the fidelity of setting a threshhold at the particular value. The maximum is chosen.

8.3 Readout in Simulation

With calibrated device parameters, implemented simulations, trust in the dispersive model and the numerical settings, we are ready to do the readout simulations. By using the SME with the dispersive model and the parameters calibrated and summarized in Section 7.4, we recreate the readout experiment from Chapter 6. We create 500 trajectories for the equilibrium state calculated from the temperature and 500 times with an x-gate applied to the equilibrium state.

The IQ trajectories were combined with optimal weights and the maximum separating line was found. The process can be seen in Figure 8.4. We remember that the phase of the IQ plot can be chosen freely, so the rotation compared to experiment (which was shown in Figure 6.4) is not alarming. The state initialization and measurement error of our readout process in the simulated system is:

$$F_{\text{SPAM}} = 0.654 \pm 0.024 \tag{8.1}$$

Which is close to the actual experiment. Comparing the two, we find a z-score[6] of 1.15. A fidelity from the same distribution as the experiment would have probability of $p = 24.8\%$ of being further away from than the estimate from the simulation. This is a good indication that we are on the right track. Even though we still have multiple additions left. This includes the ramp-up and down of the experimental readout pulse, a realistic X-gate and proper inclusion of the dynamics associated with the second excited state.

While the number is close, we can also compare the distributions. In Figure 8.5, we compare the distribution for all trajectories and for the ground and excited state separately. We can use these distributions to calculate a 2 sample Kolmogorov Smirnov Test[54] to test the probability, that the samples are drawn from the same distribution. The results of this test is shown in Table 8.3.

We see great correspondence between the full distribution, but the individual distribution are still not convincing (at 5% and 6%). Specifically we see that the ground state peak in the excited state is a bit to the right. While this could be a random artifact, we expect the

[6] $|F_e - F_s| / \sqrt{\sigma_s^2 + \sigma_e^2}$ where subscript e is the fidelity and error of the experiment and s is for simulation

Table 8.3: The results of 2-Sample Kolmogorov Smirnov test.

	KS-statistic	pval
Full	0.036	0.367
Ground	0.075	0.046
Excited	0.072	0.062

mixed state to be more anti-symmetric since the X-gate is not perfect. Furthermore, the inclusion of the second excited state, will end up having around $1-2\%$ of the trajectories following another path for both of the initialization.

The data analysis to determine these distributions also include both calculated weights and a linear discriminant analysis. Small random effects in weights or in projection axis can also lead to differences in the distribution. To achieve more stability the amount of trajectories could be increased.

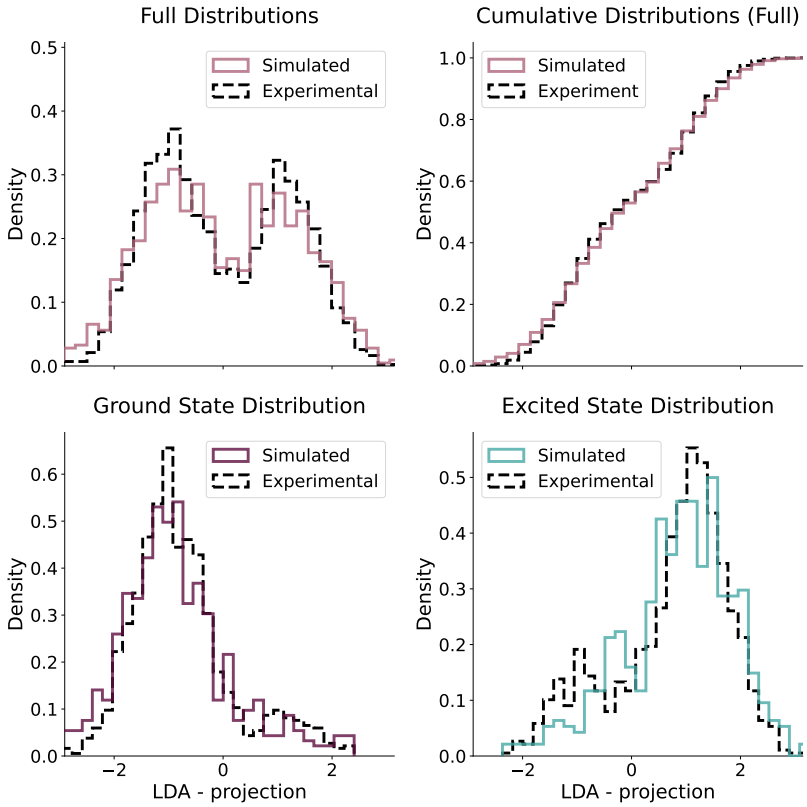

Figure 8.5: The distributions for the simulated readout integration compared to that of the experiment. Both regular histogram and a cumulative distribution is shown for all the trajectories. In the lower panels the histograms for gronud and excited state is displayed separately.

9 Readout Infidelity Budget

In this chapter, we will use the realistic simulation to estimate the contributions to state initialization and measurement infidelities. We will also estimate the fidelity gains by improving the superconducting qubit and hardware through three physical parameters.

9.1 Turning off the Contributions

In this section, we hypothesize three contributions to our SPAM fidelity. By turning them on and off in the model, we will try to quantize the effect they have on the errors of our readout procedure. The three effects we will investigate are.

1. A low readout efficiency, η, which results in an overlap between the $|0\rangle$ and $|1\rangle$ distributions in the IQ plane. This results in readout assignment error

2. The temperature, τ, contributes significantly to the initialization error. At non-zero temperature, we will expect to see a mixed state with non-zero elements for $|1\rangle\langle 1|$. These errors will not be detected during readout.

3. Energy exchanges with the environment can give a low coherence time T_1. Since relaxation or excitation during the readout will alter the trajectory and can lead to false classifications.

By using the simulation model, we can now turn off the different contributions and see which resulting fidelity the readout sequence achieves. As a start, we will model the perfect system. That is a system where the qubit has infinite lifetime $T_1 = \infty$, the system will be zero temperature, $\tau = 0$ and we detect all of the signal $\eta = 1$. A comparison of the Fidelity of this perfect system and the realistic one, which we also simulated in Section 8.3 can be seen in Table 9.1 and the corresponding IQ plot is found in Figure 9.1. To see weights, histograms and other details, we refer to appendix D.

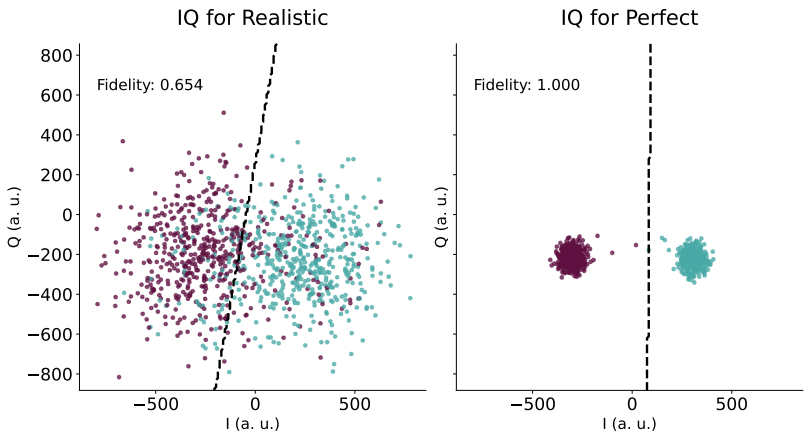

Figure 9.1: The IQ distributions for the experiment run with a realistic and an ideal set of parameters. The fidelity as well as separation line is shown on the plot.

Table 9.1: Results from running the simulation experiment for 500 samples with a realistic set of parameters and a perfect set of parameters.

Parameters Set	Fidelity
Realistic	0.654 ± 0.024
Perfect	1.000 ± 0.000

In the experiment with model with ideal parameters , we get fidelity of $F_{\text{SPAM}} = 1$. This supports our hypothesis where eliminating all thre parameters give a perfect classification . In the IQ plot few points can be seen near origo. They are suspected to come from the effect, we described in Section 8.2 where the SME in a finite dimensional Hilbert Space produces some unwanted dynamics when efficiency is high[1].

In an attempt to single out the effect on readout fidelity from the individual contributions, we can repeat the experiment with the different combinations of turning the effects on one after another. This leads to six experiments. Starting from the realistic set of parameters, we have three experiments with $\eta = 1$, $T_1 = \infty$, $\tau = 0$ respectively (each which excludes one source of SPAM errors). This is repeated with two out of three of the perfect parameters such that we exclusively have one source of SPAM errors. The IQ plots can be seen in Figure 9.2 and the associated fidelity scores in Table 9.6.

[1] The suspicion comes from seeing many more of these points with a lower dimensional Hilbert Space

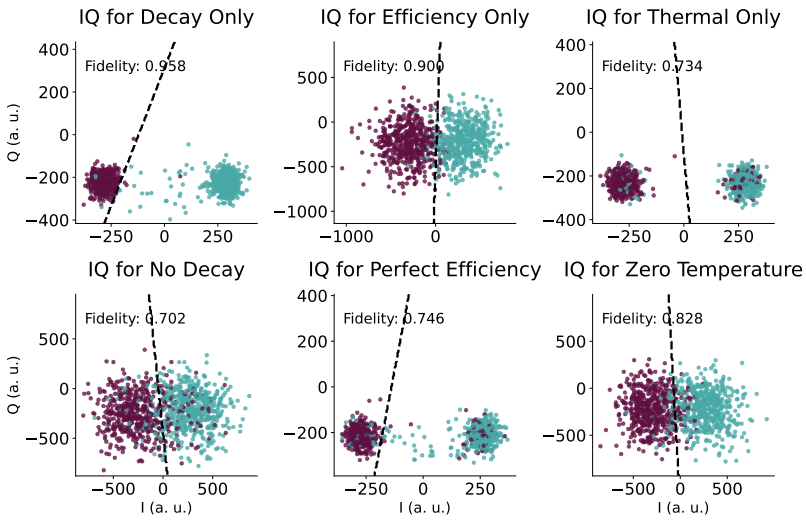

Figure 9.2: The IQ results from turning on the different sources of errors one by one. The IQ scatter plots are displayed along side the decision boundary and the readout fidelity.

Another way of visualizing the infidelity from each parameter is by

Contributions	Temperature	Energy Decay	Inefficiency
Excluding	0.828 ± 0.018	0.702 ± 0.022	0.746 ± 0.021
Exclusively	0.734 ± 0.021	0.958 ± 0.009	0.900 ± 0.014

Table 9.2: The Fidelity results of running the simulation experiment with 1000 samples given parameters that sets one or two of the three parameters to the ideal setting.

placing them in a combination tree. We now add one contribution at a time according to the possible permutations and register the increase in infidelity. This will allow us to get a good idea of the contribution from the individual sources. The combination tree can be seen in Figure 9.3. With infidelity errors of around $2-3\%$ (percent points) the differences have errors of $3-4\%$ (percent points), so we should be careful making conclusions from the specific values. We can, however, analyse the overall pattern.

At a first glance, the errors does not seem to be independent. Decay adds 7.2 % infidelity if we have inefficient measurements while the infidelity goes down if we have non-zero temperature. While this could be a 2 sigma outlier, we should be careful when separating the contributions as it looks like there are some second order effects at play as well. If we want to get a vague first order estimate, we can take the simple average over infidelity contributions for the different parameters in the combination tree. These averages are shown in Table 9.3.

Table 9.3: Average contribution to infidelity when counting in the combination tree seen in Figure 9.3

Parameter	Avg Infidelity
Temperature	0.21
Decay	0.04
Efficiency	0.09

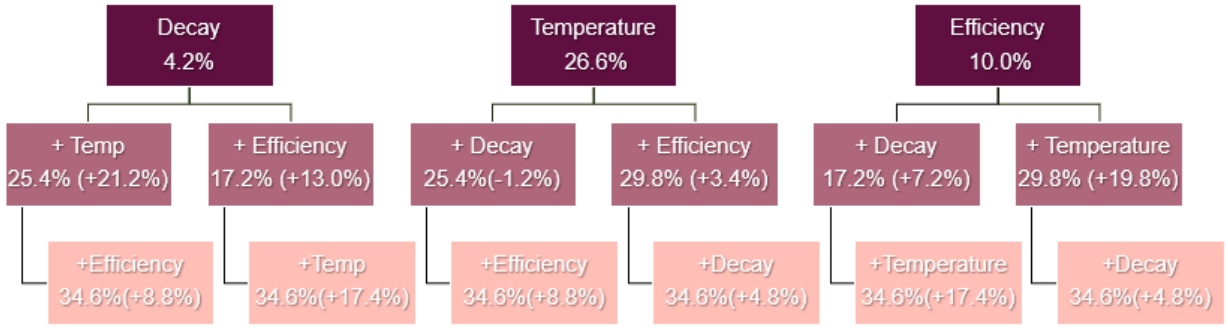

Figure 9.3: Visualizing the different ways of combining the error sources and watching their contributions at each step.

For our system with a readout pulse defined in Section 7.4, the F_{SPAM} seems to be dominated by the temperature, followed by inefficiency and only slightly by the energy decay to the environment.

9.2 Improving the Readout

In this section, we will setup a use case for the developed model: *Given the device and the readout pulse parameters used throughout the thesis, what increase in F_{SPAM} can we the expect by improving the physical device?*. We will use the model to estimate answers and use this as a basis to discuss how the parameters can be used to improve the performance in other parts of the readout sequence by applying other techniques.

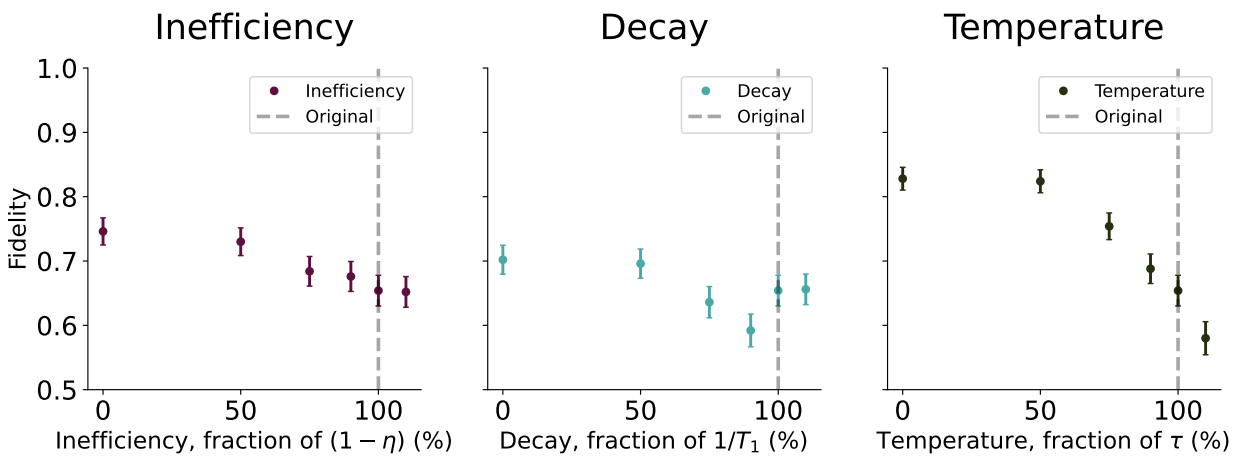

Figure 9.4: The Fidelities of the model when the parameters are changed. In each plot the two other parameters are held constant at the realistic value.

9.2.1 Modifying the Parameters

In the previous section, we considered the parameters to be on (at 0) or off (at 100%) of the considered value. We will now try more incremental improvements of one parameter while we keep the other two fixed. Again, we will run the simulation for 600 ns and do 500 trajectories for both initialization. All the fidelities of the readout sequence are summarized in Figure 9.4 and the IQ plots can be found in Figure 9.6. We will in the next three subsections discuss the results one parameter at a time. To see histogram distributions or weights, we refer to Appendix D.

9.2.2 Temperature

In our model, the temperature has two roles: to determine the mixed state in the beginning of the readout and the relation between energy excitation and decays. Especially, the first of these two affects increases the state initialization error significantly as the failed initialization of $|0\rangle$ will be indistinguishable to the proper initialization of $|1\rangle$. In Table 9.4, we have summarized the SPAM-fidelities for experiments with a reduced temperature of $-10, 0, 10, 25, 50$ and a 100 percent.

For our system, the temperature decreases the Fidelity dramatically, since the equilibrium position will be around 88 percent $|0\rangle\langle 0|$ and 12 percent of $|1\rangle\langle 1|$. Since a reduction of temperature would exponentially suppress the excited part, a reduction of temperature by 50% would reduce the state initialization error to mere $e^{-2} \approx 1/7$ of the current setup. This means that it should be highly prioritized to get to around this point, but further reduction would lead to diminishing returns.

Table 9.4: The outcome of calibrating the qubit with the methods presented in this chapter for different temperatures.

Reduction	Temperature	Fidelity (%)
-10 %	162.3 mK	58 ± 3
0 %	147.5 mK	65 ± 2
10 %	132.8 mK	69 ± 2
25 %	110.6 mK	75 ± 2
50 %	73.5 mK	82 ± 2
100 %	0.0 mK	83 ± 2

Active Reset One way of artificially "cooling down" the qubit is by initializing with readout. If the readout fidelity is larger than the state preparation, it is beneficial to start with a readout and apply an X-gate if the qubit is in state $|1\rangle$. The qubit can the be read out and

the X-gate reapplied until the outcome of the measurement is $|0\rangle$ (see Figure 9.5.

To gain an advantage from active reset, we require the qubit to have long coherence time and high efficiency such that we are confident in our readout. The long coherence time is necessary since a normal readout would try to determine the state at the beginning of the pulse. An x-gate should however only be performed if the qubit is in state $|1\rangle$ so many repetitions would be required if the qubit decays in the meantime. In addition, a readout pulse leaves the resonator filled resulting in a shifted qubit frequency. If one does not take this into account when applying gates, the gate fidelity will be highly affected. The easiest approach is to wait for the resonator to return to the vacuum state, but this also requires the qubit to stay coherent during the process.

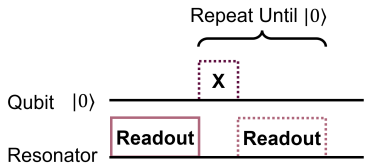

Figure 9.5: Illustration of the active reset process. A readout is performed, if it measures $|1\rangle$ an X-gate and another readout is applied. This is repeat till the readout gives $|0\rangle$.

9.2.3 Qubit Decay

Unwanted changes of the qubit between $|0\rangle \leftrightarrow |1\rangle$ is another big challenge when measuring the state of the qubit. If the qubit changes state during the readout process, it will be difficult to classify as either $|0\rangle$ or $|1\rangle$ and will often lead to points floating in between in the regular distributions in the IQ plots. In Table 9.5, we see how small reductions in the transition rate increase the readout fidelity.

Table 9.5: The outcome of calibrating the qubit with the methods presented in this chapter.

Reduction	Γ_1	T_1	Fidelity (%)
-10 %	0.256 μs^{-1}	3.91 µs	66 ± 2
0 %	0.232 μs^{-1}	4.30 µs	65 ± 2
10 %	0.209 μs^{-1}	4.78 µs	59 ± 3
25 %	0.175 μs^{-1}	5.73 µs	64 ± 2
50 %	0.116 μs^{-1}	8.60 µs	70 ± 2
100 %	0	∞	70 ± 2

In Section 6.5, we saw that we can remove most of the measurement errors from this tail by repeating the experiment and only selecting the most certain measurements. However, this will severely impact the ability to run codes and will not be feasible in scenarios like error correcting codes, where a readout is performed on 10s or 100s of qubit in every cycle.

With a pulse of 600 ns, the contribution from the energy decay during readout seems be less compared to that of efficiency and temperature. Thus, we would probably gain a lot of benefit using the active reset or increasing the pulse length a bit. If we want high-fidelity readout (> 99 %), we should however find ways to decrease the infidelity contribution from T_1 either by improving the device or applying one of the following two adjustments.

Shorter Readout Pulse One way of decreasing the effect of T_1 on readout fidelity by making a shorter readout pulse so the qubit has less time to decay. This will however require a higher efficiency since the distance between the two distributions should be at least 3-4 standard deviations to have sub-percent overlap. The width of the distribution scales with $1/\sqrt{\eta t_{\text{readout}}}$, so a higher efficiency and a shorter pulse could lead to the same results.

Further Excitement Another method for reducing the impact of qubit decay in readout is by applying a qubit pulse at frequency f_{12} such that we drive transitions $|1\rangle \rightarrow |2\rangle$. The $|0\rangle$ will not be affected. And we can choose our readout frequency such that we can draw a decision

boundary separating $|0\rangle$ or $|\text{not } 0\rangle$ with high fidelity. Since the second excited state $|2\rangle$ primarily relaxes to $|1\rangle$, this will effectively lead to a higher lifetime since $|2\rangle$ and $|1\rangle$ will be classified similarly as $|\text{not } 0\rangle$. Unfortunately, this method can not be combined with active reset, since we only want to apply and x-gate if the qubit is in state $|1\rangle$ and not in this case, the indistinguishable $|2\rangle$. This could be solved with good qutrit classification [55].

9.2.4 Efficiency

The efficiency plays a delicate role for reading out. Primarily, it scales the standard deviations of the two Gaussian distributions in the IQ plane with a factor of $\sqrt{\eta}$. The overlap between two Gaussians goes rapidly down with smaller widths, and with a separation of only three to four standard deviations, we are below the sub-percent overlap. From this points onward, we will not see much more performance gain. In Table 9.6, we see that a 4 time increase in η leads to approximately the same performance gain as by having a perfect efficiency. If it is possible to increase the efficiency more, it will most likely be more beneficial to decrease the pulse duration. Instead of improving the efficiency directly, we can use the following two strategies to combat infidelity effects from inefficiency.

Table 9.6: The outcome of calibrating the qubit with the methods presented in this chapter.

Increase	Efficiency	Fidelity (%)
-25 %	2.64 %	65 ± 2
0 %	3.30 %	65 ± 2
33 %	4.40 %	68 ± 2
100 %	6.60 %	68 ± 2
300 %	13.2 %	73 ± 2
max	100.0 %	75 ± 2

Longer Readout Pulse The duration of a pulse is a compromise between energy decay and readout efficiency. If the pulse is too short the two distributions have a big overlap making it hard to classify them, whereas a long pulse increases the probability of energy decay. If we were to have a large T_1 and a low efficiency. In future setups, the optimal pulse length could be calibrated by doing an experiment where SPAM fidelity is determined as a function of time.

High Power Readout - The efficiency helps reduce the overlap of the two distribution by making the distributions narrower. However, another approach is to move the distributions further away from each other. In this thesis, we have been limited by the photon number for numerical reasons. However, by driving the resonator with a larger amplitude, the two distributions would move further away in the IQ-space. One should however be aware of the increased shift of the qubit frequency and to still be within the critical photon number where the dispersive approximation is valid or venture into a new realm of high power readouts.

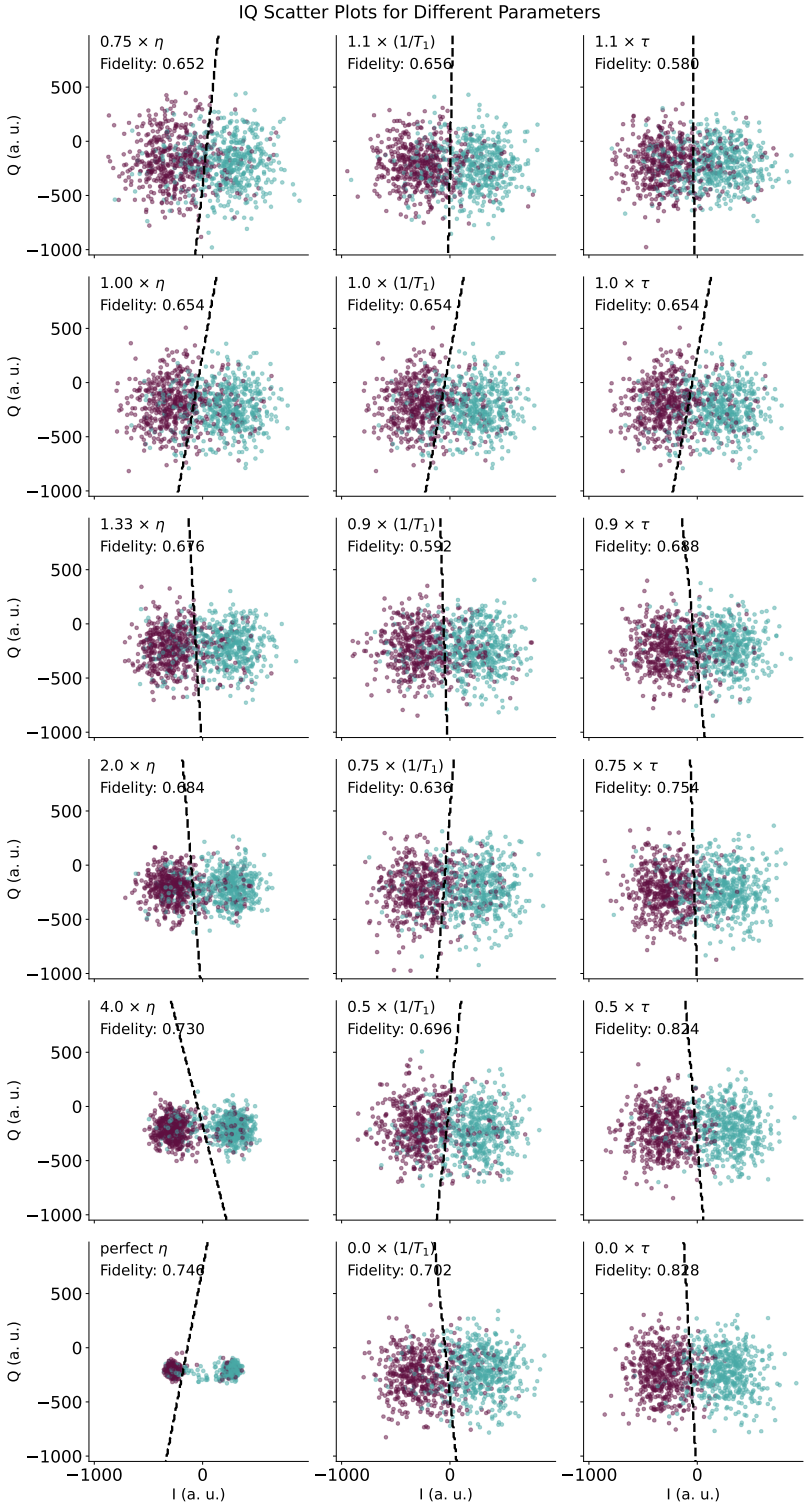

Figure 9.6: The IQ Plots for the models with different parameters. The seperation line, fidelity and parameter scaling is shown.

9.3 Further Path to Optimization

In the sections above, we have considered a first order optimization, where all except one parameter were kept constant. This gives significant improvements for reductions in temperature, less for increased η and marginal increases from better T_1. In addition to the improvements from a colder, more coherent and more efficient setup, we also discussed the possibility of "trading" a good performing parameter to improvements in the others. Some of the trade-offs are illustrated in Figure 9.7.

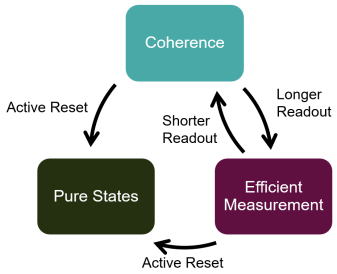

Figure 9.7: Illustration of how good coherence, low temperatures or efficient measurement can be used to reduce infidelity contribution from the other sources.

The biggest factor in our SPAM errors was the temperature providing a mixed state from the beginning. Since the T_1 seemed to be less limiting, we would probably benefit from using the active reset method in our approach. Furthermore, we saw that the contribution from efficiency is larger than that of energy decay. This indicates that we could win performance by using a longer pulse. This consideration can be used in an experiment where an accumulated demodulation gives a fidelity for each pulse duration. One can now pick the duration with the highest fidelity.

Since all improvements would lead to an altered readout sequence, the improvement gained by reducing the parameters in the section above are not very representative of what would actually happen in the laboratory. To increase performance, a changed parameter would quickly start a search for the optimal readout duration, amplitude and applying the tricks (like active reset) that would help with our setup. In order to use the simulation model we have built up through this thesis, the next steps would be to find ways of simulating these strategies, so they can be applied when we do our forecasts. This will also lead to second order effects like inefficiency contributing to the state preparation error in active reset.

Another challenge is that a stronger pulse would definitely help our readout fidelity. The increased amplitude will force us to use a larger Hilbert space as well. And since the Lindblad Equation and the Stochastic Master Equation both evolve the density matrix, we would effectively get n^2 differential equation to solve. Implementing active reset in simulation is also not trivial. In the code-module built for this thesis, the simulation of a trajectory is separate from the analysis and classification from the trajectories. In active reset, we would have to do a simulation, readout analysis and apply a conditional x-gate before simulating again[2]. We would also need to take cool down of the resonator into account along with the possibility of qubit decay in the meantime. Ultimately, this would mean a 3-10 times increase (at best) of simulation time and would require a rework of the simulations module.

[2] And might even have to repeat multiple times if the readout the second time still gives $|1\rangle$

10 Conclusion

We have now reached the end of our journey into the theory, calibration, and simulation of readout in a superconducting system. To end this thesis, we will summarize the key points before looking at some possible next steps for this project.

To create a model of superconducting qubit readout, we have reviewed the theory behind it in three stages. The unitary evolution of the system, where we described how the coupling between qubit and resonator allows us to measure the qubit by driving the resonator. The interaction with the environment, where we have described the challenges of a qubit and resonator that lose coherence or exchange energy with the environment. And finally, the stochastic evolution, which describes the unraveling of a single trajectory subject to weak measurements. The review of theory has given us the tools for simulating the dynamics and a list of parameters that we need to determine to make a realistic model.

Following the list of parameters, we have performed a sequence of calibrations, leading to a list of estimated parameters to enter the simulation model. By running the model and comparing it to the readout sequence experiment from the laboratory, we conclude that we get similar state initialization and measurement fidelity. While the distributions also look promising, they are not overwhelmingly convincing. This hints that X-gate fidelity and the second excited state should be included in the analysis.

By changing parameters to the ideal values, we used the realistic model to estimate the contributions from three different sources to the SPAM infidelity. We find that the primary contributor to infidelity is a high temperature, followed by low efficiency and low coherence time. Lastly, we have used the model to estimate the improvements to SPAM fidelity by marginal improvements in efficiency, temperature, or coherence time. These estimates were used to enter a discussion of how different strategies for the initialization and readout sequence can be used to reduce the impact of low efficiency, high temperature, or low coherence, given that the other parameters are better.

10.1 Next Steps

During the learning, writing, and coding for this thesis, my overview of the field and the methods have increased significantly. Of course, there are many things I would have liked to do differently, in another

order, or have shelved earlier, if I look back now. However, this has also come with ideas for possible paths for continuing the work. While some are straight-forward, like general model optimization and inclusion of X-gate fidelity and qutrit dynamics, others require more work. The last part of this thesis will cover a short presentation of some possible continuations.

10.1.1 Fitting the Model to Trajectories

In this thesis, the model was made by calibrating the qubit using different methods for each parameter. Instead, we could explore if the model could be directly fitted to the data to retrieve the calibrated parameters. We saw in Figure 8.1.3 that by convolving the q-function with a Gaussian, we get a good estimate for the distribution of the readout record at a given time. One could imagine using this to calculate the log-likelihood of each point at each time, given a set of parameters. If we consider this a cost function, we can leverage the development of ODE integration techniques in deep learning libraries. This allows us to maximize the likelihood by tuning the parameters, where the gradients can be found by either autograd methods or the adjoint state method. [56]

New libraries for minimizing stochastic differential equation models have also been developed and are now already used to calibrate qubit parameters [57]. Here, the qubit is however modeled without the resonator with the equations from Section 5.4. One could imagine reintroducing the resonator with the models presented in this thesis to get an even better representation of the dynamics.

10.1.2 Including Improved Strategies in Simulation

In Chapter 9, we discussed different strategies to swap good-performing variables for others. It would definitely be beneficial to include these strategies in simulation. First, the amplitude and duration of the pulse should be optimized in the realistic setting before good estimates for improved devices can be extracted. The next steps will be to include $|1\rangle \rightarrow |2\rangle$ pulses as well as active reset. This would allow for a more flexible model that does not slack a few steps behind what is happening at the fridge.

10.1.3 Bigger Hilbert Space - High Power Simulations

Lastly, we have been limited in our readout power, not by the quantum device in question but by the classical computation power used to run the simulation. By having more computational resources (and time), it would be possible to also drive the resonator to a mean photon number of approximately 30 or maybe even higher. This would give a better illustration of what is happening in the laboratory. Of course, we will need to check the dispersive approximation thoroughly when we start to add more photons.

Bibliography

[1] John J. L. Morton, Dane R. McCamey, Mark A. Eriksson, and Stephen A. Lyon. Embracing the quantum limit in silicon computing. *Nature*, 479(7373):345–353, November 2011. ISSN 1476-4687. doi: 10.1038/nature10681. URL https://www.nature.com/articles/nature10681. Number: 7373 Publisher: Nature Publishing Group.

[2] John Preskill. Quantum Computing in the NISQ era and beyond. *Quantum*, 2:79, August 2018. doi: 10.22331/q-2018-08-06-79. URL https://quantum-journal.org/papers/q-2018-08-06-79/. Publisher: Verein zur Förderung des Open Access Publizierens in den Quantenwissenschaften.

[3] Kenneth R. Brown, Jungsang Kim, and Christopher Monroe. Co-designing a scalable quantum computer with trapped atomic ions. *npj Quantum Information*, 2(1):1–10, November 2016. ISSN 2056-6387. doi: 10.1038/npjqi.2016.34. URL https://www.nature.com/articles/npjqi201634. Number: 1 Publisher: Nature Publishing Group.

[4] Jeremy L. O'Brien. Optical Quantum Computing. *Science*, 318(5856):1567–1570, December 2007. doi: 10.1126/science.1142892. URL https://www.science.org/doi/full/10.1126/science.1142892. Publisher: American Association for the Advancement of Science.

[5] Philip Krantz, Morten Kjaergaard, Fei Yan, Terry P. Orlando, Simon Gustavsson, and William D. Oliver. A Quantum Engineer's Guide to Superconducting Qubits. *Applied Physics Reviews*, 6(2):021318, June 2019. ISSN 1931-9401. doi: 10.1063/1.5089550. URL http://arxiv.org/abs/1904.06560. arXiv:1904.06560 [cond-mat, physics:physics, physics:quant-ph].

[6] Jens Koch, Terri M. Yu, Jay Gambetta, A. A. Houck, D. I. Schuster, J. Majer, Alexandre Blais, M. H. Devoret, S. M. Girvin, and R. J. Schoelkopf. Charge insensitive qubit design derived from the Cooper pair box. *Physical Review A*, 76(4):042319, October 2007. ISSN 1050-2947, 1094-1622. doi: 10.1103/PhysRevA.76.042319. URL http://arxiv.org/abs/cond-mat/0703002. arXiv:cond-mat/0703002.

[7] Vladimir E. Manucharyan, Jens Koch, Leonid I. Glazman, and Michel H. Devoret. Fluxonium: Single Cooper-Pair Circuit Free of Charge Offsets. *Science*, 326(5949):113–116, October 2009. doi: 10.1126/science.1175552. URL https://www.science.org/doi/full/10.1126/science.1175552. Publisher: American Association for the Advancement of Science.

[8] F. Motzoi, J. M. Gambetta, P. Rebentrost, and F. K. Wilhelm. Simple Pulses for Elimination of Leakage in Weakly Nonlinear Qubits. *Physical Review Letters*, 103(11):110501, September 2009. doi: 10.1103/PhysRevLett.103.110501. URL https://link.aps.org/doi/10.1103/PhysRevLett.103.110501. Publisher: American Physical Society.

[9] T. Walter, P. Kurpiers, S. Gasparinetti, P. Magnard, A. Potočnik, Y. Salathé, M. Pechal, M. Mondal, M. Oppliger, C. Eichler, and A. Wallraff. Rapid High-Fidelity Single-Shot Dispersive Readout of Superconducting Qubits. *Physical Review Applied*, 7(5):054020, May 2017. doi: 10.1103/PhysRevApplied.7.054020. URL https://link.aps.org/doi/10.1103/PhysRevApplied.7.054020. Publisher: American Physical Society.

[10] Fei Yan, Philip Krantz, Youngkyu Sung, Morten Kjaergaard, Daniel L. Campbell, Terry P. Orlando, Simon Gustavsson, and William D. Oliver. Tunable Coupling Scheme for Implementing High-Fidelity Two-Qubit Gates. *Physical Review Applied*, 10(5):054062, November 2018. doi: 10.1103/PhysRevApplied.10.054062. URL https://link.aps.org/doi/10.1103/PhysRevApplied.10.054062. Publisher: American Physical Society.

[11] R. Barends, J. Kelly, A. Megrant, A. Veitia, D. Sank, E. Jeffrey, T. C. White, J. Mutus, A. G. Fowler, B. Campbell, Y. Chen, Z. Chen, B. Chiaro, A. Dunsworth, C. Neill, P. O'Malley, P. Roushan, A. Vainsencher, J. Wenner, A. N. Korotkov, A. N. Cleland, and John M. Martinis. Superconducting quantum circuits at the surface code threshold for fault tolerance. *Nature*, 508(7497):500–503, April 2014. ISSN 1476-4687. doi: 10.1038/nature13171. URL https://www.nature.com/articles/nature13171. Number: 7497 Publisher: Nature Publishing Group.

[12] Leon Ding, Max Hays, Youngkyu Sung, Bharath Kannan, Junyoung An, Agustin Di Paolo, Amir H. Karamlou, Thomas M. Hazard, Kate Azar, David K. Kim, Bethany M. Niedzielski, Alexander Melville, Mollie E. Schwartz, Jonilyn L. Yoder, Terry P. Orlando, Simon Gustavsson, Jeffrey A. Grover, Kyle Serniak, and William D. Oliver. High-Fidelity, Frequency-Flexible Two-Qubit Fluxonium Gates with a Transmon Coupler. *Physical Review X*, 13(3):031035, September 2023. doi: 10.1103/PhysRevX.13.031035. URL https://link.aps.org/doi/10.1103/PhysRevX.13.031035. Publisher: American Physical Society.

[13] François Swiadek, Ross Shillito, Paul Magnard, Ants Remm, Christoph Hellings, Nathan Lacroix, Quentin Ficheux, Dante Colao Zanuz, Graham J. Norris, Alexandre Blais, Sebastian Krinner, and Andreas Wallraff. Enhancing Dispersive Readout of Superconducting Qubits Through Dynamic Control of the Dispersive Shift: Experiment and Theory, July 2023. URL http://arxiv.org/abs/2307.07765. arXiv:2307.07765 [quant-ph].

[14] Junan Lin, Joel J. Wallman, Ian Hincks, and Raymond Laflamme. Independent State and Measurement Characterization for Quantum Computers. *Physical Review Research*, 3(3):033285, September 2021. ISSN 2643-1564. doi: 10.1103/PhysRevResearch.3.033285. URL http://arxiv.org/abs/1910.07511. arXiv:1910.07511 [quant-ph].

[15] Philip Krantz, Morten Kjaergaard, Fei Yan, Terry P. Orlando, Simon Gustavsson, and William D. Oliver. Week 3 exercises. *Applied Physics Reviews*, 6(2):021318, June 2019. ISSN 1931-9401. doi: 10.1063/1.5089550. URL http://arxiv.org/abs/1904.06560. arXiv:1904.06560 [cond-mat, physics:physics, physics:quant-ph].

[16] Jun J. Sakurai and Jim Napolitano. *Modern quantum mechanics*. Cambridge University Press, Cambridge, United Kingdom New York, NY Port Melbourne, VIC New Delhi Singapore, third edition edition, 2021. ISBN 978-1-108-58728-0 978-1-108-47322-4. doi: 10.1017/9781108587280.

[17] Charles Kittel and Herbert Kroemer. *Thermal Physics*. W. H. Freeman, January 1980. ISBN 978-0-7167-1088-2. Google-Books-ID: coR79nyOoNMC.

[18] J. C. Butcher. Numerical methods for ordinary differential equations in the 20th century. *Journal of Computational and Applied Mathematics*, 125(1):1–29, December 2000. ISSN 0377-0427. doi: 10.1016/S0377-0427(00)00455-6. URL https://www.sciencedirect.com/science/article/pii/S0377042700004556.

[19] J. R. Johansson, P. D. Nation, and Franco Nori. QuTiP: An open-source Python framework for the dynamics of open quantum systems. *Computer Physics Communications*, 183(8):1760–1772, August 2012. ISSN 0010-4655. doi: 10.1016/j.cpc.2012.02.021. URL https://www.sciencedirect.com/science/article/pii/S0010465512000835.

[20] Alexandre Blais, Arne L. Grimsmo, S.M. Girvin, and Andreas Wallraff. Circuit quantum electrodynamics. *Reviews of Modern Physics*, 93(2):025005, May 2021. doi: 10.1103/RevModPhys.93.025005. URL https://link.aps.org/doi/10.1103/RevModPhys.93.025005. Publisher: American Physical Society.

[21] Pierre-Gilles de Gennes. *Superconductivity of metals and alloys*. New York, W.A. Benjamin, 1966. URL http://archive.org/details/superconductivit0000genn.

[22] Uri Vool and Michel H. Devoret. Introduction to Quantum Electromagnetic Circuits. *International Journal of Circuit Theory and Applications*, 45(7):897–934, July 2017. ISSN 0098-9886, 1097-007X. doi: 10.1002/cta.2359. URL http://arxiv.org/abs/1610.03438. arXiv:1610.03438 [cond-mat, physics:quant-ph].

[23] Nathan K. Langford. Circuit QED - Lecture Notes, October 2013. URL http://arxiv.org/abs/1310.1897. arXiv:1310.1897 [cond-mat, physics:quant-ph].

[24] Philipp Aumann, Tim Menke, William D. Oliver, and Wolfgang Lechner. CircuitQ: an open-source toolbox for superconducting circuits. *New Journal of Physics*, 24(9):093012, September 2022. ISSN 1367-2630. doi: 10.1088/1367-2630/ac8cab. URL https://dx.doi.org/10.1088/1367-2630/ac8cab. Publisher: IOP Publishing.

[25] Maxime Boissonneault, J. M. Gambetta, and Alexandre Blais. Dispersive regime of circuit QED: photon-dependent qubit dephasing and relaxation rates. *Physical Review A*, 79(1):013819, January 2009. ISSN 1050-2947, 1094-1622. doi: 10.1103/PhysRevA.79.013819. URL http://arxiv.org/abs/0810.1336. arXiv:0810.1336 [cond-mat, physics:quant-ph].

[26] Alexandre Blais, Ren-Shou Huang, Andreas Wallraff, S. M. Girvin, and R. J. Schoelkopf. Cavity quantum electrodynamics for superconducting electrical circuits: An architecture for quantum computation. *Physical Review A*, 69(6):062320, June 2004. doi: 10.1103/PhysRevA.69.062320. URL https://link.aps.org/doi/10.1103/PhysRevA.69.062320. Publisher: American Physical Society.

[27] Christopher Gerry and Peter Knight. *Introductory Quantum Optics*. Cambridge University Press, Cambridge, 2004. ISBN 978-0-521-52735-4. doi: 10.1017/CBO9780511791239. URL https://www.cambridge.org/core/books/introductory-quantum-optics/B9866F1F40C45936A81D03AF7617CF44.

[28] Daniel Manzano. A short introduction to the Lindblad master equation. *AIP Advances*, 10(2):025106, February 2020. doi: 10.1063/1.5115323. URL https://aip.scitation.org/doi/10.1063/1.5115323. Publisher: American Institute of Physics.

[29] Daniel Greenbaum. Introduction to Quantum Gate Set Tomography, September 2015. URL http://arxiv.org/abs/1509.02921. arXiv:1509.02921 [quant-ph].

[30] Philip Pearle. Simple derivation of the Lindblad equation. *European Journal of Physics*, 33(4):805, April 2012. ISSN 0143-0807. doi: 10.1088/0143-0807/33/4/805. URL https://dx.doi.org/10.1088/0143-0807/33/4/805. Publisher: IOP Publishing.

[31] John Preskill. Lecture Notes for Ph219/CS219: Quantum Information Chapter 3, October 2018. URL http://theory.caltech.edu/~preskill/ph219/chap3_15.pdf.

[32] Kurt Jacobs and Daniel A. Steck. A Straightforward Introduction to Continuous Quantum Measurement. *Contemporary Physics*, 47(5):279–303, September 2006. ISSN 0010-7514, 1366-5812. doi: 10.1080/00107510601101934. URL http://arxiv.org/abs/quant-ph/0611067. arXiv:quant-ph/0611067.

[33] Vlad Gheorghiu. Ito^ calculus in a nutshell.

[34] Stephen L Adler. Derivation of the Lindblad generator structure by use of the Itô stochastic calculus. *Physics Letters A*, 265(1):58–61, January 2000. ISSN 0375-9601. doi: 10.1016/S0375-9601(99)00847-6. URL https://www.sciencedirect.com/science/article/pii/S0375960199008476.

[35] Mike Giles. Numerical Methods II. URL https://people.maths.ox.ac.uk/gilesm/mc/mc/lec11.pdf.

[36] Philippe Campagne-Ibarcq. Measurement back action and feedback in superconducting circuits.

[37] Jay Gambetta, Alexandre Blais, M. Boissonneault, A. A. Houck, D. I. Schuster, and S. M. Girvin. Quantum trajectory approach to circuit QED: Quantum jumps and the Zeno effect. *Physical Review A*, 77(1):012112, January 2008. ISSN 1050-2947, 1094-1622. doi: 10.1103/PhysRevA.77.012112. URL http://arxiv.org/abs/0709.4264. arXiv:0709.4264 [cond-mat, physics:quant-ph].

[38] OPX+: Ultra-Fast Quantum Control Hardware, . URL https://www.quantum-machines.co/products/opx/.

[39] Octave: Seamless Up/Down-Conversion for Quantum Computing, . URL https://www.quantum-machines.co/products/octave/.

[40] Q. M. Technologies Ltd. QUA - API documentation. URL https://docs.quantum-machines.co/1.1.5/.

[41] Jacob Hastrup and Malthe Asmus MArciniak Nielsen. cQED at Center for Quantum Devices. URL https://github.com/cqed-at-qdev.

[42] C. Macklin, K. O'Brien, D. Hover, M. E. Schwartz, V. Bolkhovsky, X. Zhang, W. D. Oliver, and I. Siddiqi. A near–quantum-limited Josephson traveling-wave parametric amplifier. *Science*, 350(6258):307–310, October 2015. doi: 10.1126/science.aaa8525. URL https://www.science.org/doi/full/10.1126/science.aaa8525. Publisher: American Association for the Advancement of Science.

[43] Mark M. Wilde. *From Classical to Quantum Shannon Theory*. November 2016. doi: 10.1017/9781316809976.001. URL http://arxiv.org/abs/1106.1445. arXiv:1106.1445 [quant-ph].

[44] Jay Gambetta, W. A. Braff, A. Wallraff, S. M. Girvin, and R. J. Schoelkopf. Protocols for optimal readout of qubits using a continuous quantum nondemolition measurement. *Physical Review A*, 76 (1):012325, July 2007. doi: 10.1103/PhysRevA.76.012325. URL https://link.aps.org/doi/10.1103/PhysRevA.76.012325. Publisher: American Physical Society.

[45] Fabian Pedregosa, Gael Varoquaux, Alexandre Gramfort, Vincent Michel, Bertrand Thirion, Olivier Grisel, Mathieu Blondel, Peter Prettenhofer, Ron Weiss, Vincent Dubourg, Jake Vanderplas, Alexandre Passos, and David Cournapeau. Scikit-learn: Machine Learning in Python. *MACHINE LEARNING IN PYTHON*.

[46] Easwar Magesan, Jay M. Gambetta, A. D. Córcoles, and Jerry M. Chow. Machine learning for discriminating quantum measurement trajectories and improving readout. *Physical Review Letters*, 114(20):200501, May 2015. ISSN 0031-9007, 1079-7114. doi: 10.1103/PhysRevLett.114.200501. URL http://arxiv.org/abs/1411.4994. arXiv:1411.4994 [quant-ph].

[47] Colm A. Ryan, Blake R. Johnson, Jay M. Gambetta, Jerry M. Chow, Marcus P. da Silva, Oliver E. Dial, and Thomas A. Ohki. Tomography via Correlation of Noisy Measurement Records. *Physical Review A*, 91(2):022118, February 2015. ISSN 1050-2947, 1094-1622. doi: 10.1103/PhysRevA.91.022118. URL http://arxiv.org/abs/1310.6448. arXiv:1310.6448 [quant-ph].

[48] Benjamin Lienhard, Antti Vepsäläinen, Luke C.G. Govia, Cole R. Hoffer, Jack Y. Qiu, Diego Ristè, Matthew Ware, David Kim, Roni Winik, Alexander Melville, Bethany Niedzielski, Jonilyn Yoder, Guilhem J. Ribeill, Thomas A. Ohki, Hari K. Krovi, Terry P. Orlando, Simon Gustavsson, and William D. Oliver. Deep-Neural-Network Discrimination of Multiplexed Superconducting-Qubit States. *Physical Review Applied*, 17(1):014024, January 2022. doi: 10.1103/PhysRevApplied.17.014024. URL https://link.aps.org/doi/10.1103/PhysRevApplied.17.014024. Publisher: American Physical Society.

[49] David Hucul, Justin E. Christensen, Eric R. Hudson, and Wesley C. Campbell. Spectroscopy of a Synthetic Trapped Ion Qubit. *Physical Review Letters*, 119(10):100501, September 2017. doi: 10.1103/PhysRevLett.119.100501. URL https://link.aps.org/doi/10.1103/PhysRevLett.119.100501. Publisher: American Physical Society.

[50] Mahdi Naghiloo. Introduction to Experimental Quantum Measurement with Superconducting Qubits, April 2019. URL http://arxiv.org/abs/1904.09291. arXiv:1904.09291 [quant-ph].

[51] E. Knill, D. Leibfried, R. Reichle, J. Britton, R. B. Blakestad, J. D. Jost, C. Langer, R. Ozeri, S. Seidelin, and D. J. Wineland. Randomized benchmarking of quantum gates. *Physical Review A*, 77(1):012307, January 2008. doi: 10.1103/PhysRevA.77.012307. URL https://link.aps.org/doi/10.1103/PhysRevA.77.012307. Publisher: American Physical Society.

[52] C. C. Bultink, B. Tarasinski, N. Haandbæk, S. Poletto, N. Haider, D. J. Michalak, A. Bruno, and L. DiCarlo. General method for extracting the quantum efficiency of dispersive qubit readout in circuit QED. *Applied Physics Letters*, 112(9):092601, March 2018. ISSN 0003-6951. doi: 10.1063/1.5015954. URL https://doi.org/10.1063/1.5015954.

[53] Tom Lindstrøm. *Kalkulus*. Universitetforlaget, 4 edition, 2016.

[54] Dmitry Panchenko. Lecture Notes | Statistics for Applications | Mathematics. URL https://ocw.mit.edu/courses/18-443-statistics-for-applications-fall-2006/pages/lecture-notes/.

[55] Liangyu Chen, Hang-Xi Li, Yong Lu, Christopher W. Warren, Christian J. Križan, Sandoko Kosen, Marcus Rommel, Shahnawaz Ahmed, Amr Osman, Janka Biznárová, Anita Fadavi Roudsari, Benjamin Lienhard, Marco Caputo, Kestutis Grigoras, Leif Grönberg, Joonas Govenius, Anton Frisk Kockum, Per Delsing, Jonas Bylander, and Giovanna Tancredi. Transmon qubit readout fidelity at the threshold for quantum error correction without a quantum-limited amplifier. *npj Quantum Information*, 9(1):1–7, March 2023. ISSN 2056-6387. doi: 10.1038/s41534-023-00689-6. URL https://www.nature.com/articles/s41534-023-00689-6. Number: 1 Publisher: Nature Publishing Group.

[56] Grégoire Allaire. A review of adjoint methods for sensitivity analysis, uncertainty quantification and optimization in numerical codes. *Ing. Automob.*, 836, July 2015.

[57] Élie Genois, Jonathan A. Gross, Agustin Di Paolo, Noah J. Stevenson, Gerwin Koolstra, Akel Hashim, Irfan Siddiqi, and Alexandre Blais. Quantum-Tailored Machine-Learning Characterization of a Superconducting Qubit. *PRX Quantum*, 2(4):040355, December 2021. doi: 10.1103/PRXQuantum.2.040355. URL https://link.aps.org/doi/10.1103/PRXQuantum.2.040355. Publisher: American Physical Society.

[58] Svend Kroejer. Week 7 - Exercises - Superconducting Qubits, July 2023.

A Code Documentation

During this project as code bases was developed to ease the implementation of simulating many different situations with different simulation schemes. In this appendix, the documentation for the code is a attached. The code can be found on GitHub at https://github.com/JohannSeverin/QuantumDeviceSimulation.

Documentation - QuantumDeviceSimulation

This is the documentation for a simulation tool created as part of my Master Thesis. Ultimately, this module is built as a wrapper for QuTiP in an attempt to ease simulation of routine tasks in Superconducting Qubits.

The module is built up of three main parts: Devices, Simulation and Analysis which are working together to built, simulate and analyze the desired superconducting system.

The complete content of this module:

Devices

To built up the devices and quantum chips, we have all statics in the device part of the module. The main goals are to calculate and store:

- Hamiltonians from calibrated or device parameters
- Decoherence operators
- Interaction between different devices in a so called Devices/System
- Different pulses which can be send in to the devices to interact with them

---

Experiment

When devices are designed, the time evolution can be calculated at different degrees of complexity. These simulation strategies are found in this part of the module. And currently support the following:

- Unitary Evolutions using the Schrodinger Equation
- Lindblad Evolution which also take decoherence into account by evolving the total density matrix and collapse operators
  - This can be done by using the Lindblad Master Equation to do deterministically
  - Or by doing a Monte Carlo Style Experiment

Analysis

Lastly, we have a module to do common analysis of the simulation traces. This is still very much under development. The hope is, however, that it should take xarrays of the same type support in OPX Control. Hopefully this will decrease the distance between simulations and experiment to hopefully integrate the two together.

Simulation

The simulation is the module responsible for the time integration. Most of the functionality is collected in the `SimulationExperiment` - parent class which keeps track of sweeping, data storage, calculation of expectation

values etc.. The `SimulationExperiment` is subclassed in order to provide a method for simulating. This allows us to to simulate using different models like Unitary, Lindblad or Stochastic simulations.

The following subclasses are available:

- Schrödinger Experiment allows unitary evolution without loss. This is however one dimensional and can go very fast.
- Lindblad Experiment is a deterministic evolution using the Lindblad Master Equation to take care of decoherence and leakage due to interaction with the environment
- Monte Carlo Experiment takes care of decoherence and losses to the environment by applying them stochastically. This means that we can approximate the Lindblad solution by dialing up the number of trajectories.
- Stochastic Master Equation is used for simulating homodyne and heterodyne measurements of the system and how it behaves under continuous monitoring.

Simulation Experiment Class

> **Note**
>
> This class uses a `Dataclass` to store data from simulation and save it. In the future this should be changed such that it comes in the same way as from the ´OPX_control´ library which is used in the lab.

The `SimulationExperiment` call the overwritten `simulate` method to simulate a configuration. This now takes care of looping over the swept parameters defined in the Systems simulated. At the moment it supports sweeps over 1 or 2 parameters as well as the possibility to save the state or density matrix at each time in the simulation.

Subclasses
Schrödinger Experiment

The simplest implemented experiment is the Schrödinger experiment which takes states and simply evolves them using the Schrödinger equation:

$$\frac{d}{dt}|\psi\rangle = -i\hbar\hat{H}|\psi\rangle$$

The Schrödinger equation is unitary evolutions and does not support decoherences, density matrices or measurements.

Since the Schrödinger equation is unitary, it is not necessary to keep track of a whole density matrix and is for this reason the fastest of the possible simulations.

To run an experiment it can be defined using:

```
experiment = SchoedingerExperiment(
        system: System,
        states: Iterable[qutip.Qobj],
        times: Iterable[float],
        expectation_operators: list[qutip.Qobj] = [],
        store_states: bool = False,
        store_measurements: bool = False,
        only_store_final: bool = False,
        save_path: str = None,
)
```

And can then be run simply by:

```
results = experient.run()
```

The parameters of the `SchroedingerExperiment` are as follows:

Parameter	Function
system	The System that should be simulated
states	States or list of states to simulate
times	List of times for simulation
expectation_operators	List of operators for which an expectation value should be calculated
store_states	Whether the states should be stored
only_store_final	Whether only the final state should be considered in storing states and calculating expectation vaues
save_path	What path the final results should be saved to

Lindblad Experiment

To consider losses and decoherences from the system, one should use the Lindblad Master equation to simulate the time evolution of a density matrix in contact with the environment. The master equation which is evolved is given by:

$$\dot{\rho}(t) = -idt[H, \rho(t)] + \sum_a \left(L_a \rho(t) L_a^\dagger - \frac{1}{2} L_a L_a^\dagger \rho(t) - \frac{1}{2} \rho(t) L_a L_a^\dagger \right)$$

where L_α is dissipation operators.

The Lindblad Master Equation considers a linear equation for the density matrix and for this reason it scales heavy with the size of the Hilbert Space. For this reason, it is significantly slower than the Schrödinger equation for high dimensional problems.

To simulate the Lindblad Master equation the following experiment should be set up in exactly the same way as the `SchoedingerExperiment`, but will consider dissipation operators of the system:

```
experiment = LindbladExperiment(
        system: System,
        states: Iterable[qutip.Qobj],
        times: Iterable[float],
        expectation_operators: list[qutip.Qobj] = [],
        store_states: bool = False,
        store_measurements: bool = False,
        only_store_final: bool = False,
        save_path: str = None,
)
```

And can be run by:

```
experiment.run()
```

The parameters are also the same as `SchroedinerExperiment`:

Parameter	Function
system	The System that should be simulated
states	States or list of states to simulate
times	List of times for simulation
expectation_operators	List of operators for which an expectation value should be calculated
store_states	Whether the states should be stored
only_store_final	Whether only the final state should be considered in storing states and calculating expectation vaues
save_path	What path the final results should be saved to

Monte Carlo Experiment

> **Note**
>
> While the Monte Carlo method uses parallel processes, it is done at a python level and runs inefficient. This method should instead be changed like the Stochastic Master Equation, where qutip handles the parallel calls internally.

For larger dimensions it can be beneficial to add the collapse operators stochastically by using the Monte Carlo Simulation. This simulation will apply a collapse operator depending on the given rate and time step. By doing this, the problem is still one dimensional and can be repeated multiple times to approximate the Lindblad equation.

A Monte Carlo Experiment is setup using:

```
experiment = MonteCarloExperiment(
        system: System,
        states: Iterable[qutip.Qobj],
        times: Iterable[float],
        expectation_operators: list[qutip.Qobj] = [],
        store_states: bool = False,
        store_measurements: bool = False,
        only_store_final: bool = False,
        save_path: str = None,
        ntraj: int = 1,
        exp_val_method="average",
)
```

And is run by:

```
results = experiment.run()
```

The parameters of the `MonteCarloExperiment` are:

Parameter	Function
system	The System that should be simulated
states	States or list of states to simulate
times	List of times for simulation
expectation_operators	List of operators for which an expectation value should be calculated
store_states	Whether the states should be stored

Parameter	Function
only_store_final	Whether only the final state should be considered in storing states and calculating expectation vaues
save_path	What path the final results should be saved to
ntraj	How many times to repeat each subexperiment
exp_val_method	When set to "average" this will take the average of all trajectories other wise expectation values for each trajectory is returened

Stochastic Master Equation

The most complex experiment is evolving the stochastic master equation. In addition, to including decoherence and dissipation this also allows for measurement feedback and a measurement record.

The Stochastic Master Equation takes the form:

$$d\rho = -i[H,\rho]dt + \mathcal{D}[c]\rho dt + \mathcal{H}[c]\rho dW$$

Where the superoperators refer to the Lindblad dissipator:

$$\mathcal{D}[c]\rho(t) = c\rho(t)c^\dagger - \frac{1}{2}cc^\dagger\rho(t) - \frac{1}{2}\rho(t)cc^\dagger$$

And a stochastic part given by:

$$\mathcal{H}[c]\rho(t) = c\rho(t) + \rho(t)c - \langle c + c^\dagger\rangle\rho(t)$$

Here dW is a stochastic variable of the wiener process with variance dt.

Currently this is simulated either by using a homodyne or heterodyne setup of the collapse operator using the `method` keyword, depending on whether one or two quadratures should be measured.

When using `StochasticMasterEquation` the system parameter `system.stochastic_dissipators` will also be considered and add the stochastic term with weighted by the efficiency of the system: `system.readout_efficiency`.

The results of the `StochasticMasterEquation` will include `measurements`. The measurements are the result of a record of outcomes from the measurement at each timestep. In the heterodyne measurements (which is the only one implemented), the measurement record takes the form of:

$$dr = \eta\left(\langle I\rangle + i\langle Q\rangle\right)dt + \frac{dW_I + dW_Q}{\sqrt{2}}$$

The experiment is defined using:

```
experiment = StochasticMasterEquation(
        system: System,
        states: Iterable[qutip.Qobj],
        times: Iterable[float],
        expectation_operators: list[qutip.Qobj] = [],
        store_states: bool = False,
        store_measurements: bool = False,
        only_store_final: bool = False,
        save_path: str = None,
        ntraj: int = 1,
        exp_val_method="average",
        method: str =  "heterodyne",
        store_measurements: bool = True,
        nsubsteps: int = 1,
)
```

And run like the others by:

```
results = experiment.run()
```

The parameters are:

Parameter	Function
system	The System that should be simulated
states	States or list of states to simulate
times	List of times for simulation
expectation_operators	List of operators for which an expectation value should be calculated
store_states	Whether the states should be stored
only_store_final	Whether only the final state should be considered in storing states and calculating expectation vaues
save_path	What path the final results should be saved to
ntraj	How many times to repeat each subexperiment
exp_val_method	When set to "average" this will take the average of all trajectories other wise expectation values for each trajectory is returened
method	Set to "homodyne" or "heterodyne" depending on one or two quadrature measurement
store_measurements	whether to store the measurement record
nsubsteps	If there should be substeps in the simulation between returned points

Devices

All the physical devices and pulses are written as children to the `Device`-class.

All devices are collected in three main categories:

- **Device** store the physical devices with Hamiltonian, decays and other parameters
- **Systems** are connecting physical devices from the Device class. This can be to combine multiple qubits, qubit and a resonator, or drive them with pulses.
- **Pulses** are different time dependent functions which can be coupled at the appropriate keyword in a System.

List of Devices:

A running list of devices, systems and pulses are found here:

- Device
  - Simple Qubit
  - Transmon
  - Resonator
- Systems
  - Qubit System
  - Qubit Resonator System
  - [Approximated Systems](Systems#Approximated Systems)
- Pulses
  - GaussianPulse

- SquareCosinePulse
- CloakedPulse

Device Parent Class

The Device Parent Class:

```
Device(ABC):

        def set_operators(self) -> None:
                SHOULD BE OVERWRITTEN TO SET DEVICES OPERATORS GIVEN PARAMETERS
```

is an abstract class made to keep track of static and sweepable parameters. It has the following methods. When subclassed it should have a new version which creates a new init calling the parent and overwriting the `Device.set_operators` method.

The `init(self)` should define a `self.sweepable_parameters` a list with strings referring to the defined parameters which should have the ability to be swept in an .md. Furthermore, it should also include `self.update_methods</<code>`

An example could be the following:

```
def NewDevice(Device):

        def __init__(self, ...):
                DEFINE NEW PARAMETERS HERE FOR THE CLASS
                self.sweepable_parameters = ["PARAM1", "PARAM2"]
                self.update_methods = [self.set_operators]
                super().__init__()

        def set_operators(self):
                SET HAMILTONIAN AND OTHER OPERATORS HERE
                self.hamiltonian = qutip.number(self.levels) # For Example a harmonic oscillator
```

Device

Device is part of the Devices submodule which contains the different children classes to the [Device Parent Class] (Devices#Device Parent Class).

Qubits

Simple Qubit

The most basic device is the simple qubit. This is simply defined from a qubit frequency given in GHz which defines the energy gap between $|0\rangle$ and $|1\rangle$, along with the anharmonicity. If the anharmonicity is None, the Qubit is a simple two-level system, but with it defined, there will be a third level $|2\rangle$ with energy $2f_{01} + \alpha$ where α is the anharmonicity.

Furthermore, the qubit can be defined with a decay by defining a $T_1 \neq 0$.

```
SimpleQubit(
        frequency: float,
        anharmonicity: float = None,
        T1: float = 0.0,
):
```

The sweepable parameters of the SimpleQubit are:

Parameter	Use	Sweepable
frequency	The energy spacing between the 0 and 1 level in GHz	x
anharmonicity	The difference in energy splitting between 2-1 and 1-0 . (Given in Ghz)	x
T1	The characteristic time of qubit decay	x

And the update methods calculates the following operators/dissipators:

- Hamiltonian
- Charge Matrix
- Dissipators
  - Qubit Decay

Transmon

The Transmon qubit defines an n-level anharmonic system from the physical parameters Transmon Device. The Hamiltonian and Charge Matrix are calculated numerically by diagonalizing the Hamiltonian in the charge basis of the charge matrix. (see CircuitQ: an open-source toolbox for superconducting circuits)

To define the Transmon call the following:

```
SimpleQubit(
        self,
        EC: float,
        EJ: float,
        n_cutoff: int = 20,
        ng: float = 0.0,
        levels: int = 3,
        T1: float = 0.0,
)
```

The parameters of the Transmon qubit are:

Parameter	Use	Sweepable
EC	Energy associated with capacitor in GHz	x
EJ	Energy assiciated with Josephson Junction in GHz	x
n_cutoff	Number of charges to include in calculations of hamiltnonian.	
ng	Charge offset in units of 2e	x
levels	Define how many energy levels of the Transmon should be considered.	
T1	The characteristic time of qubit decay process	x

And the update methods calculates the following operators/dissipators:

- Hamiltonian

- Charge Matrix
- Dissipators
  - Qubit Decay

Resonator

The resonator is a defined as a quantum harmonic oscillator with energy levels $(n+\frac{1}{2})2\pi f$ with f the frequency of the resonator. It further supports decay of the resonator given by the characteristic time κ.

To define a resonator use the following:

```
Resonator(
        frequency: float,
        levels=10,
        kappa: float = 0
)
```

The sweepable parameters of the Resonator are:

Parameter	Use	Sweepable
frequency	The energy spacing between levels in GHz	x
levels	The number of levels to consider	
kappa	The characteristic time of photon decay	x

Which updates the following operators and dissipators:

- Hamiltonian
- Coupling Operator
- Dissipators
  - Qubit Decay

Systems

In this module, a **system** is made to simulate the interaction between different devices such that different interactions can be calculated. The system class also takes care of propagating updates directly to the devices which it is built of while also maintaining its own sweepable parameters.

System Parent Class

The **System parent class** defines much of the logistics for the updating parameters in the overall system or in the device which it is made of.

The parent class takes the following abstract form:

```
class System(ABC):
    @abstractmethod
    def set_operators(self):
                WRITE THIS FUNCTION SUCH THAT IT UPDATES THE OPERATORS
                DEVICE OPERATORS ARE UPDATED BEFORE THIS FUNCTION IS CALLED

    @abstractmethod
```

```
    def get_states(self):
        THIS FUNCTION SHOULD BE USED TO GET THE BASIS STATES OF THE SYSTEM
```

In addition to the new methods, the new `init()` function should also define a `self.sweepable`*`parameters`* *and a* `self.update_methods`. *_Maybe also even a self.dimensions?*

An example for defining a new system can be seen here:

```
class NewSystem(System):

        def __init__(self, qubit, PARAM1, PARAM2):
                CALCULATIONS HERE

                self.sweepable_parameters = ["PARAM1"]
                self.update_method = [self.update_operators, self.update_dissipators]

        def set_operators(self):
                CALCULATE HAMILTNONIAN FOR THE ENTIRE SYSTEM HERE

        def set_dissipators(self):
                CALCULATE THE DISSIPATORS HERE

        def get_states(self, state_numbers):
                states = FIND THE STATES HERE
                return states
        ```


Systems
Some simple systems are already defined in the module and are documented below. Some systems are
approximation of these systems and will be found in the new section.

QubitSystem
The simplest system connects a qubit to a pulse drive line. It can be defined by:

```python
QubitSystem(
        self,
        qubit: Device,
        qubit_pulse: Pulse = None,
)
```

To get a state, one can call the following code with state being the integer of the desired level.

```
state = QubitSystem.get_states(state: int)
```

A few simple methods are defined to get common expectation value operators.

```
# An operator  for finding the number operator
QubitSystem.qubit_state_operator()

# Or the occupation for a specific state
QubitSystem.qubit_state_occupation_operator(state: int = 1)
```

QubitResonatorSystem

The QubitResonatorSystem is made for combing one Device > Qubits class element with a Device > Resonator along with pulses each.

The QubitResonatorSystem is called with the following syntax:

```
QubitResonatorSystem(
        qubit: Device,
        resonator: Device,
        coupling_strength: float,
        resonator_pulse: Pulse = None,
        qubit_pulse: Pulse = None,
)
```

The qubit and resonator are connected with the $g\,\hat{n} \otimes (a + a^\dagger)$ where g is the coupling strength, $\hat{n}$ is the charge matrix of the qubit and a and $a^\dagger$ are the lowering and raising operators of the resonator.

Initial states are found as $|\text{qubit state}\rangle \otimes |\text{resonator state}\rangle$ calling:

```
QubitResonatorSystem.get_states(qubit_states: int = 0, resonator_states: int = 0)
```

And the following operators can be found to calculate common expectation values:

```
# The photon number operator by tracing out the qubit
QubitResonatorSystem.photon_number_operator()

# The qubit number operator is found:
QubitResonatorSystem.qubit_state_operator()

# The occupation operator for a specifcic qubit state can be found
QubitResonatorSystem.qubit_state_occupation_operator(state: int = 1)

# And the I and Q operator for measuring the quadratures of resonator can be found as
QubitResonatorSystem.resonator_I()
QubitResonatorSystem.resonator_Q()
```

Approximated Systems

As some system very complex to simulate. For this reason a few approximations are made and implemented in order to get simpler simulations.

DispersiveQubitResonatorSystem

By taking the dispersive approximation of the QubitResonatorSystem subject to a Pulses > Square Cosine Pulse, one can do the dispersive approximation. The dispersive approximation, is most easily calculated by using the `.dispersive_approximation()` when a *QubitResonatorSystem* is defined with a *Square Cosine Pulse*.

As an example, the system can be defined by:

```
QubitResonatorSystem(
        qubit: Device,
        resonator: Device,
        coupling_strength: float,
        resonator_pulse: Pulse = None,
        qubit_pulse: Pulse = None,
```

```
).dispersive_approximation(dispersive_shift: float = None)
```

where the `resonator_pulse` must be a **SquareCosinePulse** and the **qubit_pulse** is ignored if defined. The DispersiveQubitResonatorSystem inherits the dissipators and stochastic dissipators from the QubitResonatorSystem, but redefines. One can give the function explicit dispersive shifts, otherwise it will be calculated using the frequencies of the qubit and the resonator together with the coupling strength.

Pulses

Pulse Parent Class

At the moment the Pulse Parent class mostly serves a typing help. It just has single abstract method inheriting most functionality from the [Device Parent Class](Devices#Device Parent Class). A Pulse class takes the structure:

```
class Pulse(Device):

    @abstractmethod
    def set_pulse(self):
            A FUNCTION THAT DEFINES A PULSE AS
            self.pulse: callable(t, args) -> float
```

> **Note**
>
> With `np.piecewise` it should be possible to write this in a vectorized form. This could hopefully help with performance.

Square Cosine Pulse

The simplest pulse is the cosine pulse with a simple rectangular envelope. It is defined using the following:

```
SquareCosinePulse(
        frequency: float,
        amplitude: float,
        start_time: float = 0,
        duration: float = None,
        phase: float = 0,
)
```

Parameter	Function	Sweepable
`frequency`	Set the frequency of the pulse	x
`amplitude`	The amplitude	x
`start_time`	When the pulse starts	x
`duration`	How long it lasts	x
`phase`	A phase to give to the oscillating term	x

Gaussian Pulse

The simplest pulse is the square cosine pulse. It has the following arguments:

```
GaussianPulse(
        frequency: float,
        amplitude: float,
        sigma: float,
        start_time=0,
        duration=0,
        phase=0,
        drag_alpha=0,
):
```

Where the parameters are given by the following:

Parameter	Function	Sweepable
`frequency`	Set the frequency of the pulse	x
`amplitude`	The amplitude	x
`sigma`	The width of the pulse given as standard deviation of the gaussian envelope	x
`start_time`	When the pulse starts	x
`duration`	How long it lasts	x
`phase`	A phase to give to the oscillating term	x
`drag_alpha`	if DRAG should be applied to the pulse, this $\alpha_{DRAG} \neq 0$	x

Analysis

The analysis module serves as a convenient way for plotting results from the Simulations class. It is in a preliminary stage and is mostly used for overview and debugging purposes. At the current stage, it is built of two groups.

- Sweep Analysis - Which serves as way of plotting different sweeps or time dependent behavior from a simulation. The different sweep-analysis methods can be chosen automatically by using `automatic_analysis` from `analysis.auto`.
- Q Function Analysis - Is used to calculate and visualize the Q function for density matrices from simulations.

Sweep Analysis

At the moment, the sweep analysis have four functions which both support multiple initial states and multiple expectation values, which will be shown in a grid.

- `plot_one_dimensional_sweep(results: SimulationResults, **kwargs)`, which takes a `SimulationResults` object with one sweep parameter and plots the expectation values against it.
- `plot_two_dimensional_sweep(results: SimulationResults, **kwargs)`, which takes a `SimulationResults` object with two sweep parameters and plot a heatmap with the expectation values as function of both.
- `plot_time_evolution(results: SimulationResults, **kwargs)`, which takes a `SimulationResults` object with no sweep parameters, but with `only_store_final = False` and plots the time-dependence of the expectation values.
- `plot_time_evolution_with_single_sweep(results: SimulationResults, **kwargs)`, which takes a `SimulationResults` object with one sweep parameter and `only_store_final = False`. It then plots the a heatmap of the expectation values where the axis are the sweep parameter and time.

Instead of choosing, one can use the automatic analysis:

```
# With results from some experiment
results = experiment.run()

from analysis.auto import automatic_analysis
automatic_analysis(results)
```

which automatically detects the amount of sweep parameters and if a time-axis is available to determine which of the sweep plots above should be shown.

Q Function Analysis

The Q Function Analysis consists of one utility function:

```
Q_of_rho(
         rhos: iterable[qutip.Qobj],
         x: np.ndarray,
         y: np.ndarray,
         rotate: iterable[float] = 0
 )
```

Which takes a list of state along with a list of x, y coordinates where the q function should be calculated for these states. To support demodulation behavior a rotation amount can be given in radians for each of the states. This will rotate the x-y coordinate system with the desired amount.

And two plotting functions:

- `qfunc_plotter(results: SimulationResults, interval=10, resolution=100)` which takes a simulation result and plots the Q function of the resonator after tracing out the qubit state.
- `qfunc_plotter_with_time_slider(results: SimulationResults, interval=10, resolution=100, time_steps=1, demod_frequency=0)` which plots the time-dependent q function with slider which chooses at what time the Q function should be displayed.

B Generalization of Dispersive Model for Multi Level Qubit

In section 3.2.2 the dispersive model was derived for 2-level-qubit. In this appendix, we will expand this to general form where we consider an m-level instead of the qubit. This derivation is based on the exercise from a ph.d. course in superconducting Qubits at the Niels Bohr Institute developed by Svend Krøjer [58]. As earlier, we have energy for the resonator given by: $H_{res} = \omega_r a^\dagger a$ while the energy for an M-level qubit can be written generally as:

$$H_q = \sum_{k=0}^{M-1} \omega_k |k\rangle \langle k| \tag{B.1}$$

Where $|k\rangle$ is the k'th energy eigenstate of the qubit with corresponding energy of ω_k. Allowing the M-level qubit to interact with the resonator by the Generalized Jaynes-Cumming model:

$$H_1 = \sum_{i,j} g_{ij} |i\rangle \langle j| (a + a^\dagger) \tag{B.2}$$

Where the jump strength g_{ij} is related to the overlap of the eigenstates with the charge operator and the coupling energy: $g_{ij} = g \langle i|\hat{n}|j\rangle$. This gives the full Hamiltonian:

$$H = H_0 + H_1 = \omega_r a^\dagger a + \sum_{k=0}^{M-1} \omega_k |k\rangle \langle k| + \sum_{i,j} g_{ij} |i\rangle \langle j| (a + a^\dagger) \tag{B.3}$$

As in the two-level-system, we can make use of the Schrieffer-Wolff transformation to diagonalize the Hamiltonian to second order in the perturbation variable. We want to apply the transfomration:

$$\begin{aligned} H' = e^S H e^{-S} &= H + [S, H] + \frac{1}{2}[S, [S, H]] + \dots \\ &= H_0 + H_1 + [S, H_0 + H_1] + \frac{1}{2}[S, [S, H_0 + H_1]] + \dots \end{aligned} \tag{B.4}$$

Where S has to be an anti-hermitian operator to make this a unitary transformation. The goal is now to choose S such that the linear terms in our perturbation disappear. This gives the condition $[S, H_0] = -H_1$. If we were to choose:

$$S = \sum_{ij} g_{ij} |i\rangle \langle j| \left(\frac{1}{\omega_{ij} - \omega_r} a + \frac{1}{\omega_{ij} + \omega_r} a^\dagger \right) \tag{B.5}$$

with $\omega_{ij} = \omega_i - \omega_j$. The commutator gives:

$$
\begin{aligned}
[S, H_0] &= \sum_{ijk} g_{ij} \left[|i\rangle \langle j| \left(\frac{1}{\omega_{ij} - \omega_r} a + \frac{1}{\omega_{ij} + \omega_r} a^\dagger \right), \omega_r a^\dagger a + \omega_k |k\rangle \langle k| \right] \\
&= \sum_{ij} g_{ij} |i\rangle \langle j| (\omega_j - \omega_i) \left(\frac{1}{\omega_{ij} - \omega_r} a + \frac{1}{\omega_{ij} + \omega_r} a^\dagger \right) \\
&+ \sum_{ij} g_{ij} |i\rangle \langle j| \omega_r \left(\frac{1}{\omega_{ij} - \omega_r} \left[a, a^\dagger a \right] + \frac{1}{\omega_{ij} + \omega_r} \left[a^\dagger, a^\dagger a \right] \right)
\end{aligned}
$$

And with $\left[a^\dagger, a^\dagger a\right] = -a^\dagger$ and $\left[a^\dagger, aa\right] = +a$. We obtain:

$$
\begin{aligned}
&= \sum_{ij} g_{ij} |i\rangle \langle j| \left(\frac{\omega_j - \omega_i - \omega_r}{\omega_{ij} + \omega_r} a + \frac{\omega_j - \omega_i - \omega_r}{\omega_{ij} + \omega_r} a^\dagger \right) \\
&= -\sum_{ij} g_{ij} |i\rangle \langle j| (a + a^\dagger) = -H_1
\end{aligned}
$$

With this result, our transformed Hamiltonian now becomes:

$$
\begin{aligned}
H' &= H_0 + [S, H_1] + \frac{1}{2}[S, [S, H_0 + H_1]] \dots \\
&= H_0 + [S, H_1] + \frac{1}{2} \left(-[S, H_1] + [S, [S, H_1]] \right) \dots \qquad \text{(B.6)} \\
&= H_0 + \frac{1}{2}[S, H_1] + \dots \qquad \text{(B.7)}
\end{aligned}
$$

In the dispersive limit, the coupling strength is much weaker than the detuning: $g_{ij} \ll w_{ij}$. Since S contains g_{ij}/w_{ij} terms, we only go to the linear term in the dispersive approximation, and drop everything with higher orders of S.

In this transformed basis, we find the "pertubation" entirely from: $H_{shift} = \frac{1}{2}[S, H_1]$ which can be calculated to:

$$
\begin{aligned}
2H_{shift} &= \left[\sum_{ij} g_{ij} |i\rangle \langle j| \left(\frac{1}{\omega_{ij} - \omega_r} a + \frac{1}{\omega_{ij} + \omega_r} a^\dagger \right), \sum_{kl} g_{kl} |k\rangle \langle l| (a + a^\dagger) \right] \\
&= \sum_{ijkl} g_{ij} g_{kl} \left[|i\rangle \delta_{jk} \langle l| \left(\frac{1}{\omega_{ij} - \omega_r} a + \frac{1}{\omega_{ij} + \omega_r} a^\dagger \right) (a + a^\dagger) \right] \\
&- \sum_{ijkl} g_{ij} g_{kl} \left[|k\rangle \delta_{li} \langle j| (a + a^\dagger) \left(\frac{1}{\omega_{ij} - \omega_r} a + \frac{1}{\omega_{ij} + \omega_r} a^\dagger \right) \right]
\end{aligned}
$$

Going into the rotating frame terms proportional to aa or $a^\dagger a^\dagger$ will be negligible since they are not energy conserving. Furthermore, the Scrieffer Wolf diagonalized to first order, so we will only keep diagonal elements proportional to $|i\rangle \langle i|$. We find:

$$
2H_{shift} = \sum_{ij} |g_{ij}|^2 |i\rangle \langle i| \left[\frac{1}{\omega_{ij} - \omega_r} aa^\dagger - \frac{1}{\omega_{ji} + \omega_r} a^\dagger a + \frac{1}{\omega_{ij} - \omega_r} a^\dagger a - \frac{1}{\omega_{ji} + \omega_r} aa^\dagger \right]
$$

Using the commutation relation $\left[a, a^\dagger\right] = 1$, we can write it in the following form:

$$H_{shift} = \sum_{ij} |i\rangle \langle i| \, |g_{ij}|^2 \left(\frac{1}{\omega_{ij} - \omega_r} + \left(\frac{1}{\omega_{ij} - \omega_r} + \frac{1}{\omega_{ij} + \omega_r} \right) a^\dagger a \right) \tag{B.8}$$

And by defining the following quantities:

$$\chi_{ij} = |g_{ij}|^2 \left(\frac{1}{\omega_{ij} - \omega_r} + \frac{1}{\omega_{ij} + \omega_r} \right) \tag{B.9}$$

$$\delta_{ij} = \frac{|g_{ij}|^2}{\omega_{ij} - \omega_r} \tag{B.10}$$

$$\chi_i = \sum_j \chi_{ij} \tag{B.11}$$

$$\delta_i = \sum_j \delta_{ij} \tag{B.12}$$

The dispersive m-level qubit and resonator system can be written as:

$$H' = \omega_r a^\dagger a + \sum_k \omega_k |k\rangle \langle k| + \sum_{kl} |k\rangle \langle k| \, (\delta_{kl} + \chi_{kl} a^\dagger a) \tag{B.13}$$

Or in a more interpretable manner:

$$H' = \left(\omega_r + \sum_k \chi_k |k\rangle \langle k| \right) a^\dagger a + \sum_k (\omega_k + \delta_k) |k\rangle \langle k| \tag{B.14}$$

This equation allows us to investigate the effect of the coupling between resonator and qubit. When coupled the qubit state shift the resonator frequency with χ_k. While every qubit frequency is shifted slightly y δ_k.

Or by considering reducing the multi-level system to only the two lowest, we can write the equation in the simple form:

$$H = (\tilde{\omega}_r + \chi \sigma_z) a^\dagger a + \frac{1}{2} \tilde{\omega}_{01} \sigma_z \tag{B.15}$$

where the shifts from the higher order terms have been absorbed into the new redefined frequencies.

C Fit Parameters

During this project as code bases was developed to ease the implementation of simulating many different situations with different simulation schemes. In this appendix, the documentation for the code is a attached.

C.1 Qubit

In the following tables, the fits for the qubit parameters are shown.

C.1.1 Qubit Spectroscopy

Qubit spectroscopy was fitted with

$$y = \text{offset} + A\gamma^2/(\gamma^2 + (x - f_0)^2) \tag{C.1}$$

Parameter	Value
Chi-squared	127.33 for 96 dof with p-value 0.018
f_0	$5.98203 \times 10^9 \pm 8.24256 \times 10^4$
A	$6.63190 \times 10^{-4} \pm 1.44000 \times 10^{-5}$
γ	$3.93462 \times 10^6 \pm 1.40260 \times 10^5$
Offset	$9.01520 \times 10^{-5} \pm 4.01262 \times 10^{-6}$

Table C.1: The results from fitting the qubit spectroscopy data.

and anharmonicity by:

$$y = \text{offset} + A_1\gamma_1^2/(\gamma_1^2 + (x - f_{01})^2) + A_2\gamma_2^2/(\gamma_2^2 + (x - (f_{02}/2)^2) \tag{C.2}$$

Parameter	Value
Chi-squared	882.06 for 293 dof with p-value 0.000
f_{01}	$5.97946 \times 10^9 \pm 6.11718 \times 10^4$
A_1	$7.76935 \times 10^{-4} \pm 2.37875 \times 10^{-5}$
γ_1	$1.96132 \times 10^6 \pm 8.54273 \times 10^4$
Offset	$2.41042 \times 10^{-4} \pm 1.74947 \times 10^{-6}$
f_{02}	$5.83506 \times 10^9 \pm 4.57718 \times 10^4$
A_2	$8.02353 \times 10^{-4} \pm 2.68230 \times 10^{-5}$
γ_2	$1.30993 \times 10^6 \pm 6.32462 \times 10^4$
Anharmonicity	$-2.88806 \times 10^8 \pm 1.52801 \times 10^5$

Table C.2: Results from fitting the anharmonicity experiment.

C.1.2 Rabi

Rabi was fitted with:

$$y = \text{Offset} + \text{Amplitude} \cdot \cos\left(2\pi \cdot \text{Frequency} \cdot x + \text{Phase}\right) \tag{C.3}$$

Parameter	Value
Chi-squared	85.54 for 96 dof with p-value 0.769
Amplitude	$-5.87664 \times 10^{-4} \pm 3.89923 \times 10^{-6}$
Frequency	$5.54590 \pm 1.17750 \times 10^{-2}$
Phase	$-4.06622 \times 10^{-3} \pm 7.75219 \times 10^{-3}$
Offset	$7.76880 \times 10^{-4} \pm 3.05453 \times 10^{-6}$

Table C.3: Results from fitting the Rabi experiment.

C.1.3 T1

T1 time was fitted with:

$$y = \text{Offset} + \text{Amplitude} \cdot \exp\left(-x/T_1\right) \tag{C.4}$$

Parameter	Value
Chi-squared	95.49 for 72 dof with p-value 0.034
Amplitude	$1.38798 \times 10^{-3} \pm 2.10499 \times 10^{-5}$
Offset	$-1.65994 \times 10^{-3} \pm 5.65962 \times 10^{-6}$
T1	$4.30197 \times 10^{-6} \pm 1.23942 \times 10^{-7}$

Table C.4: Results from fitting the T1 experiment.

C.1.4 T2

T2 was fitted with:

$$y = \text{Offset} + \exp(-x/T_2) \sum_i \text{Amplitude}_i \cdot \cos\left(2\pi \cdot \text{Frequency}_i \cdot x + \text{Phase}_i\right) \tag{C.5}$$

where $i \in \{1, 2\}$ for the new data and $i = 1$ for the old data.

Parameter	Value
Chi-squared	621.01 for 179 dof with p-value 0.000
Amplitude_1	$2.52602 \times 10^{-4} \pm 1.15859 \times 10^{-5}$
Frequency_1	$4.40050 \times 10^{6} \pm 1.41730$
Phase_1	$3.96978 \times 10^{-1} \pm 3.75929 \times 10^{-2}$
Amplitude_2	$1.56321 \times 10^{-4} \pm 9.88497 \times 10^{-6}$
Frequency_2	$5.00000 \times 10^{6} \pm 1.41485$
Phase_2	$3.98596 \times 10^{-1} \pm 5.71422 \times 10^{-2}$
Offset	$-8.71766 \times 10^{-4} \pm 2.87661 \times 10^{-6}$
T_2	$1.64514 \times 10^{-6} \pm 1.18271 \times 10^{-7}$

Table C.5: Results from fitting the two oscillating model to the new data in the T2 model.

Parameter	Value
Chi-squared	188.50 for 161 dof with p-value 0.068
Amplitude	$1.29900 \times 10^{-4} \pm 2.17201 \times 10^{-6}$
Frequency	$5.01652 \times 10^{6} \pm 3.39729 \times 10^{3}$
Phase	$-1.00263 \times 10^{-3} \pm 1.67711 \times 10^{-2}$
Offset	$-1.69752 \times 10^{-4} \pm 6.03841 \times 10^{-7}$
T_2	$1.69875 \times 10^{-6} \pm 5.92495 \times 10^{-8}$

Table C.6: Results from fitting the old data with the proper model.

C.2 Resonator

And the resonator fits

C.2.1 Spectroscopy

Spectroscopy of the resonator in the ground state is fitted by:

$$y = \text{offset} + A\gamma^2/(\gamma^2 + (x - f_0)^2) \tag{C.6}$$

and for the excited state:

$$y = \text{offset} + \sum_{i \in 0,1} A_i\gamma_i^2/(\gamma_i^2 + (x - f_0)^2) \tag{C.7}$$

Parameter	Value
Ground State	
Chi-squared	33.35 for 16 dof with p-value 0.007
f_0	$7.555893 \times 10^{9} \pm 3.293863 \times 10^{3}$
A_0	$-1.853905 \times 10^{-3} \pm 1.942156 \times 10^{-5}$
γ_0	$6.164246 \times 10^{5} \pm 1.185079 \times 10^{4}$
Offset	$3.480317 \times 10^{-3} \pm 2.088801 \times 10^{-5}$
Excited State	
Chi-squared	77.24 for 37 dof with p-value 0.000
f_0	$7.555801 \times 10^{9} \pm 1.983607 \times 10^{4}$
A_0	$-7.907930 \times 10^{-4} \pm 1.692275 \times 10^{-5}$
γ_0	$1.042611 \times 10^{6} \pm 4.626130 \times 10^{4}$
Offset	$3.689660 \times 10^{-3} \pm 1.987719 \times 10^{-5}$
f_1	$7.554366 \times 10^{9} \pm 6.967312 \times 10^{3}$
A_1	$-1.491251 \times 10^{-3} \pm 1.863746 \times 10^{-5}$
γ_1	$5.562317 \times 10^{5} \pm 1.150527 \times 10^{4}$

Table C.7: Fit Outcomes for Ground and Excited States of the resonator spectroscopy.

C.2.2 Kappa

kappa was fitted with:

$$y = \text{Offset} + \text{Amplitude} \cdot \exp(-\kappa x) \tag{C.8}$$

Parameter	Value
New Set	
Chi-squared	46.67 for 73 dof with p-value 0.993
Amplitude	$6.45500 \times 10^{-2} \pm 2.40723 \times 10^{-2}$
Offset	$1.26682 \times 10^{-3} \pm 2.49725 \times 10^{-4}$
κ	$3.80033 \times 10^{6} \pm 5.75194 \times 10^{5}$

Table C.8: Fit Outcomes from the model to fit kappa.

C.2.3 Photon Counting

For the photon counting, the fit was done with a parabola:

$$y = ax^2 + bx + c \tag{C.9}$$

Parameter	Value
Chi-squared	56.91 for 47.0 dof with p-value 0.153
a	$-1.89715 \times 10^{7} \pm 3.78078 \times 10^{5}$
b	$3.04349 \times 10^{6} \pm 5.67926 \times 10^{5}$
c	$5.97798 \times 10^{9} \pm 1.75053 \times 10^{5}$

Table C.9: Results from fitting the photon counting experiment.

C.3 System

Finally, fits used to extract temperature and efficiency.

C.3.1 Temperature

The temperature was extracted by fitting with the t1 decay in a continuous measurement. For the ground, it was fitted with:

$$y = \text{steady\_state} - (\text{steady\_state} - \text{initial\_error}) \cdot \exp(-x/\text{decay\_time}) \tag{C.10}$$

and for the excited state:

$$y = \text{steady\_state} + (1 - (\text{steady\_state} - \text{initial\_error})) \cdot \exp(-x/\text{decay\_time}) \tag{C.11}$$

Parameter	Value
Ground State	
Chi-squared	19.69 for 47 dof with p-value 1.000
Steady State	$9.35013 \times 10^2 \pm 1.61621 \times 10^2$
Initial Error	$8.75143 \times 10^2 \pm 3.71799 \times 10^0$
Decay Time	$1.20234 \times 10^2 \pm 3.94611 \times 10^2$
Excited State	
Chi-squared	54.26 for 47 dof with p-value 0.217
Steady State	$1.01789 \times 10^2 \pm 3.24616 \times 10^0$
Initial Error	$-8.77383 \times 10^2 \pm 7.12052 \times 10^0$
Decay Time	$1.07728 \times 10^1 \pm 2.22305 \times 10^{-1}$

Table C.10: Results from fitting the continuous modeled data to determine temperature.

C.3.2 Efficiency

The SNR was fitted by a linear fit:

$$y = ax + b \tag{C.12}$$

and the dephasing experiment with a gaussian:

$$y = Ae^{-(x-\mu)^2/\sigma^2} \tag{C.13}$$

Parameter	Value
Chi-squared	17.40 for 49 dof with p-value 1.000
a	$2.43444 \pm 1.45927 \times 10^{-1}$
b	$4.36653 \times 10^{-2} \pm 2.55083 \times 10^{-2}$

Table C.11: Results from linear fit to determine SNR as a function of amplitude strength.

Parameter	Value
Chi-squared	45.67 for 48 dof with p-value 0.569
A	$1.24481 \times 10^{-5} \pm 2.36924 \times 10^{-7}$
μ	$-8.97090 \times 10^{-4} \pm 1.52904 \times 10^{-3}$
σ	$6.93066 \times 10^{-2} \pm 1.51261 \times 10^{-3}$

Table C.12: Results from gaussian fit to determine the width of the dephasing experiment for determining efficiency.

D Plots of Fidelity Calculations

In chapter 9 many IQ plots were displayed along with the fidelity. In this appendix, we have collected the plots showing the full IQ calculations.

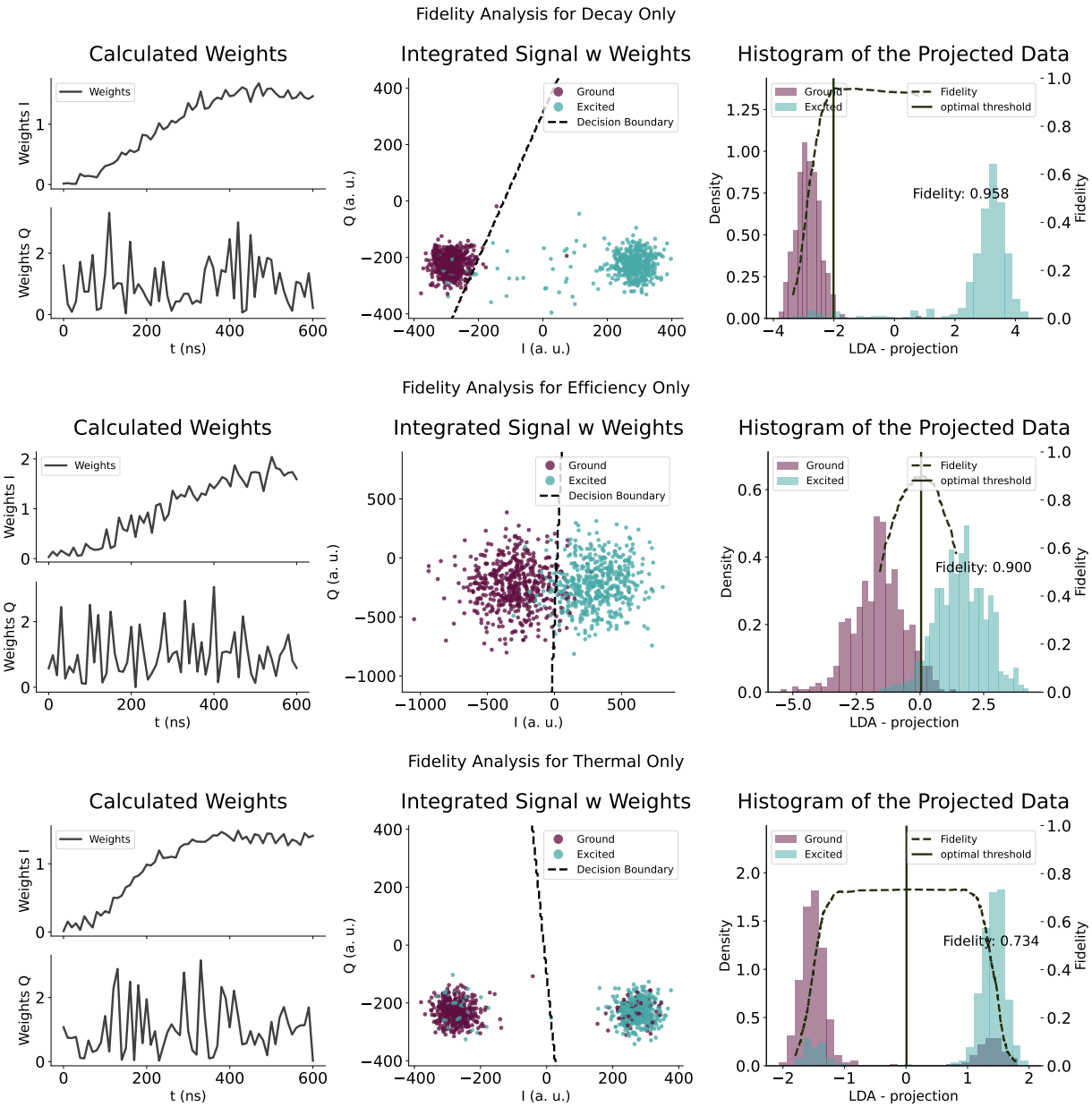

Figure D.1: The fidelity-analysis plots with the isolated contributor to infidelity.

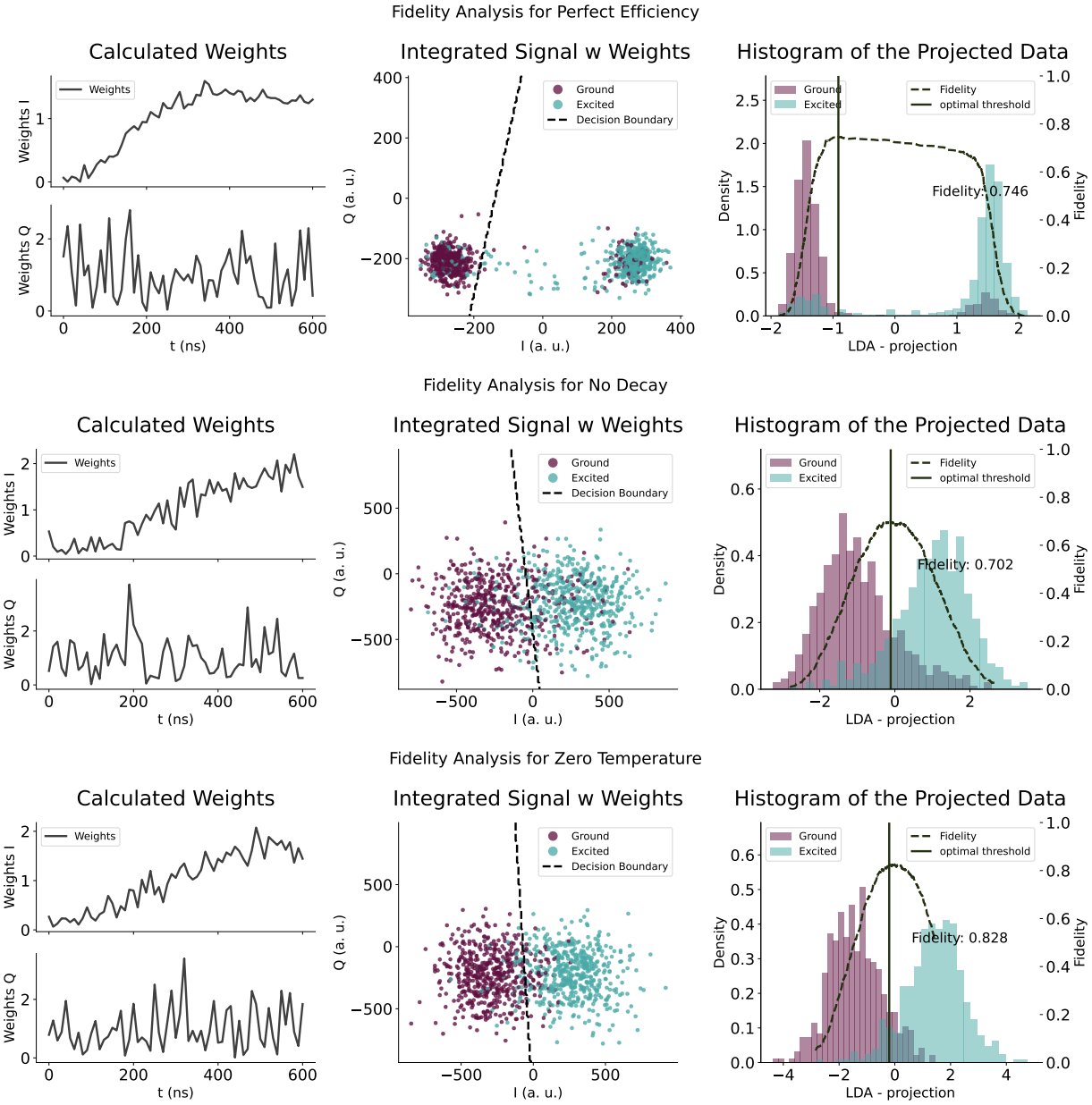

Figure D.2: The fidelity-analysis plots with contributors turned off.

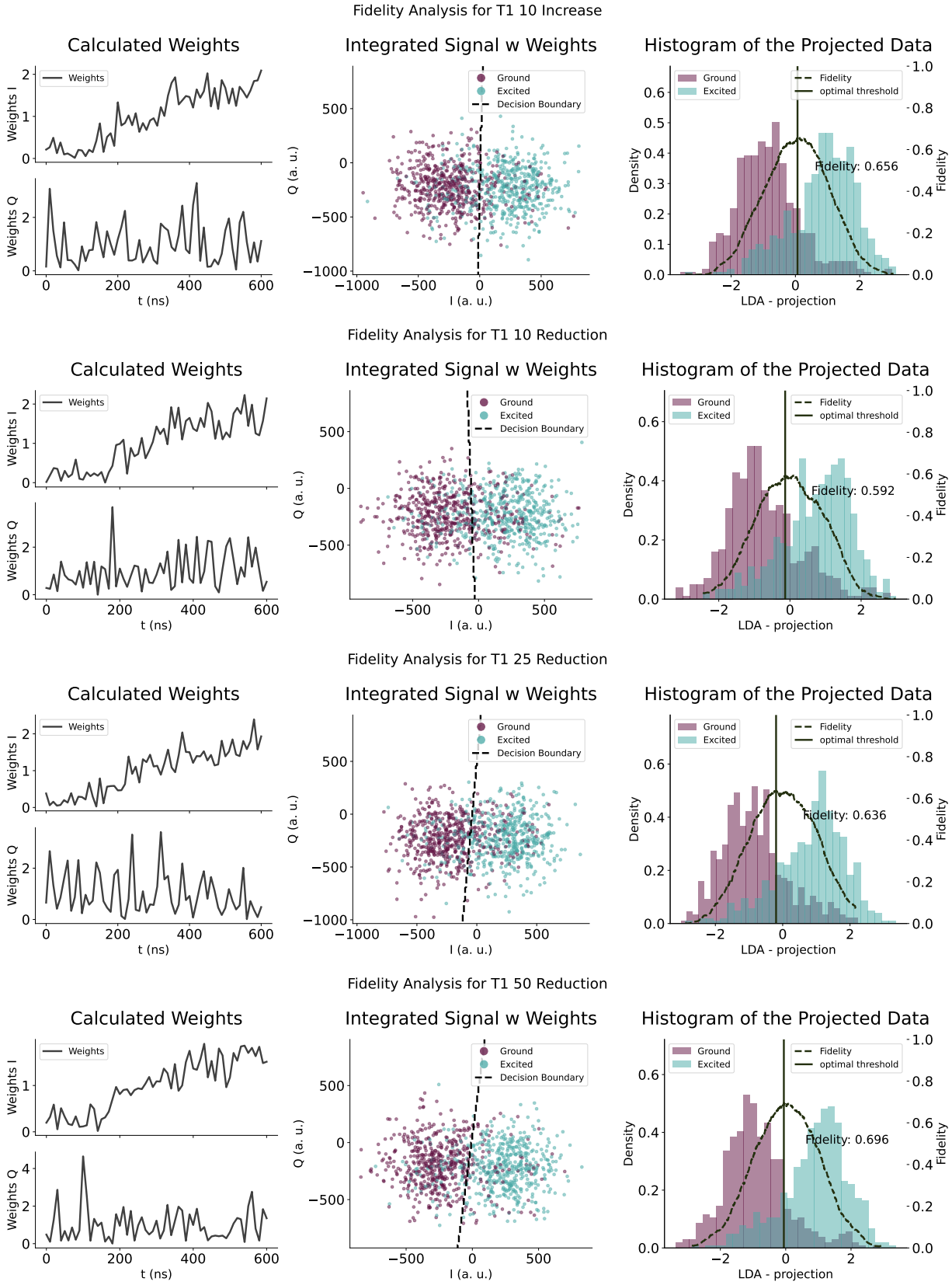

Figure D.3: The fidelity-analysis plots with marginal changes to T_1.

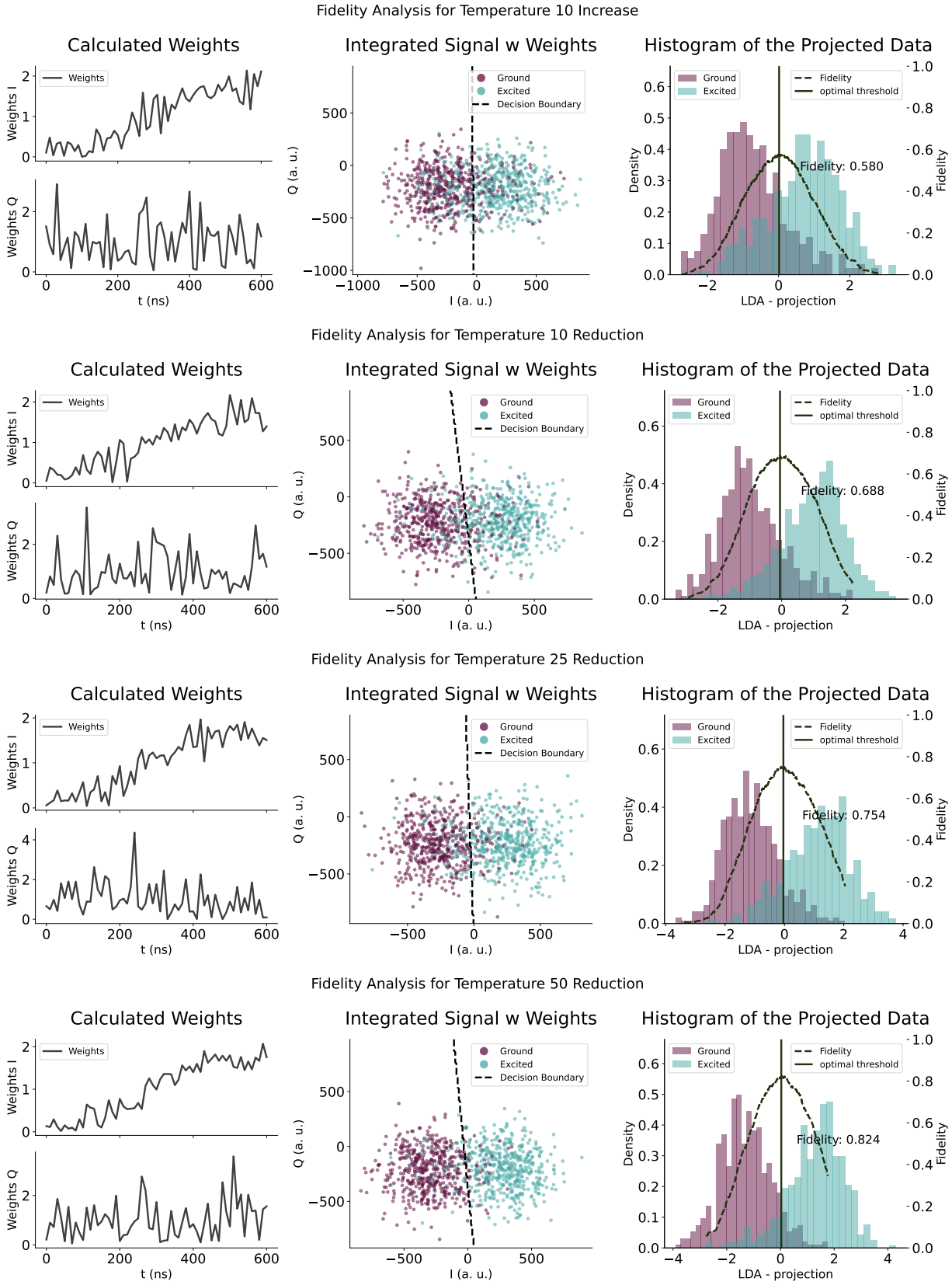

Figure D.4: The fidelity-analysis plots with marginal changes to temperature.

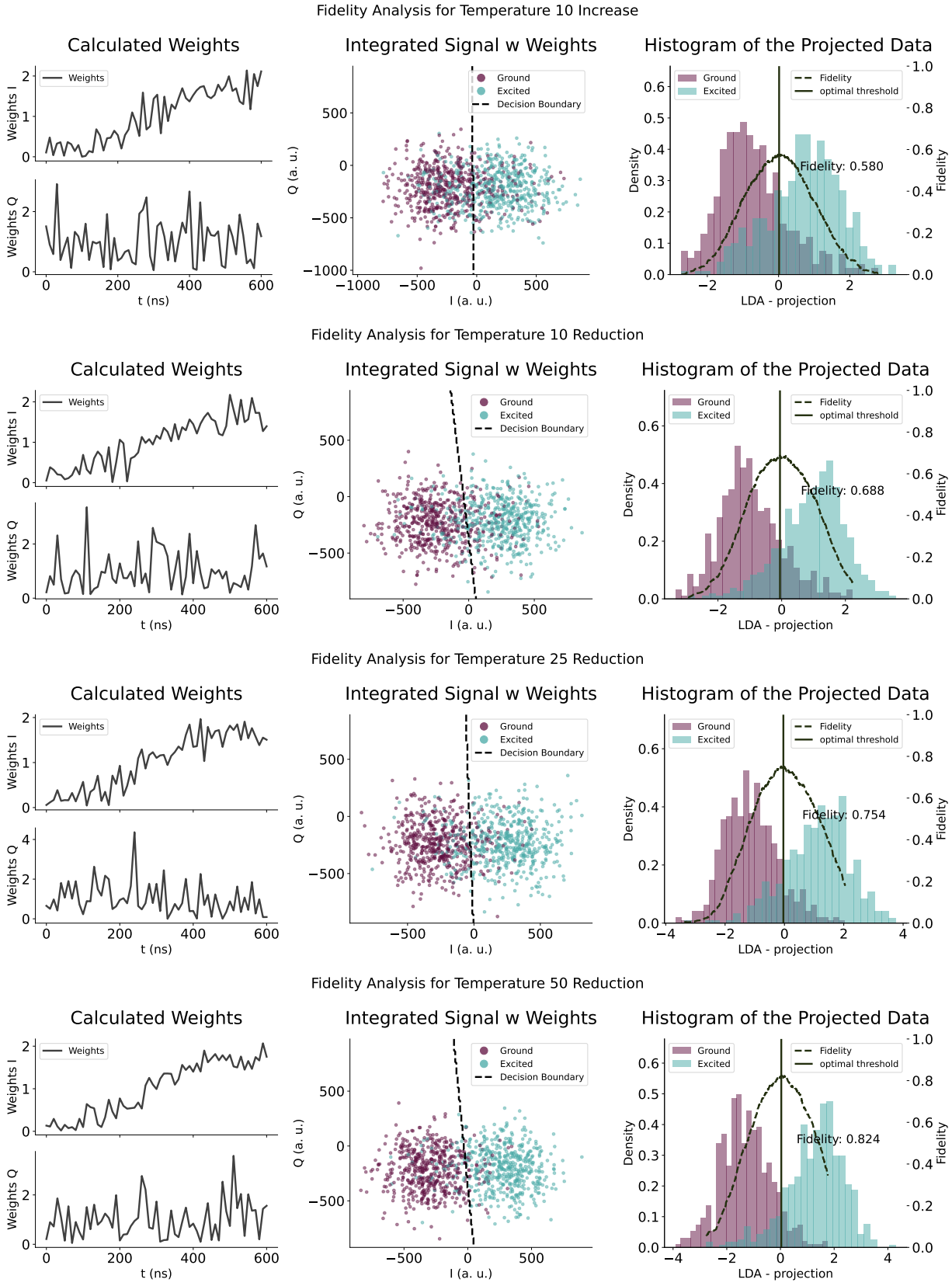

Figure D.5: The fidelity-analysis plots with marginal changes to η.